

Aus der Neurologischen Universitätsklinik Tübingen
Abteilung Neurologie mit Schwerpunkt neurovaskuläre
Erkrankungen und Neuroonkologie

**The role of C-C motif chemokine ligand 7, C-C motif chemokine
ligand 11 and interleukin-9 in T helper type 9 cell mediated
neuronal damage**

**Inaugural-Dissertation
zur Erlangung des Doktorgrades
der Medizin**

**der Medizinischen Fakultät
der Eberhard Karls Universität
zu Tübingen**

**vorgelegt von
Nakov, Philipp**

2019

Dekan: Professor Dr. I. B. Autenrieth

1. Berichterstatter: Privatdozent Dr. F. Bischof

2. Berichterstatter: Professor Dr. K. Ghoreschi

Tag der Disputation: 28.11.2018

I. Table of Contents

I.	Table of contents	I
II.	List of figures	V
III.	List of tables	VI
IV.	List of abbreviations	VII
1.	Introduction	1
1.1	Immune cells and the central nervous system (CNS)	1
1.1.1	T helper cells (T _h cells)	1
1.1.2	T helper type 9 (T _h 9) cells and their signature cytokine Interleukin-9 (IL-9)....	2
1.1.3	The immune privilege of the central nervous system (CNS)	3
1.1.4	Interactions of T helper cells (T _h cells) and neurons	4
1.1.5	Chemokines: signal mediators between the immune and the nervous system...	5
1.1.5.1	The C-C motif chemokine ligand 7 (CCL7)	6
1.1.5.2	The C-C motif chemokine ligand 11 (CCL11)	7
1.2	T helper cell mediated neuroinflammatory diseases.....	8
1.2.1	Multiple sclerosis (MS)	8
1.2.2	Experimental autoimmune encephalomyelitis (EAE) as a T _h cell mediated neuroinflammatory disease and the role of excitotoxicity in EAE.....	9
1.3	Aim of this work	11
2.	Materials and Methods	12
2.1	Animals	12
2.2	Generation of defined cell cultures for the identification of neuronal toxicity of T helper type 9 cells.....	12
2.2.1	Buffer Preparation	12
2.2.2	Generation of defined T helper type 9 cell cultures	13
2.2.2.1	Preparing of T helper type 9 cell cultures	13
2.2.2.2	Control of T helper type 9 cell cultures	15
2.2.3	Generation of defined neuronal cultures from embryonic day 16 (E16) mouse pups	16

2.2.4	Generation of defined astrocytic-neuronal mixed cultures from postnatal day 0 (P0) mouse pups	17
2.2.5	Generation of defined pure astrocytic cultures from P2 mouse pups.....	18
2.3	Gene expression analysis by quantitative real-time polymerase chain reaction (qPCR).....	19
2.3.1	Treatment of cell cultures with cytokines and glutamate for gene expression analysis	19
2.3.2	RNA extraction.....	20
2.3.3	Reverse transcription into complementary deoxyribonucleic acid (DNA)	20
2.3.4	Quantitative real-time polymerase chain reaction (qPCR).....	21
2.3.5	Analysis of measured qPCR files	22
2.4	Ca ²⁺ -imaging of neurons.....	22
2.4.1	Treatment of cells with cytokines.....	22
2.4.2	Conditioning of Magnesium free Locke's buffer (LB) with T _h 9 cells.....	23
2.4.3	Staining of neurons with a fluorescent Ca ²⁺ -dye.....	23
2.4.4	Microscopy of stained neurons.....	24
2.4.5	Analysis of Ca ²⁺ -imaging series	25
2.4.6	Statistical Analysis	26
2.5	Immunocytochemistry, microscopy and analysis of defined neuronal, astrocyte or mixed cultures	26
2.5.1	Treatment of cells	27
2.5.2	Immunostaining.....	28
2.5.3	Microscopy of immunostained samples	29
2.5.4	Analysis of immunostained samples	30
2.6	Detection of CCL7, CCL11 and IL-9 in an experimental autoimmune encephalomyelitis (EAE) mouse model	30
2.6.1	Induction of EAE.....	30
2.6.2	Dissection of the spinal cord	31
2.6.3	RNA extraction, reverse transcription and qPCR.....	31
3.	Results	32
3.1	Analysis of the generation of defined cell cultures.....	32
3.1.1	Analysis of the generation of defined T helper type 9 cell cultures.....	32

3.1.2	Analysis of the generation of defined neuronal cultures from E16 mouse embryos	33
3.1.3	Analysis of the generation of defined astrocyte cultures from P0 and P2 mouse pups	33
3.2	Identification of the effect of cytokine exposure (CCL7, CCL11, IL-9) on cytokine mRNA expression of defined cells	33
3.2.1	The effect of cytokines on cytokine gene expression in mouse astrocytes	34
3.2.2	The effect of defined cytokines on cytokine gene expression in mouse neurons	37
3.3	The effect of CCL7, CCL11 and IL-9 preincubation on E16 mouse neurons	39
3.4	Analysis of the effect of defined cytokines and T _h 9 cell conditioned imaging buffer on Ca ²⁺ levels in cultured E16 mouse neurons using Ca ²⁺ -imaging.....	42
3.4.1	General notes regarding Ca ²⁺ -imaging.....	42
3.4.2	Direct effect of the application of mouse T _h 9 cell supernatant on Ca ²⁺ levels in E16 mouse neurons	44
3.4.3	Direct effect of the application of CCL7, CCL11 and IL-9 on Ca ²⁺ levels in E16 mouse neurons	46
3.4.4	The effect of preincubation of E16 mouse neurons with CCL7, CCL11 and IL-9 on glutamate-induced Ca ²⁺ influx.....	48
3.4.4.1	Notes for all samples.....	48
3.4.4.2	The effect of 50 nM CCL7 preincubation on glutamate-induced Ca ²⁺ influx in neurons DIV 7.....	49
3.4.4.3	The effect of 50 nM CCL7 preincubation on glutamate-induced Ca ²⁺ influx in neurons DIV 14	51
3.4.4.4	The effect of 5 nM CCL7 preincubation on glutamate-induced Ca ²⁺ influx in neurons DIV 14	53
3.4.4.5	The effect of 50 nM CCL11 preincubation on glutamate-induced Ca ²⁺ influx in neurons DIV 7	55
3.4.4.6	The effect of 5 nM IL-9 preincubation on glutamate-induced Ca ²⁺ influx in neurons DIV 7	57
3.4.4.7	The effect of 30 nM IL-9 preincubation on glutamate-induced Ca ²⁺ influx in neurons DIV 14	59
3.4.4.8	The effect of 5 nM IL-9 preincubation on glutamate-induced Ca ²⁺ influx in neurons DIV 14	61

3.5	The effect of CCL7, CCL11 and IL-9 preincubation on glutamate-mediated excitotoxicity in neurons	63
3.6	Detection of CCL7, CCL11 and IL-9 in an experimental autoimmune encephalomyelitis (EAE) mouse model	68
3.7	Summary of the results	69
4.	Discussion	71
4.1	Culturing of neurons and of T _h 9 cells	71
4.1.1	Assessment of the T _h 9 cell cultures	71
4.1.2	Assessment of the neuronal cultures	71
4.2	CCL7- and CCL11-mRNA expression in neurons and astrocytes	73
4.3	The role of CCL7, CCL11 and IL-9 in neuronal damage.....	74
4.4	Analysis of neuronal Ca ²⁺ levels.....	76
4.4.1	General limitations of the Ca ²⁺ -imaging experiments	76
4.4.2	The effect of T _h 9 supernatant on neuronal Ca ²⁺ levels.....	78
4.4.3	The effect of CCL7, CCL11 and IL-9 on neuronal Ca ²⁺ levels	79
4.4.4	The enhancement of the glutamate-mediated increase of neuronal Ca ²⁺ levels by CCL7 and IL-9	80
4.5	The effect of CCL7, CCL11 and IL-9 on glutamate-mediated excitotoxicity.....	83
4.6	Detection of CCL7-, CCL11- and IL-9-mRNA in an EAE mouse model	83
5.	Summary	86
6.	Summary (native language of the faculty)	87
7.	Literature	88
8.	Declaration of Authorship	102
9.	Danksagung	103
10.	Curriculum Vitae	104

II. List of figures

Figure 1: IL-9-mRNA expression in a T _H 9 cell culture.	32
Figure 2: Effect of IL-9, CCL7 and Ccl11 on CCL7-mRNA expression in astrocytes.	35
Figure 3: Effect of IL-9, CCL7 and CCL11 on CCL11-mRNA expression in astrocytes.	36
Figure 4: Effect of IL-9, CCL7 and CCL11 on CCL7-mRNA expression in neurons DIV 12.	37
Figure 5: Effect of IL-9, CCL7 and CCL11 on CCL11-mRNA expression in neurons DIV 12.	38
Figure 6: Neuronal morphology and apoptosis after incubation with CCL7, CCL11 and IL-9.	41
Figure 7: Examples of neurons stained with the Ca ²⁺ fluorescent dye Fluo-4AM and their reaction to KCl and glutamate.	43
Figure 8: Effect of T _H 9 conditioned Locke's Buffer (LB-T _H 9) on Ca ²⁺ levels in neurons and its antagonization by the NMDA-receptor antagonist MK-801.	45
Figure 9: Ca ²⁺ levels in neurons (DIV 7 and 14) upon addition of CCL7, CCL11 and IL-9.	48
Figure 10: The effect of 50 nM CCL7 on glutamate-mediated Ca ²⁺ rise in neurons DIV 7.	50
Figure 11: The effect of 50 nM CCL7 on glutamate-mediated Ca ²⁺ rise in neurons DIV 14.	52
Figure 12: The effect of 5 nM CCL7 on glutamate-mediated Ca ²⁺ rise in neurons DIV 14.	54
Figure 13: The effect of 50 nM CCL11 on glutamate-mediated Ca ²⁺ rise in neurons DIV 7.	56
Figure 14: The effect of 5 nM IL-9 on glutamate-mediated Ca ²⁺ rise in neurons DIV 7.	58
Figure 15: The effect of 30 nM IL-9 preincubation on glutamate-mediated Ca ²⁺ rise in neurons DIV 14.	60
Figure 16: The effect of 5 nM IL-9 on glutamate-mediated Ca ²⁺ rise in neurons DIV 14.	62
Figure 17: The effect of CCL7 pretreatment on glutamate induced excitotoxicity in neurons.	66
Figure 18: mRNA expression of CCL7, CCL11 and IL-9 in spinal cords of EAE-mice....	69

III. List of tables

Table 1: Sequences of primers used in qPCR reactions	22
Table 2: Effect of IL-9, CCL7 and Ccl11 on CCL7-mRNA expression in astrocytes.....	35
Table 3: Effect of IL-9, CCL7 and CCL11 on CCL11-mRNA expression in astrocytes....	36
Table 4: Effect of IL-9, CCL7 and CCL11 on CCL7-mRNA expression in neurons DIV 12.....	38
Table 5: Effect of IL-9, CCL7 and CCL11 on CCL11-mRNA expression in neurons DIV 12.....	39
Table 6: The effect of CCL7 50 nM on glutamate mediated Ca ²⁺ rise in neurons DIV 7...	51
Table 7: The effect of CCL7 50 nM on glutamate mediated Ca ²⁺ rise in neurons DIV 14.	53
Table 8: The effect of CCL7 5 nM on glutamate mediated Ca ²⁺ rise in neurons DIV 14...	55
Table 9: The effect of CCL11 50 nM on glutamate mediated Ca ²⁺ rise in neurons DIV 7.	57
Table 10: The effect of IL-9 5 nM on glutamate mediated Ca ²⁺ rise in neurons DIV 7.. ...	59
Table 11: The effect of IL-9 30 nM on glutamate mediated Ca ²⁺ rise in neurons DIV 14.	61
Table 12: The effect of IL-9 5 nM on glutamate mediated Ca ²⁺ rise in neurons DIV 14. ..	63

IV. List of abbreviations

- Units of measurement

%	percent
°C	degree Celsius
d	days
h	hours
µg	microgram
µl	microliter
µm	micrometer
µM	micromolar
min	minute
ml	milliliter
mM	millimolar
nM	nanomolar
ng	nanogram
IE	Internationale Einheit = International Unit
s	seconds

- Abbreviations

AB	antibody
ACK	ammonium-chloride-potassium lysing
aDMSO	anhydrous dimethyl sulfoxide
APC	antigen presenting cell
AGM	astrocyte growth medium
AMPA	α-amino-3-hydroxy-5-methyl-4-isoxazolepropionic acid
AraC	cytosine β-D-arabinofuranoside

β_{III} -tubulin	neuronal class 3 beta-tubulin
BBB	blood brain barrier
BDNF	brain derived neurotrophic factor
BSA	bovine serum albumin
Ca^{2+}	calcium
$CaCl_2$	calcium chloride
cDNA	complementary deoxyribonucleic acid
CO_2	carbon dioxide
CCL	C-C motif chemokine ligand
CCR	C-C motif chemokine receptor
CD4	cluster of differentiation membrane protein 4
CNS	central nervous system
C_t	cycle threshold
DEPC	diethylpyrocarbonate
DIV	days in vitro
DMEM	Dulbecco's Modified Eagle Medium
DNA	deoxyribonucleic acid
DRG	dorsal root ganglion
E	embryonic
EAE	experimental autoimmune encephalomyelitis
EBSS	Earl's balanced salt solution
EDTA	ethylenediaminetetraacetic acid
FACS	fluorescence activated cell sorting
FasL	Fas ligand
FBS	fetal bovine serum
Fluo-4	Fluo-4 acetoxymethyl ester
GABA	γ -aminobutyric acid

GFAP	glial fibrillary acidic protein
GnRH	gonadotropin-releasing-hormone
GPCR	G-protein coupled receptor
H ₂ O	water
HEPES	4-(2-hydroxyethyl)-1-piperazineethanesulfonic acid
Ig	Immunoglobulin
ICAM	intercellular adhesion molecule
IFA	incomplete Freund's adjuvant
IFN	interferon
IL	interleukin
KCl	potassium chloride
KHCO ₃	potassium bicarbonate
KH ₂ PO ₄	potassium dihydrogen phosphate
LB or Locke's Buffer	magnesium-free Locke's Buffer
LB-T _h 9	magnesium-free Locke's Buffer in which T _h 9 cells had been incubated
LFA	lymphocyte function-associated antigen
MACS	magnetic activated cell sorting
MCP-3	monocyte-chemotactic protein 3
MEA	mast cell growth enhancing activity
MHC I/II	major histocompatibility complex class I/II proteins
mGluR	metabotropic glutamate receptors
MBP	myelin basic protein
MK-801	dizocilpine
MOG	myelin oligodendrocyte glycoprotein
MOG ₃₅₋₅₅	myelin oligodendrocyte glycoprotein peptide 35-55
mRNA	messenger ribonucleic acid

MS	multiple sclerosis
NaCl	sodium chloride
NaHCO ₃	sodium hydrogen carbonate
Na ₂ HPO ₄	di-sodium hydrogen phosphate
NaN ₃	sodium azide
NBQX	2,3-dihydroxy-6-nitro-7-sulfamoylbenzo (F) quinoxaline
NGM	neuronal growth medium
NMDA	N-methyl-D-aspartate
P	postnatal
PBS	phosphate buffered saline
PDL	poly-D-lysine
qPCR	quantitative real-time polymerase chain reaction
ROI	regions of interest
RNA	ribonucleic acid
rpm	rounds per minute
TBS	tris buffered saline
TCR	T cell receptor
TGF- β	transforming growth factor beta
T _h	T helper
T _h 9	T helper type 9
TNF- α	tumor necrosis factor alpha
VCAM-1	vascular cell adhesion molecul

1. Introduction

1.1 Immune cells and the central nervous system (CNS)

The central nervous system (CNS) and the immune system interact in many ways. On the one hand, neurons need to be protected from excessive inflammation and the subsequent damage to the neurons. On the other hand, the immune system protects the CNS from pathogens. This work aims at identifying damaging mechanisms of the immune system in the CNS.

1.1.1 T helper cells (T_h cells)

T cells or T lymphocytes are a subtype of lymphocytes. They mature within the thymus and play an important role in the adaptive immune system. T cells are characterized by their T cell receptor (TCR), which enables the recognition of antigens by T lymphocytes.

T lymphocytes are divided into subsets such as cytotoxic T cells, T helper cells (T_h cells) and others.

T_h cells express the cluster of differentiation membrane protein 4 (CD4) and interact with major histocompatibility complex class II proteins (MHC II)¹. MHC II is expressed by professional antigen presenting cells (APCs), namely macrophages, B-lymphocytes and dendritic cells. T_h cells can recognize antigens presented by these MHC II proteins and are then stimulated to divide, differentiate and exert their varying effector functions.

Originally, two subsets of T_h cells were discovered, namely T_h1 cells and T_h2 cells.

T_h1 cells play an important role in the immune response to intracellular pathogens by inducing macrophages to kill pathogenic agents, which persist inside the macrophages. In addition, T_h1 cells stimulate B cells to produce antibodies against extracellular pathogens. Likewise, T_h2 cells can stimulate B cells to produce immunoglobulin (Ig) E. One of their primary functions is the protection against parasitic infections².

The different subsets of T_h cells are characterized by their production of specific cytokines³. For example, T_h1 cells are defined by their production of interleukin-2 (IL-2) and interferon- γ (IFN- γ), T_h2 cells by their production of IL-4, IL-5 and IL-13, as well as IL-9 and IL-10^{3,4,5} (for a review see Vahedi et al.⁶). This dichotomy of T_h cells was expanded with the discovery of other types of T_h cells, such as T_h17 cells and T_h9 cells. Since T_h9 cells are of importance to this work, the following paragraph describes them in detail.

1.1.2 T helper type 9 (T_h9) cells and their signature cytokine Interleukin-9 (IL-9)

T_h9 cells are a subset of T_h cells, which has been recently identified^{7,8}. T_h9 cells can be generated from antigen-unexperienced CD4 positive T cells *in vitro*, by culturing in the presence of IL-4 and transforming growth factor beta (TGF- β)^{7,8}. They are characterized by the expression of high amounts of IL-9 and IL-10 and by the transcription factor PU.1⁹, with IL-9 being their signature cytokine. Since they do not co-express cytokines like IL-4 or IL-5, T_h9 cells are viewed as a distinct subset of T_h cells⁷.

IL-9 (also called P40 or mast cell growth enhancing activity(MEA)) was discovered much earlier than T_h9 cells^{10,11,12,13,14}. It is not only produced by T_h9 cells, but also by T_h2 cells⁴, T_h17 cells^{15,16}, mast cells¹⁷ and eosinophils¹⁸.

Physiologically, IL-9 has a variety of effects on different cell types, including the promotion of mast cell growth¹² and regulation of hematopoiesis¹⁹. IL-9 influences neuronal cells: During the development of the CNS, IL-9 and its receptor protect against neuronal, developmental apoptosis²⁰. It also helps in the process of differentiation of T_h17 cells and increases the suppressive effect of regulatory T cells²¹, as well as enhances the IL-4 induced production of Ig by B-lymphocytes²². In addition, IL-9 was found to decrease the activity of pathogenic T_h17 cells in autoimmune gastritis²³ and protect against intestinal parasites such as *Trichuris muris*²⁴. Taken together, IL-9 has many beneficial, physiological functions in protective immune responses, but in addition, contributes to detrimental self-directed immunity:

T_h9 cells were shown to play a significant role in a mouse model disease of allergic asthma. In this model, their pathophysiological effect is primarily mediated by IL-9 and neutralization of IL-9 ameliorates the course of the disease²⁵. In line with this, the IL-9 gene was linked to allergic asthma in humans²⁶. Additionally, myelin oligodendrocyte glycoprotein (MOG)-specific T_h9 cells induce experimental autoimmune encephalomyelitis (EAE), an animal model for multiple sclerosis (MS) upon adoptive transfer in mice²⁷.

1.1.3 The immune privilege of the central nervous system (CNS)

The interaction between immune cells and neurons is carefully balanced between being able to protect the CNS from pathogens and preventing inflammatory damage. Since neurons are limited in their regeneration, the brain needs to be protected from excessive immune processes. The reduced immune activity of the brain compared to other organs of the body is termed *immune privilege* (for a review see Galea et al.²⁸). The immune privilege results mostly from a reduced afference of immunity, a term that indicates that antigen presentation within the CNS is delayed or inhibited. There are several mechanisms contributing to this reduced immunity in the brain, some of which are explained here:

1. The brain parenchyma is separated from the blood by the blood brain barrier (BBB). Under non-inflammatory conditions, naive T_h cells cannot pass this barrier. Immunohistochemistry of the human brain showed, that basically no T-lymphocytes are in the CNS under physiological conditions²⁹. Activated T cells however, can penetrate the BBB³⁰, regardless of their antigen specificity³¹. However, only activated T-lymphocytes with a CNS antigen specificity stay in the CNS or reenter it. The retention of T-lymphocytes within the CNS is thus antigen dependent, while the entering of the CNS is not³¹. Different cell types such as astrocytes can influence this migration of T-lymphocytes into the CNS³². Migration of lymphocytes across the BBB is controlled by a range of distinct chemokines, integrins and cytokines^{33,34}.
2. Few neuronal cells in the CNS have constitutive expression of MHC I and II. Originally, it was thought that MHC I is in fact not constitutively expressed in

neurons at all³⁵, but can be induced by for example axotomy³⁶ or exposure to cytokines³⁷. Later studies revealed that MHC I is expressed constitutively by neuronal subsets such as hippocampal pyramidal neurons³⁸. Subsequent studies revealed that in addition to its immune function, MHC I directly interacts with CNS resident cells. For example, it plays an important role in synaptic plasticity³⁹. Although the brain is lacking typical APCs, MHC II is expressed by microglia⁴⁰ as well as astrocytes⁴¹.

3. Once inside the CNS, encephalitogenic T cell activity is inhibited by e.g. neurons⁴² or astrocytes⁴³. Neurons were shown to be able to induce differentiation of encephalitogenic T cells into regulatory T cells and thus suppress EAE⁴². Astrocytes were shown to inhibit the proliferation and inflammatory cytokine production of encephalitogenic T cells during the early phases of CNS-directed immune responses. During prolonged inflammation however, astrocytes have the potential to exaggerate inflammation⁴³.

1.1.4 Interactions of T helper cells (T_h cells) and neurons

Activated T_h cells can have a major influence on neuronal cells. Activated T_h cells secrete a diversity of cytokines. IFN- γ , which is produced by T_h1 cells amongst others, induces neuronal apoptosis mediated via the ionotropic glutamate receptors alpha-amino-3-hydroxy-5-methyl-4-isoxazolepropionic acid (AMPA) and kainate receptors. Consequently, IFN- γ enhances neuronal excitotoxicity mediated by AMPA receptors⁴⁴.

Excitotoxicity is a damaging process in the nervous system. An excessive amount of extracellular glutamate leading to an activation of glutamate receptors is followed by a large intracellular calcium (Ca²⁺) rise. This in turn, triggers intracellular pathways, which result in the destruction of the neuron⁴⁵. Excitotoxicity plays a major role in a variety of diseases, for example stroke⁴⁶.

Cytokines in general can serve as attractants to other immunological cell types and can disrupt the BBB, thereby facilitating the entry of further inflammatory cells into the CNS⁴⁷, which in turn influence neurons in various ways.

It was also discovered that T_h cells can make direct cell to cell contact with neurons and induce cell death. This cell death can be mediated by the Fas ligand (FasL), lymphocyte function-associated antigen 1 (LFA-1) and CD40. It is independent of MHC interaction and selectively damages neuronal cells⁴⁸. Cell death can also be mediated by an increase in intracellular Ca²⁺. This damage can be inhibited by AMPA and N-methyl-D-aspartate (NMDA) receptor antagonists⁴⁹. Additionally, stimulation of the AMPA/kainate receptor leads to enhanced expression of MHC I in neurons⁵⁰ and would thus be able to increase the susceptibility to damage induced by cytotoxic T cells, which recognize antigens presented by MHC I.

T_h cells also have beneficial functions on neurons. T_h1 cells and T_h2 cells produce brain derived neurotrophic factor (BDNF) upon antigen stimulation, which supports neuronal survival *in vitro*⁵¹. Autoimmune T cells specific for myelin basic protein (MBP) have been shown to protect neurons of the CNS from secondary degeneration⁵² and pro-inflammatory T_h1-conditioned cells have been shown to increase the recovery after spinal cord injury in rats⁵³.

Taken together, T_h cells have a diversity of effects on neuronal cells, which can be beneficial or detrimental. Intracellular neuronal Ca²⁺ levels play a pivotal role in some of these processes.

1.1.5 Chemokines: signal mediators between the immune and the nervous system

Chemokines are a family of secreted proteins with chemotactic functions. Their name is a combination of the terms “chemotaxis” and “cytokine”. Chemokines are divided into four families, depending on the first two NH₂-terminal cysteines of their protein structure. In the family of the C-X-C chemokines, these cysteines are separated by an amino acid, in the family of the C-C chemokines, these cysteines are next to each other. Two smaller families include the C family and the C-X-X-X-C family. Chemokines bind to G-protein coupled receptors (GPCR) and lead to transient Ca²⁺ rises in their effector cells. Ten receptors for

C-C chemokines have been identified, namely C-C chemokine receptor (CCR) 1-10 (for a review see Rollins⁵⁴).

Chemokines serve as attractors and activators of leukocytes in physiological and inflammatory conditions. Other functions include angiogenesis and hematopoiesis (for a review see Rollins⁵⁴). They have been linked to various inflammatory diseases such as EAE⁵⁵ and MS⁵⁶.

Additionally, novel non-immune functions of chemokines were reported. Various chemokine receptors are expressed on neurons and astrocytes, notably CCR2⁵⁷. This receptor is constitutively expressed, thus having functions independent of neuroinflammation, for example playing a role in neurotransmission⁵⁸. Physiological roles, such as the release of glutamate from astrocytes upon CXCR4 activation in neuromodulation, has been linked to neurotoxicity, when paired with activated microglia⁵⁹. Hence, the role of chemokines is no longer confined to the chemotaxis of leukocytes, but include complex physiological and pathophysiological functions in the CNS, often independent of immune cells.

The following paragraphs explain two C-C chemokines, namely C-C motif chemokine ligand (CCL) 7 and 11 in more detail, since these two were investigated in this thesis. They were selected, firstly because previous results from our lab showed, they were discovered to be upregulated in a neuron culture co-cultivated with T_h9 cells (S. Ray, K. Forsberg, F. Bischof, unpublished results). Secondly, the gene locus for C-C chemokines has already been associated with MS⁶⁰, making CCL7 and CCL11 possibly relevant for the damaging mechanisms of T_h9 cells *in vivo*.

1.1.5.1 The C-C motif chemokine ligand 7 (CCL7)

The C-C motif chemokine ligand 7 (CCL7, also called monocyte-chemotactic protein 3, MCP-3) was first discovered in 1992⁶¹ and is produced by a variety of cells including monocytes⁶¹, smooth muscle cells⁶² and astrocytes⁶³. Tumor necrosis factor alpha (TNF- α) stimulates the CCL7 production in astrocytes⁶³.

One of the main functions of CCL7 is chemotaxis. It attracts a broad spectrum of cells such as monocytes⁶¹, CD4+ and CD8+ T-lymphocytes⁶⁴ and dendritic cells⁶⁵. CCL7 also causes the release of enzymes in its effector cells. It induces the release of arachidonic acid in monocytes⁶⁶ and granzyme A and N-acetyl- β -D-glucosaminidase in dendritic cells and CD8+ T-lymphocytes⁶⁷.

The effect of CCL7 on non-immune cells has not yet been extensively investigated. CCL7 was shown to be produced by a gonadotropin-releasing-hormone (GnRH) producing neuronal cell line and to chemotactically attract astrocytes⁶⁸. Expression of CCL7 is induced by TNF- α in cortical neurons⁶⁹. One recently emerged function of CCL7 is its role in CNS development: CCL7 increases the axonal outgrowth during neuronal morphogenesis⁷⁰ and it was linked to dopamine neuron development as well as promoting neuritogenesis⁷¹.

Finally, CCL7 has been associated with several diseases: CCL7 expression was detected in MS lesions⁵⁶ and atopy⁷².

1.1.5.2 The C-C motif chemokine ligand 11 (CCL11)

The C-C motif chemokine ligand 11 (CCL11, also called eotaxin-1) was first described in an *in vivo* model of allergic inflammation⁷³. It is produced by endothelial cells and epithelial cells upon stimulation with TNF- α , IL-1 α and IFN- γ , as well as by eosinophils cultured in the presence of IL-3⁷⁴. CCL11 was also detected in lymphocytes, macrophages⁷⁵ and in dermal fibroblasts, where it is constitutively expressed. The expression in fibroblasts is upregulated by IL-1 α and TNF- α ⁷⁶.

In contrast to CCL7, CCL11 serves as a chemoattractant for a smaller spectrum of cells: CCL11 selectively attracts eosinophils, but not neutrophils^{73,75}, lymphocytes⁷⁵, dendritic cells⁷⁷ or mononuclear cells⁷⁴. Later studies also revealed a chemoattractant role of CCL11 for basophils⁷⁸.

CCL11 mainly effects immune cells. It activates the respiratory burst in eosinophils⁷⁹. In basophils, CCL11 induces the release of histamine and leukotriene C₄⁷⁸. Additionally,

CCL11 was shown to upregulate the expression of intercellular adhesion molecule 1 (ICAM-1) and vascular cell adhesion molecule 1 (VCAM-1) in endothelial cells⁸⁰.

As a proinflammatory chemokine, CCL11 has been associated with many inflammatory diseases: In asthma, it was shown to contribute to the recruitment of eosinophils to the site of inflammation⁸¹. It was also associated with allergic rhinitis and non-allergic sinusitis⁸², as well as ulcerative colitis, Crohn's disease⁷⁴ and atopic myelitis⁸³.

Although constitutive expression of CCL11 in the brain was not observed⁷⁴, newer studies revealed the influence of CCL11 in the CNS. CCL11 binds to oligodendrocyte precursor cells, thereby being linked to the process of myelination⁸⁴. Additionally, CCL11 plasma levels have been associated with ageing and reduced neurogenesis⁸⁵.

Furthermore, CCL11 was shown to be secreted by activated astrocytes. These astrocytes thus stimulated microglia, thereby promoting neuronal excitotoxicity⁸⁶. Finally, a recent study showed that CCL11 expression has protective, modulatory functions in an EAE model in rats. Here, CCL11 was mainly produced by neurons in the brain and could be detected in the cerebrospinal fluid⁸⁷.

All in all, recent publications point towards novel roles of chemokines, which were classically seen as purely chemoattractant. A variety of non-immune cells exhibit receptors for these molecules and their effect on these cells is under investigation.

1.2 T helper cell mediated neuroinflammatory diseases

Some neuroinflammatory diseases are viewed as being primarily mediated by T_h cells. Two of these are introduced below.

1.2.1 Multiple sclerosis (MS)

MS is a neuroinflammatory, demyelinating disease of the CNS, mediated through immunological processes. Immune cells attack the myelin sheath and lead to the formation of inflammatory lesions in the brain and spinal cord. These lesions can emerge at any

location inside the CNS and impair the neuronal functions, finally resulting in neurodegeneration and scar formation (sclerosis). The cause for MS is still unknown and a multifactorial genesis is assumed. Hereby, hereditary, environmental and autoimmune mechanisms play a central role in the development of MS⁸⁸.

Depending on the location of the inflammatory lesions, a variety of clinical symptoms can occur. The most common symptoms include muscular weakness, tingling sensations, ataxia and visual impairment⁸⁸.

The clinical course of the disease is often characterized by attacks of symptoms with some recovery in between, sometimes followed by a secondary progressive course of the disease⁸⁸.

During the past 15 years, a range of drugs have been approved that allow the efficient suppression of inflammatory disease activity and accumulation of neurological deficits (Robinson et al. show some examples⁸⁹).

1.2.2 Experimental autoimmune encephalomyelitis (EAE) as a T_h cell mediated neuroinflammatory disease and the role of excitotoxicity in EAE

EAE is a neuroinflammatory, demyelinating disease of the CNS. It can be induced in animals such as rats or mice and shares a lot of clinical and pathological elements with MS. Thus, it is considered as an animal model for this disease. The main early clinical symptom is a progressive ascending paralysis of the muscles.

EAE needs to be induced either actively or passively:

1. In the active induction, mice are immunized with CNS-specific antigens, like MOG, and pertussis toxin⁹⁰. Myelin-specific T-lymphocytes are activated and cross the BBB, made permeable by pertussis toxin. The myelin-specific T-lymphocytes are reactivated in the CNS and cause inflammation, demyelination and axonal damage.
2. In the passive induction, myelin-specific T-lymphocytes are isolated from mice already actively induced with EAE. The T-lymphocytes are restimulated *in vitro* and transferred into mice, which had not been immunized yet⁹¹. This adoptive

transfer of T_h cells indicates that EAE is a T_h cell mediated disease. Ben-Nun et al.⁹² were the first to show that MBP-specific T-lymphocytes could passively induce EAE. The passive induction of EAE has been demonstrated for a number of different T_h cells, including T_h1 cell⁹³, T_h17 cell⁹⁴, as well as T_h9 cells²⁷. Each of these inductions lead to a distinct phenotype.

The ability to passively induce EAE indicates, that T_h cells play a crucial role in the pathogenesis of EAE. Both the role of T_h1 cells and T_h17 cells has been elucidated to some extent. Experiments suggest that the disease is mainly caused by T_h17 cells and T_h1 cells. T_h1 cells facilitate the entry of T_h17 cells into the CNS, which in turn damage the CNS⁹⁵.

Different cytokines produced by T_h cells or cytokines effecting T_h cells, have been shown to increase the severity of EAE symptoms. IL-23 is critical for the development of EAE. IL-23 deficient mice are resistant to EAE⁹⁶. Neutralization of IL-9 using monoclonal antibodies led to a decrease in EAE severity by inhibition of the generation of MOG-specific T_h cells^{15,97}. Both IL-23⁹⁴ and IL-9²¹ effect T_h17 cells by promoting the generation of these cells. Through this, T_h17 cells are considered as one of the main contributors in EAE pathophysiology.

Although it is assumed that EAE is a demyelinating disease, axonal and neuronal damage seem to play a central part in EAE as well as in MS pathology⁹⁸. Excitotoxicity has been shown to be one reason for this neuronal damage. The AMPA receptor antagonist 2,3-dihydroxy-6-nitro-7-sulfamoylbenzo (F) quinoxaline (NBQX)⁹⁹ ameliorates the EAE disease, thereby affecting the tissue inflammation, but functioning solely by inhibiting excitotoxicity^{100,101}. Siffrin et al.¹⁰² showed that T_h17 cells directly contact neurons by forming immune synapses and induce fluctuations of intracellular Ca²⁺ in neurons, as well as neuronal cell death in an antigen independent way. These Ca²⁺ fluctuations were partly reversible by blocking the NMDA receptor¹⁰², thereby linking excitotoxicity with T_h17 cells.

The study of EAE has revealed many fundamental mechanisms of neuroinflammation in general and MS in particular. Many MS therapies are based on the EAE model such as the

α 4-integrin antibody (AB) *Natalizumab*¹⁰³. However, there are differences between MS and EAE and this model has certain limitations (for a review see Gold et al.¹⁰⁴). In line with this, some therapies which were shown to be efficient in EAE¹⁰⁵ failed to show beneficial effects in MS patients¹⁰⁶.

1.3 Aim of this work

Previous experiments in our lab (S. Ray, K. Forsberg, F. Bischof, unpublished results) on primary mouse cell cultures showed that T_h9 cells lead to neuronal deterioration, both when only co-culturing T_h9 cells and neurons and when exposing neurons to T_h9 cell supernatant. This damage could be ameliorated by pre-treating the neurons with the glutamate receptor antagonists dizocilpine (MK-801), which is an antagonist for NMDA receptors, and NBQX, which is an antagonist for AMPA receptors. A whole genome analysis was performed on neurons exposed to T_h9-supernatant and revealed an upregulation of several genes, including the chemokines CCL7 and CCL11.

This work aims at elucidating the role of the two chemokines CCL7 and CCL11, as well as of the cytokine IL-9, in this damaging process.

Firstly, the gene regulation of these cytokines was analysed in neurons and astrocytes. Secondly, the damaging potential of each cytokine in neurons was investigated and the influence of these cytokines on neuronal Ca²⁺ levels was examined. Thereby the direct effect of each cytokine on neurons was observed, as well as the sensitization of neurons to glutamate-mediated Ca²⁺ rise by these cytokines. Thirdly, the influence on glutamate-mediated excitotoxicity was analysed. All of these experiments intend to determine, whether these cytokines can damage neurons either directly or by enhancing excitotoxicity.

Finally, we tried to detect CCL7, CCL11 and IL-9 in an EAE mouse model. These experiments intend to explore a novel role for CCL7, CCL11 and IL-9 in neuronal damage and link them to neuroinflammation *in vivo*.

2. Materials and Methods

2.1 Animals

For the primary cell cultures female mice of the C57BL/6N strain were used. All experiments were conducted in accordance with the German ‘Law on Protecting Animals’ (§ 4/03 Tierschutzgesetz) as well as the regulations set by the Universitätsklinikum Tübingen (“Mitteilung nach §4 vom 04.06.2014”). Pregnant mice, necessary for neuronal und astrocyte cultures, were determined by plug check or ordered at a specific gestational age.

2.2 Generation of defined cell cultures for the identification of neuronal toxicity of T helper type 9 cells

2.2.1 Buffer Preparation

Several buffers were prepared in the laboratory. The protocols for these are listed below.

- Phosphate buffered saline (PBS), pH to 7.4:
 - 137 mM Sodium chloride (NaCl, *Merck*, #1.06404.1000)
 - 2.7 mM Potassium chloride (KCl, *Merck*, #1049360250)
 - 10 mM di-Sodium hydrogen phosphate (Na₂HPO₄, *Merck*, #1065860500)
 - 1 mM Potassium dihydrogen phosphate (KH₂PO₄, *Merck*, #1048730250) all in water (H₂O)
- Tris buffered saline (TBS), pH to 7,5:
 - 50 mM TRIS-hydrochlorid (*ROTH*, #9090.3)
 - 150 mM NaCl all in H₂O
- Magnetic activated cell sorting (MACS) buffer, stored at 2-8 °C:
 - 0,5 % Bovine serum albumin (BSA, *Sigma-Aldrich*, #A7906-100g)
 - 2 mM Ethylenediaminetetraacetic acid (EDTA, *Merck*, #1084181000) all in PBS

- Magnesium-free Locke's Buffer (Locke's Buffer or LB), stored at 2-8 °C, pH to 7.4:
 - 154 mM NaCl
 - 5.6 mM KCl (*Merck, #1049360250*)
 - 3.6 mM Sodium hydrogen carbonate (NaHCO₃, *ROTH, #8551.1*)
 - 1.3 mM Calcium chloride (CaCl₂, *ROTH, #1023780500*)
 - 5.6 mM alpha-D(+)-Glucose-Monohydrat (*ROTH, #6780.1*)
 - 5 mM 4-(2-hydroxyethyl)-1-piperazineethanesulfonic acid (HEPES, *ROTH, #9105.2*) all in H₂O
- Fluorescence activated cell sorting (FACS) buffer, stored at 2-8 °C:
 - 2 % Fetal bovine serum (FBS, *Sigma-Aldrich, #12003C*)
 - 2 mM EDTA
 - 0,02 % Sodium azide (NaN₃, *ROTH, #K305.1*) all in PBS
- Ammonium-chloride-potassium lysing (ACK) buffer, pH to 7,3:
 - 150 mM Ammonium chloride (NH₄Cl, *ROTH, #5470.1*)
 - 10 mM Potassium bicarbonate (KHCO₃, *ROTH, #P748.1*)
 - 0,1 mM EDTA all in H₂O

2.2.2 Generation of defined T helper type 9 cell cultures

2.2.2.1 Preparing of T helper type 9 cell cultures

For preparation, 96-well flat bottom plates (*Greiner Bio One, #655161*) were coated with 2 µg/ml anti-mouse CD3 (*Biolegend, #100314*) and 2 µg/ml anti-mouse CD28 (*Biolegend, #102112*) in PBS and left at 4 °C in the fridge overnight. Before usage, the plates were washed with PBS once and then dried shortly.

8-16 week-old female mice were killed using carbon dioxide (CO₂). The abdomen was then cut open and the spleen was removed. For one culture, approximately ten spleens were taken, washed with PBS and pushed through a 40 µm cell strainer (*Corning Life Sciences, #352340*) using a plunger (*BD, #309646*), all the time rinsing the cells with PBS.

Subsequently, the cell suspension was centrifuged at 1400 rounds per minute (rpm) for

5 min at 4 °C in a *Heraeus Multifuge 35-R (Thermo Scientific)* and the supernatant was discarded. The cells were suspended in 5 ml of ACK buffer and incubated for up to one minute.

Next, the solution was centrifuged again at 1400 rpm for 5 min at room temperature. The supernatant was discarded and the cells suspended in 10 ml of PBS. This step was repeated once more. Finally, the cells were suspended in PBS and counted under a microscope (*Nikon Eclipse TS100, Nikon*), first diluting it 1:1 with Trypan blue (*Sigma Aldrich, #T8154-100ML*) to sort out dead cells.

Magnetic activated cell sorting (MACS) of CD4 positive (CD4+) cells was performed using CD4 (L3T4) MicroBeads (*Miltenyi Biotec, #130-049-201*) and LS Columns (*Miltenyi Biotec, #130-042-401*) following the instructions of *Miltenyi Biotec*.

After the separation, the cells were counted again and dissolved in T cell-growth medium consisting of ~94 % Iscove's Modified Dulbecco's Medium (*Life Technologies, #11960-044*), 5 % heat inactivated FBS (*Life Technologies, #10500-064*), 1 % Penicillin-Streptomycin (*Life Technologies, #15140-122*), 50 nM 2-Mercaptoethanol (*Life Technologies, #31350-010*) at a concentration of one million cells per ml. For the CD4+ cells to differentiate into T_H9 cells, recombinant murine IL-4 (*Tebu, #214-14*) and recombinant murine TGF-β (*eBioscience, #14-8342-62*) were added at a concentration of 10 ng/ml and 1 ng/ml respectively. The cells were then plated at 350*10³ cells per well onto the coated 96-well flat bottom plates already prepared and subsequently incubated at 37 °C and 5 % CO₂.

In the following steps, the cells were always counted under the microscope using Trypan blue and then centrifuged at 1400 rpm for 5 min at room temperature. Between steps, the cells were put in the incubator at 37 °C and 5 % CO₂.

Three days (d) after the first stimulation, the cells were collected, counted and centrifuged. The supernatant was carefully removed and kept for later use. The cells were then suspended at a concentration of 1 million cells per ml in resting medium, consisting of growth medium and the differentiation medium collected earlier at a ratio of 1:1. Next,

5 IE/ml recombinant human IL-2 (*Miltenyi*, #130-097-743) was added. The cells were seeded on uncoated 24-well flat bottom plates (*Greiner Bio-One*, #662160) at 2×10^6 cells per well and kept in the incubator. They were monitored daily. In case of a change in pH, indicated by the color indicator of the medium, the cells were recollected and reseeded again at 2×10^6 cells per well.

After another five to seven days, the cells were collected again, spun down, counted and suspended in growth medium at a concentration of 1 million cells per ml. As in the first stimulation, IL-4 and TGF- β were added in the concentrations mentioned above. Cells were seeded on 96-well flat bottom plates coated with 2 μ g/ml anti-mouse CD3 and 2 μ g/ml anti-mouse CD28 again and put in the incubator.

Finally, the cells were ready to be used for experiments three days after the second stimulation.

2.2.2.2 Control of T helper type 9 cell cultures

T_h9 cultures were analyzed twice for their purity, once after magnetic separation and a second time directly before use in further experiments. FACS was used for analysis after MACS. The final analysis was performed with quantitative real-time polymerase chain reaction (qPCR, see 2.3). After MACS, the cells were controlled for CD4 positivity by flow cytometry. In addition, the purity of T_h9 cell cultures was determined by flow cytometry after intracellular staining for the T_h9 signature cytokine IL-9.

Before and after magnetic separation, about $2 \times 200 \times 10^3$ cells were set aside in 96-well round bottom plates (*Greiner Bio-One*, #650 101) and then stained for CD4: The cells were centrifuged at 1400 rpm for 5 min at 4 °C. This setting was used for all subsequent centrifugation steps. The supernatant was discarded and the cells were suspended in 25 μ l Fc-Block (1:1000 CD16/32, *BD Biosciences*, #553141). They were incubated at 4 °C for 5 min. Without washing, 20 μ l of FACS buffer was added in each of the four wells. Anti-mouse CD4-FITC (*BD Biosciences*, #561835) 1:100 in 5 μ l of FACS buffer was added to

the cells set aside before and after the MACS. In the remaining two wells, another 5 µl of FACS buffer was added. The cells were now incubated for 20 min at 4 °C.

The cells were then centrifuged, the supernatant was discarded and the cells were suspended in 150 µl of FACS buffer. This step was repeated twice. The solution was finally transferred into tubes and stored protected from light until the analysis with CyAnADP FACS (*Beckman Coulter*) and Summit software (*DakoCytomation*).

First, gates were set for forward and side scatter to sort out dead cells. Unstained cells were used to adjust PMT voltages and then the single stainings were run. Usually, the yield of CD4⁺ cells after MACS was above 90 %. If the yield was below 90 %, the culturing was not continued.

The final control for T_h9 cell yield is usually done using flow cytometry, which allows exact distinctions between T_h9 cells and other types of T_h cells for each single cell. In our experiments, the T_h9 cell yield was assessed by qPCR (see 3.1.1 and 4.1.1).

Here, total ribonucleic acid (RNA) was isolated and compared for their IL-9 expression. An older T_h9 cell culture, which had been analyzed by FACS and had consisted of 90 % T_h9 cells, served as a reference. The method of RNA isolation and qPCR is described in 2.3.

2.2.3 Generation of defined neuronal cultures from embryonic day 16 (E16)

mouse pups

One day prior to the preparation of the culture, plates were coated with Poly-D-Lysine (PDL, *Sigma Aldrich*, #P6407), at a concentration of 50 µg/ml in H₂O and incubated overnight at 37 °C and 5 % CO₂. Afterwards, plates were washed once with sterile H₂O and dried subsequently. For Ca²⁺-imaging, coverslips (*VWR*®, #631-0169) treated with UV-radiation were put in wells of a 48-well flat bottom plate (*Greiner Bio-One*, #677 180) coated as above.

For the pure neuronal culture, 16 d old embryos (E16) were dissected. Pregnant mice from the C57BL/6N strain were killed using CO₂. The abdomen was cut open using sterile

scissors. The embryos were removed from the amniotic sac and placed in Earl's Balanced Salt Solution (EBSS, *Sigma Aldrich*, #E2888).

Mouse cortices were dissected following the protocol from Beaudoin et al¹⁰⁷. In contrast to the protocol, the hippocampi were not removed. The cortices and hippocampi were then dissociated using a Papain Dissociation Kit (*Worthington Biochemical Corporation*, #LK003150) according to the protocol supplied therein. The cells were counted and placed in neuronal growth medium (NGM) consisting of Neurobasal[®] Medium (*Life Technologies*, #21103-049) containing 2 % of B-27 Supplement (*Life Technologies*, #17504-044), 1 % Penicillin-Streptomycin and 2 mM L-Glutamine (*Life Technologies*, #25030-024). Then, the cells were seeded on 96-well-F-bottom plates at a density of 40×10^3 cells per well for immunostainings, on 48-well-F-bottom plates with coverslips at a density of 120×10^3 cells per well for Ca²⁺-imaging and on 6-well-F-bottom plates (*Greiner Bio-One*, #657 160) at a density of 1×10^6 cells per well for RNA extraction.

The cells were cultured for approximately two weeks in the incubator at 37 °C and 5 % CO₂. After two days of culturing, E16 neurons were treated with 2 μM cytosine β-D-arabinofuranoside (*AraC*, *Sigma-Aldrich*, #C1768) to prevent the growth of glial cells. The AraC medium was removed completely on days *in vitro* 4 (DIV 4) and fresh NGM was placed in the wells. Some cultures were not treated with AraC. If a culture was not treated with AraC, non-AraC is mentioned next to the age of the neurons.

One third of the medium was changed twice a week. At DIV 7 and DIV 14 immunostainings for astrocyte contamination were made (see 2.5.2), and neurons were used for experiments from DIV 7 onwards.

2.2.4 Generation of defined astrocytic-neuronal mixed cultures from postnatal day 0 (P0) mouse pups

Mixed cultures were made from newborn P0 pups of the C57BL/6N strain. P0 mouse pups were used on the same day they were born (postnatal day 0; P0). Following quick decapitation of the newborn mice, the rest of the procedure was as described in the

generation of E16 pure neuronal cultures (see 2.2.3). As the survival rate of the neurons in cultures from neurons of postnatal mouse pups is lower compared to embryonic neurons, the initial seeding density was adjusted to 1.5×10^6 cells per well on 6-well plates, 240×10^3 cells per well on 48-well plates and 80×10^3 cells per well on 96-well plates. Cells were cultured at 37 °C and 5 % CO₂.

In contrast to E16 cultures, P0 cultures were not treated with AraC on DIV 2 in order to not inhibit the astrocyte growth. The subsequent medium change was identical to the change described in 2.2.3. Mixed cultures were used for experiments on DIV 7 and DIV 10.

Mixed cultures were controlled for the growth of microglia by immunocytochemistry (see 2.5.2) on DIV 7.

2.2.5 Generation of defined pure astrocytic cultures from P2 mouse pups

For pure astrocyte cultures, P2 mouse pups were used. The procedure was the same as in astrocytic-neuronal mixed culture described in 2.2.4. Pure astrocyte cultures were placed in astrocyte growth medium (AGM) consisting of 10 % FBS and 1 % Penicillin-Streptomycin in high glucose Dulbecco's Modified Eagle Medium (DMEM, *Life Technologies*, #11965-92) in a PDL-coated 175cm² cell culture flask (*Corning Life Sciences*, #431466) at a density of 1.25×10^6 cells in 50 ml AGM.

When the cells reached confluence after approximately one week of culturing, cells were shaken at 180 rpm for 30 min in a Certomat M0II (*Braun Biotech Int*) at 37 °C to remove microglia. Afterwards, the medium containing the now detached microglia was removed, and fresh AGM was put into the flask. The shaking was then continued for another 6 h at 240 rpm in the Certomat M0II at 37 °C to remove oligodendrocyte precursor cells. Subsequently, the flask was shaken vigorously by hand for 1 min. The medium was removed completely and the flask rinsed with PBS. The PBS was removed.

Next, 0.25 % trypsin-EDTA (*ThermoFisher Scientific*, #25200072) was added to detach the astrocytes for 3-5 min at 37 °C and 5 % CO₂. Finally, the flask was hit manually to improve the detachment and controlled for detachment of all cells under the microscope. Detached

astrocytes were collected by rinsing the flask with AGM, putting the AGM now containing the astrocytes into a 50 ml tube (*Cellstar Greiner, #227261*) and spinning it down at 750 rpm for 5 min at 20 °C. The cells were suspended in fresh medium and put on fresh PDL coated flasks again at a density of $1.25 \cdot 10^6$ cells in 50 ml AGM.

The astrocytes were monitored until they reached confluence again. They were then detached with 0.25 % trypsin-EDTA as before (see above) and put on PDL-coated plates at a density of $25 \cdot 10^3$ cells per well for 96-well plates, $60 \cdot 10^3$ cells per well for 48-well plates or $350 \cdot 10^3$ cells per well for 6-well plates. One to two days after this procedure, the cells were ready to be used for experiments. If cultivation for prolonged periods was warranted, the astrocytes were put in coated flasks again at the mentioned density. If necessary, this cycle was repeated when the cells reached confluence again.

Astrocyte culture medium was changed once a week during all these steps, by replacing half of the medium. Control stainings for microglia contamination were made each time a culture was used for experiments (see 2.5.2).

2.3 Gene expression analysis by quantitative real-time polymerase chain reaction (qPCR)

2.3.1 Treatment of cell cultures with cytokines and glutamate for gene expression analysis

For gene expression analysis, neuronal and mixed cultures were taken at DIV 7 or DIV 14. Recombinant murine IL-9 (*Peptotech, #219-19*) at a concentration of 5 nM or 30 nM, recombinant mouse CCL11 (*BioLegend, #582902*) at a concentration of 10 nM or 50 nM, or recombinant mouse CCL7 (*BioLegend, #586102*) at a concentration of 10 nM or 50 nM were diluted in warm NGM, the volume being one third of the volume contained in one well. The same amount of medium was then carefully removed from one well and the cytokine dilution carefully added alongside the wall of the well. In control samples, the medium was changed without adding cytokines. Cell cultures in 6-well flat bottom plates

were used. After 24h, messenger ribonucleic acid (mRNA) was extracted as described below.

2.3.2 RNA extraction

RNA was extracted from pure neuronal, pure astrocytic and mixed cultures, as well as spinal cord tissue samples using peqGOLD Trifast (*peqlab*, #30-2010), following the manufacturer's protocol. For homogenization of tissue samples, the tissue was pulled several times through 21G and 27G needles (*Becton Dickinson*, #304432 and #302200). Heating was performed using a PTC-2000 Peltier Thermal Cycler (*MJ Research*). The other reagents, not supplied with the Trifast, were chloroform (*MERCK*, #1.02445.0250), isopropanol (*MERCK*, #109634,2511), ethanol and diethylpyrocarbonate (DEPC) treated water, which was supplied with a DNase I, Amplification Grade kit (*Life Technologies*, #18068-015). Each was used according to the manufacturer's instructions. In order to prevent RNA degradation, all steps were performed with RNase free equipment including safe seal filter-tips 10 µl, 100 µl and 1000 µl (*Biozym*, #770010, #770100, #770400 respectively). The samples were transferred to RNase-free 200 µl tubes (*Biozym*, #711030) with caps (*Biozym*, #621816) after redissolving the RNA. Previously, Eppendorf cups (*Eppendorf AG*, #D159102R) were used.

Having finished the extraction and re-dissolved the RNA in 10 µl of DEPC-water, the concentration of the extracted RNA using the Peqlab ND1000 Spectrophotometer (*PeqLab*) was measured.

The RNA was stored at -80 °C until usage.

2.3.3 Reverse transcription into complementary deoxyribonucleic acid (DNA)

First, deoxyribonucleic acid (DNA) was degraded using DNase I, Amplification Grade (*Life Technologies*, #18068-015). All steps were performed following the manufacturer's protocol. Next, mRNA was reverse transcribed to generate cDNA using SuperScript II Reverse Transcriptase (*Life Technologies*, #18064-022), again following the manufacturer's

instructions. Other reagents used were Oligo-dT₁₂₋₁₈ Primer (*Life Technologies, #18418-020*), dNTP Mix (*Life Technologies, #R0192*) and Ribolock RNase Inhibitor (*Thermo Scientific, #E00381*). The heater and the centrifuge were the same as in 2.3.2 . All steps were performed using RNase and DNase free equipment.

cDNA was stored at -20°C until usage.

2.3.4 Quantitative real-time polymerase chain reaction (qPCR)

qPCR was used to analyze gene expression of defined samples. Therefore, mRNA was extracted from the samples to be analyzed as described above. In general, each sample was pipetted in triplicates to account for and rule out inaccuracy of pipetting and sample variation. Additionally, one negative control was run, which did not contain any sample in order to exclude contamination of primers, SYBR green or water.

For qPCR, Micro Amp fast optical 96-well Reaction plates (*Life technologies, #4346906*) were used. Each well was filled with 10 µl of SYBR green Absolute QPCR Mix (*Life Technologies, #AB-1322/B*), 0.5 µl of 10 µM Forward and 0.5 µl of 10 µM Reverse Primer and 8 µl of DEPC-water. Primer Sequences used are listed in Table 1. The Primers were dissolved in DEPC-water to obtain a concentration of 100 µM. Working dilutions were further diluted to a final concentration of 10 µM.

These reagents were mixed directly prior to addition to the plate. Finally, 5 µl of sample, diluted 1:25 with water from the original cDNA, was added to each well. The plate was then covered with optically clear adhesive seal sheets (*Thermo Scientific, #AB-1170*) and centrifuged at 1000 rpm for 20 min at 4 °C, all the time taking care not to soil the bottom of the plate. Plates were measured using *Applied Biosciences 7500 Fast Real-Time PCR System*. One run consisted of 15 min at 95 °C, followed by 40 cycles, each composed of 15 s at 95 °C and 1 min at 60 °C.

Table 1: Sequences of primers used in qPCR reactions

Gene	Direction	Sequence
β-Actin	<i>Forward</i>	CCACCATGTACCCAGGCATT
	<i>Reverse</i>	CGGACTCATCGTACTCCTGC
IL-9	<i>Forward</i>	CACATGGGGCATCAGAGACA
	<i>Reverse</i>	AGAGACACAAGCAGCTGGTC
CCL7	<i>Forward</i>	ACCAGTAGTCGGTGTCCCTG
	<i>Reverse</i>	AGGCTTTGGAGTTGGGGTTT
CCL11	<i>Forward</i>	GCTCACGGTCACTTCCTTCA
	<i>Reverse</i>	AGGGTGCATCTGTTGTTGGT

2.3.5 Analysis of measured qPCR files

Results were analyzed using Microsoft Excel with the $\Delta\Delta C_t$ -method¹⁰⁸. β -Actin was used as the reference gene. Statistical analysis was performed using statistical tools provided by Microsoft Excel. Standard deviations were calculated based on the technical replicates, if no biological replicates were present. Otherwise, biological replicates were used for the calculation. A two-tailed paired student's t-test was performed to assess statistical significance with $p < 0.05$ being significant. Again, biological replicates were tested. If none were present, technical replicates were used.

2.4 Ca²⁺-imaging of neurons

2.4.1 Treatment of cells with cytokines

Two different approaches were used: First, the direct effect of cytokines and T_h9 cell secreted factors on neuronal Ca²⁺ levels was determined, which did not require any pretreatment of the cells. The second approach can show a sensitization to glutamate-mediated Ca²⁺ influx in neurons. Neuronal cells were treated with cytokines two days prior to the imaging experiments as in 2.3.1.

2.4.2 Conditioning of Magnesium free Locke's buffer (LB) with T_h9 cells

In order to see the reaction of neurons to the secreted molecules of T_h9 cells in Ca²⁺-imaging, these molecules needed to be secreted in LB. Normal T cell growth medium contained glutamate and was thus not suitable for the imaging experiment. LB in contrast does not excite the neurons by itself. T_h9 cells were spun down at 1200 rpm at room temperature, counted and suspended in LB at 5 million cells/ml. This step was repeated twice to wash off all of the T cell growth medium. The T_h9 cells were then kept in the LB for 30 min at 37 °C and 5 % CO₂. Finally, the cells were spun down again and the supernatant was carefully removed without any cells. The LB conditioned with T_h9 cells (LB-T_h9) was now ready to be used for Ca²⁺-imaging experiments or be kept at -80 °C until use.

2.4.3 Staining of neurons with a fluorescent Ca²⁺-dye

For preparation, Fluo-4 acetoxymethyl ester (Fluo-4 AM, *Life Technologies*, #F-14201) was dissolved in anhydrous dimethyl sulfoxide (aDMSO, *Sigma Aldrich*, #276855) in order to gain a concentration of 2 mM for storage, which was further diluted 1:1000 to a 2 μM working dilution on the day of usage. This dilution was kept at room temperature and protected from light. It was used for all samples measured that day. Fluo-4 AM is a cell permeable fluorescent dye. It can increase its light emission upon binding to Ca²⁺.

Cover slips containing neurons were carefully removed with forceps and put in a 24-well flat bottom plate filled with LB, taking care to put the side containing the neurons on top. The buffer was removed and 200 μl of 2 μM Fluo-4 AM were added. The cells were incubated for 20 min at room temperature protected from light. The well was subsequently washed 4 times with LB with the last 2 washes lasting 3 min and transferred to 200 μl of LB. The cells were incubated again for 25 min at room temperature and protected from light, ready to use for Ca²⁺-imaging. If neurons were to be pretreated with glutamate antagonists, the NMDA-receptor antagonist MK-801 (*Sigma Aldrich*, #M107) was added to the LB for the last 25 min of the incubation at a concentration of 10 μM.

2.4.4 Microscopy of stained neurons

The principles of microscopy of both approaches are identical.

The microscope used was an Axio Observer.Z1 microscope with an AxioCam HRc camera, a HXP 120 Illuminator, an EC Plan-Neofluar 10x/0.3 Ph1 objective and the AxioVision 4.8 software at 10x magnification. The fluorescent dye Fluo-4 AM was excited with 488 nM and the wavelength of the emission measured was 516 nM.

The plate was fitted in the microscope frame tightly in order to fixate it. An area of cells, which contained a moderate cell density and few to no astrocytes, was focused to evaluate the Ca^{2+} levels in single cells and to minimize overlapping cell bodies and neurites. The exposure time was adjusted for the cells to be just bright enough to see the neuronal cell bodies. If the exposure time was set too high, further increase of brightness upon glutamate challenge would not be detectable. The usual exposure time was set between 500 ms and 1 s. It was kept the same during samples, which were going to be compared in the analysis. One picture series was taken for 12 to 30 min, depending on whether we wanted to see an early or a late reaction to the additions. Pictures were taken every 2 s automatically.

For the first approach, LB- $\text{T}_\text{H}9$ or the cytokines CCL7, CCL11 and IL-9 were added in varying concentrations between 5 nM and 100 nM after 3 min, taking care not to shift the plate as this would make an analysis of the cellular Ca^{2+} levels impossible. They were added in 100 μl dropwise. 60 mM KCl was added as a positive control in 300 μl 8 min after starting the picture series. The increase in extracellular K^+ by KCl leads to a depolarization of the neuronal membrane and opens voltage gated Ca^{2+} channels, ultimately leading to Ca^{2+} influx. Even if the neurons would not react to the cytokines, their general ability to generate action potentials could be shown through their reaction to KCl. Also, the functionality of the Ca^{2+} indicator could be shown. Neurons, which were already dead or died during the experiment, were thus sorted out. The cells not reacting to KCl were not considered in the later analysis.

In the second approach, glutamate (*Sigma-Aldrich*, #G8415-100g) was added instead of the cytokines. The concentrations were 0.5 μM , 1 μM and 10 μM . These concentrations just led

to a slight increase in Ca^{2+} levels (0.5 μM) or led to a big increase in Ca^{2+} levels but did not saturate the dye (10 μM). Tests for the most suitable glutamate concentration have been conducted prior to the other experiments. The reaction to glutamate served as the positive control. The cells not reacting to glutamate were eliminated from later analysis.

Each approach sometimes contained addition of the glutamate antagonist MK-801 at later time points in a volume of 100 μl . KCl was then scaled up accordingly to 400 μl . Time points used for this addition were usually 5 or 6 min.

During subsequent measurements, the fluorescence of the Ca^{2+} dye decreased, resulting in a decrease in fluorescence intensity of the neurons before and after the glutamate addition. To account for this decrease in fluorescence, the control sample was always measured right before its corresponding treated sample. This prevents the decrease of dye fluorescence from interference with the results. An increase in Ca^{2+} influx thus cannot be attributed to higher fluorescence of Fluo-4 AM at earlier time points.

2.4.5 Analysis of Ca^{2+} -imaging series

Ca^{2+} -imaging series were analyzed using *ImageJ V1.48*. First, the background was subtracted, using a *Rolling Ball Radius* set at 100 pixels (*Process* \rightarrow *Subtract Background*). Next, regions of interest (ROI) of all neurons were selected. This was done automatically by duplicating an image of the series through *Image* \rightarrow *Duplicate* first and selecting the image required. Mostly an image directly after glutamate or KCl addition was used, since only the cells reacting to these stimuli were relevant to our analysis. By the selection of this image, cells not reacting to this positive control could be excluded directly. Another reason for choosing this image is, that some cells were detected sufficiently only after this stimulation.

Subsequently, the threshold was adjusted by *Image* \rightarrow *Adjust* \rightarrow *Threshold* to have all neurons visible but not converging into another. Next, converged neurons were divided by *Process* \rightarrow *Binary* \rightarrow *Convert to mask* and *Process* \rightarrow *Binary* \rightarrow *Watershed*. Finally, the images were analyzed through *Analyze* \rightarrow *Analyze Particles* excluding cells on edges and marking

Add to manager. ROIs not corresponding to a neuron and ROIs containing several cells at once were manually excluded. All ROIs were now in the manager and could be selected and used to analyze the mean grey values of every single cell in the image. Additionally, the total number of cells was determined this way.

In the final step, ROIs were selected and the mean grey values of the ROIs of the full imaging series were analyzed through *Analyze* → *Analyze Particles*. The results were now in an Excel sheet and could be further evaluated.

2.4.6 Statistical Analysis

Two approaches were applied:

1. The “absolute difference” as the difference of the mean intensity value relative to the baseline of a treated sample and the corresponding control sample.
2. The “relative difference” at the time point 300 s as the mean intensity value relative to the baseline of the treated sample relative to its corresponding control.

In the calculation for the absolute difference, for every single cell the mean baseline was determined by calculating the average of the grey values of the first 3 min of the measurement. This baseline was set as 100 %. All the following grey values were calculated as percent of the baseline by dividing the grey value by the baseline value and multiplying the result with 100 %. Next, the averages out of this percentage of all cells of a single time point and the standard deviation were calculated. These final values were plotted on a timeline. Values, which showed an increase in fluorescence intensity of less than 50 % of the baseline (values < 150 %) upon glutamate or KCl addition, were excluded from the analysis.

Furthermore, the average of samples, which were treated equally, was determined by calculating the average out of every value at corresponding time points of each single sample. Standard deviations were calculated by using the Gaussian propagation of error law.

In the calculation of the relative difference, values of the time point at 300 s of the control sample were set as 100 %. The corresponding treated sample is shown relative to this control sample: The values of the treated samples were divided by the control and the result was multiplied by 100 %. These results are called the *change in percent of the control value at its peak* and presented in the tables in 3.4.4.

2.5 Immunocytochemistry, microscopy and analysis of defined neuronal, astrocyte or mixed cultures

2.5.1 Treatment of cells

The immunocytochemistry was performed using two different approaches.

In the first approach, the effect of the cytokines CCL7, CCL11 and IL-9 on neurons was to be identified. CCL7, CCL11 and IL-9 were added to neuronal cell cultures in 96-well flat bottom plates at a concentration of 5 nM, 30 nM, 50 nM, 100 nM, 500 nM or 1 μ M (see 2.3.1). The cell damage was analyzed by immunostaining after 24h.

In the second approach, the influence of CCL7, CCL11 and IL-9 on glutamate-mediated excitotoxicity in neurons was to be detected. As in the first approach, neurons in 96-well flat bottom plates were treated with cytokines for 3 h to 2 d (see 2.3.1) at the concentrations mentioned above. Subsequently, the cells were treated with glutamate at a concentration of 0.5 μ M or 10 μ M to cause excitotoxic neuronal deterioration. 0.5 μ M of glutamate just slightly damaged neurons, 10 μ M of glutamate caused severe neuronal deterioration. Accordingly, enhancement or reduction of glutamate mediated excitotoxicity could be analyzed. The glutamate was added in neuronal growth of one third of the total volume of one well. After various time points ranging from 6 h to 2 d, cells were fixed and stained.

Additionally, the glutamate addition of this second approach was conducted in another variation in order to remove factors previously secreted by the neurons: Glutamate was diluted in LB instead of neuronal growth medium. The growth medium from one well was completely removed and kept for later use. The glutamate dilution was added quickly to

ensure that the cells would not be left dry for too long. The cells were then incubated for 5 min, 10 min or 30 min and subsequently washed with fresh growth medium twice, again taking care to not let the cells dry out between removing and adding the fresh growth medium. At last, the cells were placed in their own growth medium again.

2.5.2 Immunostaining

All the following steps were conducted at room temperature. The growth medium was carefully removed from one well at a time, taking care not to damage the neuronal cell layer at the bottom of the well. The wells were quickly and gently rinsed with PBS and the PBS was removed again. Next, the cells were fixed with 4 % Paraformaldehyde (*MERCK*, #1040051000) in PBS for 15 min. The cells were washed with PBS for 5 min and subsequently permeabilized with 0.3 % Triton X-100 (*Sigma-Aldrich*, #X100) in PBS for 5 min. In order to block non-specific binding of the ABs, which were added in the following steps, the cells were put in 8 % BSA (*Sigma-Aldrich*, #A7906-100g) in TBS for 1 h. All ABs were diluted in 2 % BSA/ 0.3 % Tx100 in TBS overnight at 4 °C. The primary ABs used next depended on the type of cells stained:

- Astrocytic cell cultures were stained with anti-glia fibrillary acidic protein (anti-GFAP, rabbit polyclonal) (*Millipore*, #AB5804), diluted at a ratio of 1:1000 and rat anti-mouse CD11b (*AbD Serotec*, #MCA711GT), diluted at a ratio of 1:400, for the evaluation of microglia contamination.
- Neuronal cell cultures were stained with neuronal class 3 beta-tubulin (β_{III} -tubulin, TUJ1) mouse monoclonal AB purified (*Covance*, #MMS-435P-250), diluted at a ratio of 1:2000, cleaved caspase 3 (D175) rabbit AB (*Cell Signaling Technology*, #9661S), diluted at a ratio of 1:400, and anti-GFAP, rabbit polyclonal, for the evaluation of astrocyte contamination.

Following this incubation, the cells were washed with 0.1 % Tween® 20 (*ROTH*, #9127,1) in TBS three times for 6 min each. Afterwards, the secondary fluorescent ABs were added, each depending on the primary AB:

- Goat anti-rabbit IgG (H+L) secondary AB, Alexa Fluor® 568 conjugate (*Life Technologies, #A-11011*),
- Goat anti-mouse IgG (H+L) secondary AB, Alexa Fluor® 488 conjugate (*Life Technologies, #A-11029*)
- Goat anti-rat IgG (H+L) secondary AB, Alexa Fluor® 568 conjugate (*Life Technologies, #A-11077*).

ABs were diluted 1:2000 in 2 % BSA/ 0.3 % Tx100 in TBS. Due to the light sensitivity of the secondary ABs, all consecutive steps were conducted protected from light. The plates were incubated for 1 h at room temperature and subsequently washed with TBS/ 0.1 % Tween for 6 min each. Eventually, the nuclei were stained with 1 µg/ml Hoechst 33342 (*Life Technologies, #H3570*) in TBS for 1 min, rinsed once with PBS and kept in PBS from here on at 4 °C until further use.

2.5.3 Microscopy of immunostained samples

Stained cells were observed with an Axiovert 200M microscope equipped with an AxioCam MRm camera at 10x magnification using AxioVision 4.8 software (*Zeiss*). The excitation wavelength depended on the stainings used. 358 nM was used for the Hoechst staining, 490 nM for the Alexa Fluor® 488 conjugate and 578 nM for the Alexa Fluor® 568 conjugate. The emission of light was 461 nM for the Hoechst staining, 525 nM for the Alexa Fluor® 488 conjugate and 603 nM for the Alexa Fluor® 568 conjugate.

The cells were observed under the microscope. Samples were eliminated based on signs of contamination of the cells or signs of excessive neuronal damage, which could not be contributed to the previous treatment of the cells. The samples of different treatment conditions were compared and an overview of each sample was established.

In a second step, five images per sample were taken blindly at set positions of the well: one each in the middle, on the right, at the top, on the left and at the bottom.

2.5.4 Analysis of immunostained samples

Samples were analyzed for the general appearance of the neurites and cell bodies, thereby comparing different treatment groups in a descriptive way. The total number of nuclei present was determined as described in 2.4.5.

Cells positive for cleaved caspase 3 or CD11b were counted manually using the *ImageJ cell counter* plugin and calculated as percent of the total number of nuclei using the statistical tools provided by Microsoft Excel. Averages and the standard deviation of the five images taken for each sample were calculated.

In general, only the samples of the same cell culture and age could be compared as the neurons of different cultures and different ages would often differ from one another.

2.6 Detection of CCL7, CCL11 and IL-9 in an experimental autoimmune encephalomyelitis (EAE) mouse model

2.6.1 Induction of EAE

For the induction of EAE in one mouse, an emulsion of 60 µg myelin oligodendrocyte glycoprotein peptide 35-55 (MOG₃₅₋₅₅), dissolved in 100 µg PBS (*PAA Laboratories, Pasching, Austria*) and 100 µl incomplete Freund's adjuvant (IFA) (*Sigma-Aldrich, Steinheim, Germany*) containing 400 µg *Mycobacterium tuberculosis* (*Difco Laboratories, Detroit, MI, USA*) was prepared using a syringe.

10-week-old female C57BL/6N mice were injected subcutaneously with the emulsion in several areas around the back using a 1 ml syringe (*Braun, #4600177*) and a 27G needle. On the day of the immunization as well as two days after, 200 ng *Bordetella pertussis* toxin (*MERCK, Darmstadt, Germany*) was injected subcutaneously. Four mice were immunized in total and dissected. Another four control mice were not treated but only dissected.

The mice were monitored daily and scored according to the score described in Miller et al¹⁰⁹. At a score of one ("limp tail or hind limb weakness but not both"), the mice were sacrificed.

2.6.2 Dissection of the spinal cord

Mice were euthanized using CO₂. The skin as well as all the abdominal and thoracic organs and muscles were removed completely in order to reach the spine. The carcass was pinned onto styrofoam and the mouse was decapitated using scissors. From the cranial opening of the spine downwards, each vertebral arc was clipped on both sides using small scissors. The corpus vertebrae was removed to expose the spinal cord. When reaching the conus medullaris, the spinal cord was carefully removed, whilst severing the spinal nerves. The cord was frozen using liquid nitrogen and stored at -80 °C.

2.6.3 RNA extraction, reverse transcription and qPCR

These steps were conducted as already described in 2.3.

3. Results

Based on previous results from this laboratory, which revealed neuronal damage, when neurons were co-cultured with T_h9 cells (S. Ray, K. Forsberg, F. Bischof, unpublished results), the following experiments were designed. Further results revealed an upregulation of CCL7 and CCL11 in this co-culture. Here, we analyzed the neuron-damaging capacity of CCL7, CCL11 and IL-9.

3.1 Analysis of the generation of defined cell cultures

Cell cultures were assessed by flow cytometry and qPCR in the case of T_h9 cell cultures and by immunocytochemistry in the case of neuronal and astrocyte cultures, in order to identify possible contaminations of the cultures and the purity of the cells.

3.1.1 Analysis of the generation of defined T helper type 9 cell cultures

T_h9 cell cultures were analyzed for their yield of T_h9 cells by qPCR. After magnetic separation, cells were analyzed for their yield of CD4⁺-cells. Thus, it could be determined whether the culturing and differentiation of the T_h9 cells could be continued.

In addition, the final cell analysis, after the differentiation of the T_h9 cells, was carried out using qPCR. An old T_h9 cell culture containing over 80 % T_h9 cells (analyzed by FACS) was used as a reference. IL-9-mRNA was used as the parameter for T_h9 cell yield.

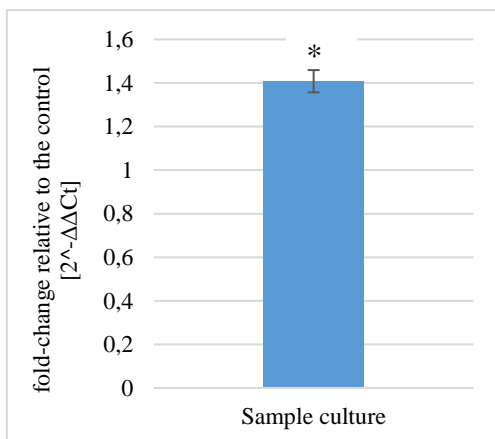


Figure 1: IL-9-mRNA expression in a T_h9 cell culture. cDNA gained from these cells was used for a qPCR for the target *IL-9* in technical triplicates. Averages of these triplicates are shown as the fold-change of the sample culture compared to a reference culture ($\Delta\Delta C_t$ -method). Error bars represent the positive and negative errors derived from the standard deviation. **** $p < 0.001$, ** $p < 0.01$, * $p < 0.05$, n.s.=non-significant, determined by student's t-test.

The quantity of IL-9 mRNA was comparable to the reference culture (Figure 1), with a fold-change of 1.4. The significance of the fold-change shows the accuracy of the measurement. This implies a high percentage of IL-9 producing cells, T_h9 cells being the biggest producer of this protein. However, contamination with other cell types cannot be ruled out (see 4.1.1).

3.1.2 Analysis of the generation of defined neuronal cultures from E16 mouse embryos

Pure neuronal cultures were analyzed for their grade of contamination with astrocytes. This analysis was performed by immunocytochemistry for GFAP, a signature molecule for astrocytes. Three cultures treated with AraC and three cultures were not treated with AraC were analyzed.

The percentage of astrocytes in the total number of cells present was below 1 % in cultures treated with AraC and below 20 % in cultures not treated with AraC.

3.1.3 Analysis of the generation of defined astrocyte cultures from P0 and P2 mouse pups

Neuronal and astrocytic mixed cultures, as well as pure astrocyte cultures, were stained for microglia by immunocytochemistry for CD11b to ensure their purity. Two cultures were analyzed.

The percentage of microglia in the total number of cells present was below 5 %.

3.2 Identification of the effect of cytokine exposure (CCL7, CCL11, IL-9) on cytokine mRNA expression of defined cells

Parallel to the following experiments, gene expression of neuronal and astrocyte cultures was analyzed. Here, the regulation of the studied cytokines by the studied cytokines themselves was determined. Neuronal and astrocyte cultures were exposed to the cytokines in question, namely CCL7, CCL11 and IL-9. Previous work has shown that CCL7-mRNA

in astrocytes is upregulated by exposure of astrocytes to T_H9 cells (S. Ray, K. Forsberg, F. Bischof, unpublished results). The following experiment was performed in order to determine whether IL-9, as the T_H9 cell signature cytokine, is responsible for this upregulation. Additionally, it could determine cross regulation between the cytokines CCL7, CCL11 and IL-9 in astrocytes.

3.2.1 The effect of cytokines on cytokine gene expression in mouse astrocytes

Analysis of qPCR results targeting CCL7 in astrocytes treated with different cytokines (Figure 2) shows that CCL7-mRNA is upregulated 1.5 – 4.5-fold by 5 nM and 30 nM IL-9. The fold-changes vary in between samples, however CCL7-mRNA is consistently upregulated by IL-9. This indicates that despite the variance of results, IL-9 has an upregulating effect on CCL7 gene expression in astrocytes. CCL7 and CCL11 did not alter CCL7-mRNA expression in astrocytes significantly. In Table 2, the average cycle threshold (C_t) -values of the same samples are listed. High C_t-values indicate low mRNA expression. With around 28, these values show that the mRNA expression of CCL7 is moderate to low in astrocytes.

A similar analysis of CCL11-mRNA expression in astrocytes (Figure 3) demonstrates a non-significant effect of CCL7, CCL11 or IL-9 on CCL11-mRNA expression.

C_t-values in the CCL11 target group were higher than in the CCL7 group (33.5 vs 29 in control samples respectively, see Table 3 and Table 2 respectively) demonstrating a low expression of CCL11-mRNA in astrocytes. Additionally, this very low expression of CCL11-mRNA leads to inaccurate measurements, as seen in the large error bars of the IL-9 treated sample (Figure 3).

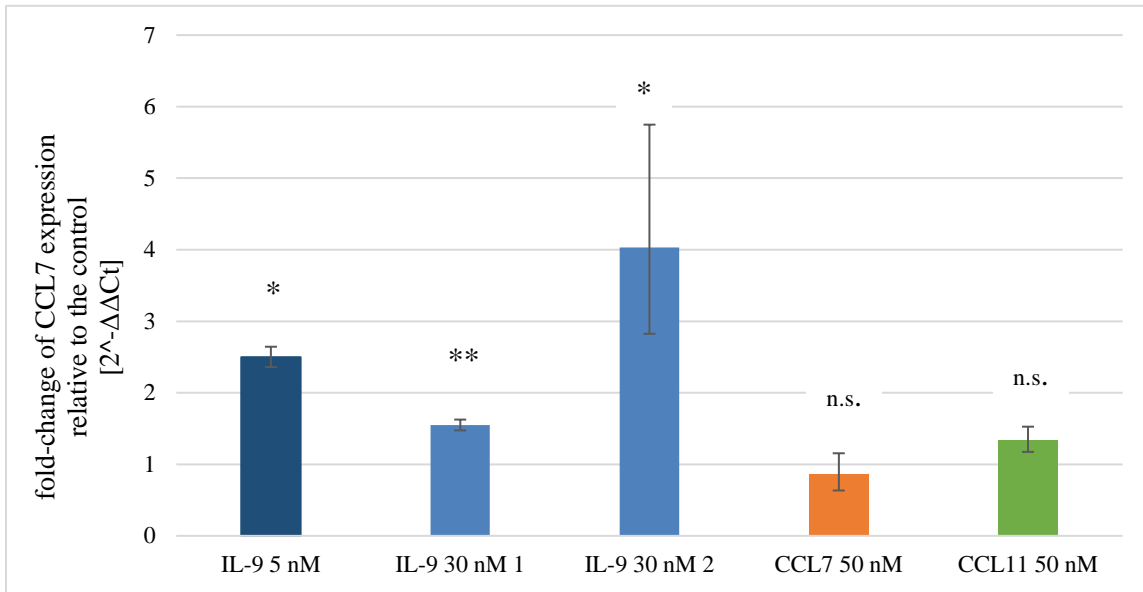


Figure 2: Effect of IL-9, CCL7 and CCL11 on CCL7-mRNA expression in astrocytes. Astrocytes were exposed to cytokines for 24 h at the concentrations indicated. Subsequently, cDNA gained from these cells was used for a qPCR for the target *CCL7* in technical triplicates. Averages of these triplicates are shown as the fold-change of treated samples versus control samples normalized to actin ($\Delta\Delta C_t$ -method). N=1 for CCL7 and CCL11 treated samples, N=1 for 5 nM IL-9, N=2 for 30 nM IL-9, all samples are shown. Error bars represent the positive and negative errors derived from the standard deviation. *** $p < 0.001$, ** $p < 0.01$, * $p < 0.05$, n.s.=non-significant, determined by student's t-test.

Table 2: Effect of IL-9, CCL7 and CCL11 on CCL7-mRNA expression in astrocytes. Astrocytes were exposed to cytokines for 24 h at the concentrations indicated. Subsequently, cDNA gained from these cells was used for a qPCR for the target *CCL7* in technical triplicates. Averages of the C_t -values of the technical replicates of all samples are shown.

Sample	C_t -Value
Control	28,92578761
IL-9 5 nM	28,67501
IL-9 30 nM 1	29,6910629
IL-9 30 nM 2	28,0316639
CCL7 50 nM	28,1976242
CCL11 50 nM	28,2468643

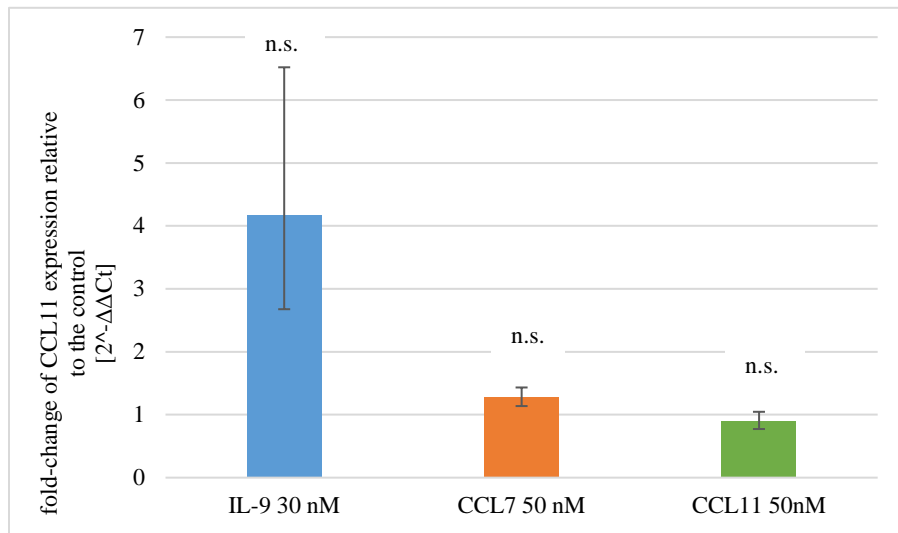


Figure 3: Effect of IL-9, CCL7 and CCL11 on CCL11-mRNA expression in astrocytes. Astrocytes were exposed to cytokines for 24 h at the concentrations indicated. Subsequently, cDNA gained from these cells was used for a qPCR for the target *CCL11* in technical triplicates. Averages of these triplicates are shown as the fold-change of treated samples versus control samples normalized to actin ($\Delta\Delta C_t$ -method). N=1, all samples are shown. Error bars represent the positive and negative errors derived from the standard deviation. *** p<0.001, ** p<0.01, * p<0.05, n.s.=non-significant, determined by student's t-test.

Table 3: Effect of IL-9, CCL7 and CCL11 on CCL11-mRNA expression in astrocytes. Astrocytes were exposed to cytokines for 24 h at the concentrations indicated. Subsequently, cDNA gained from these cells was used for a qPCR for the target *CCL11* in technical triplicates. Averages of the C_t -values of the technical replicates of the samples are shown.

Sample	C_t -Value
Control	33,2500089
IL-9 30 nM	32,4406617
CCL7 50 nM	32,0818977
CCL11 50 nM	33,2824796

3.2.2 The effect of defined cytokines on cytokine gene expression in mouse neurons

Previous work has shown that CCL11-mRNA in neurons is upregulated by exposure of neurons to T_h9 cells (S. Ray, K. Forsberg, F. Bischof, unpublished results). The following experiment was performed in order to determine whether IL-9, as the T_h9 cell signature cytokine, is responsible for this upregulation. Additionally, cross regulation between the cytokines CCL7, CCL11 and IL-9 in neurons was determined.

Quantitative PCR analysis of CCL7-mRNA expression in neurons (Figure 4) revealed that IL-9, CCL7 and CCL11 downregulate CCL7-mRNA. The C_t-values are around 31 (Table 4). As in 3.2.1, this indicates a very low expression of CCL7-mRNA in neurons.

The CCL11-mRNA expression in neurons (Figure 5) was not significantly altered by CCL7, CCL11 or IL-9.

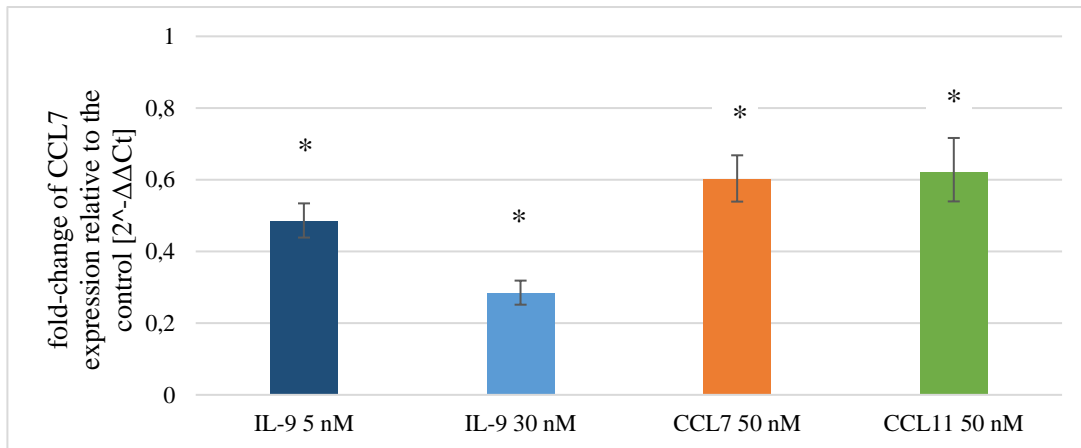


Figure 4: Effect of IL-9, CCL7 and CCL11 on CCL7-mRNA expression in neurons DIV 12. Neurons were exposed to cytokines for 24 h at the concentrations indicated. Subsequently, cDNA gained from these cells was used for a qPCR for the target *CCL7* in technical triplicates. Averages of these triplicates are shown as the fold-change of treated samples versus control samples normalized to actin ($\Delta\Delta C_t$ -method). N=1, all samples are shown. Error bars represent the positive and negative errors derived from the standard deviation. *** p<0.01, * p<0,05, n.s.=non-significant, determined by student's t-test.

Table 4: Effect of IL-9, CCL7 and CCL11 on CCL7-mRNA expression in neurons DIV 12. Neurons were exposed to cytokines for 24 h at the concentrations indicated. Subsequently, cDNA gained from these cells was used for a qPCR for the target *CCL7* in technical triplicates. Averages of the C_t -values of the technical replicates of the samples are shown.

Sample	C_t -Value
Control	31,12078094
IL-9 5 nM	31,410553
IL-9 30 nM	31,1217321
CCL7 50 nM	30,7899526
CCL11 50 nM	31,3494212

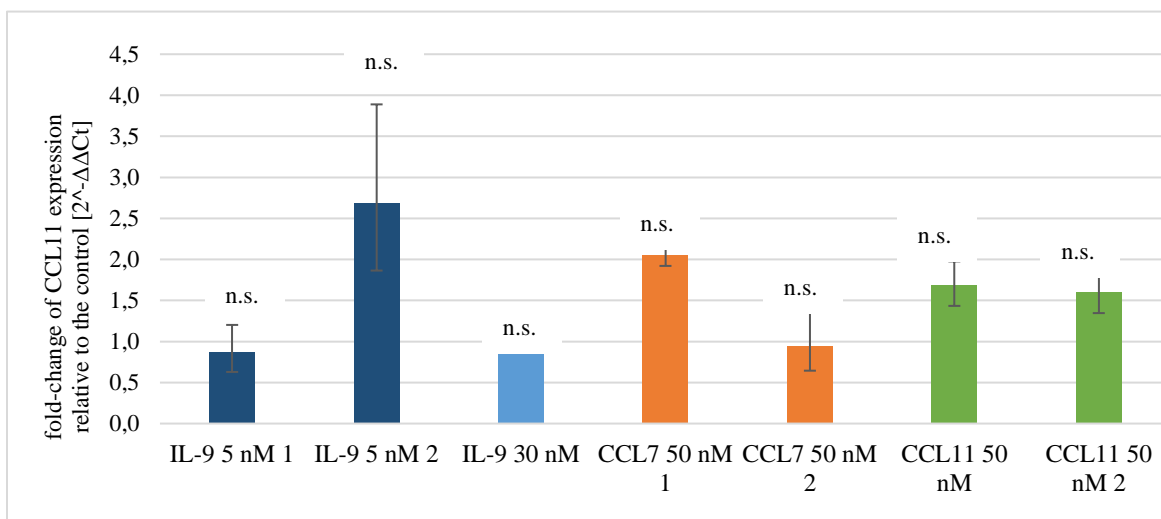


Figure 5: Effect of IL-9, CCL7 and CCL11 on CCL11-mRNA expression in neurons DIV 12. Neurons were exposed to cytokines for 24 h at the concentrations indicated. Subsequently, cDNA gained from these cells was used for a qPCR for the target *CCL11* in technical triplicates. Averages of these triplicates are shown as the fold-change of treated samples versus control samples normalized to actin ($\Delta\Delta C_t$ -method). N=2, all samples are shown. Error bars represent the positive and negative errors derived from the standard deviation. *** $p < 0.001$, ** $p < 0.01$, * $p < 0.05$, n.s.=non-significant, determined by student's t-test.

Table 5: Effect of IL-9, CCL7 and CCL11 on CCL11-mRNA expression in neurons DIV 12. Neurons were exposed to cytokines for 24 h at the concentrations indicated. Subsequently, cDNA gained from these cells was used for a qPCR for the target *CCL11* in technical triplicates. Averages of the C_t -values of technical replicates of the samples are shown.

Sample	C_t-Value
Control	28,8649089
IL-9 5 nM 1	27,7887707
IL-9 5 nM 2	31,8713633
IL-9 30 nM 1	27,5251509
CCL7 50 nM 1	26,7588266
CCL7 50 nM 2	32,4702212
CCL11 50 nM 1	27,6568375
CCL11 50 nM 2	31,2757654

The C_t -values (Table 5) range from 26 to 32 in different neuronal cultures, as indicated by the numbering of the samples. This points to a moderate to low expression of CCL11-mRNA in neurons.

In summary, CCL7-mRNA is upregulated in astrocytes by IL-9. IL-9, CCL7 and CCL11 downregulate CCL7-mRNA in neurons. None of the other treatments revealed a consistent effect on CCL7- or CCL11-mRNA in neurons or astrocytes. Finally, CCL7-mRNA is mainly expressed in astrocytes (see 3.2.1), all other samples revealed lower expression levels in astrocytes and neurons on average (see 3.2.1 and 4.2).

3.3 The effect of CCL7, CCL11 and IL-9 preincubation on E16 mouse neurons

In a first step in identifying the damaging potential of CCL7, CCL11 and IL-9, neurons were exposed to these cytokines and then stained for their DNA, cytoskeleton and cleaved caspase 3 (Figure 6). As a correlation of neuronal damage, two parameters were analyzed: neuronal morphology in form of cytoskeletal deterioration and neuronal apoptosis as

indicated by expression of cleaved caspase 3. For each condition five pictures were taken. A small part of one picture is presented in the figure to ensure a better visualization of neurites and nuclei on a single cell level.

There were no differences between the treated and the control samples with respect to the cellular morphology (Figure 6 a, β_{III} -tubulin staining). Particularly the neurites were well preserved in all conditions. Samples treated with other concentrations of the mentioned cytokines (5 nM, 50 nM and 500 nM CCL7 and CCL11, 5 nM and 30 nM IL-9, samples not shown) did not show any damage induced by CCL7, CCL11 or IL-9.

The cleaved caspase 3 positivity was very low, with almost no cells positive (see Figure 6). This is in line with the morphological analysis, which showed no neuronal deterioration.

Taken together, the neurons appeared very healthy in all conditions, indicating that the studied cytokines do not directly damage neurons.

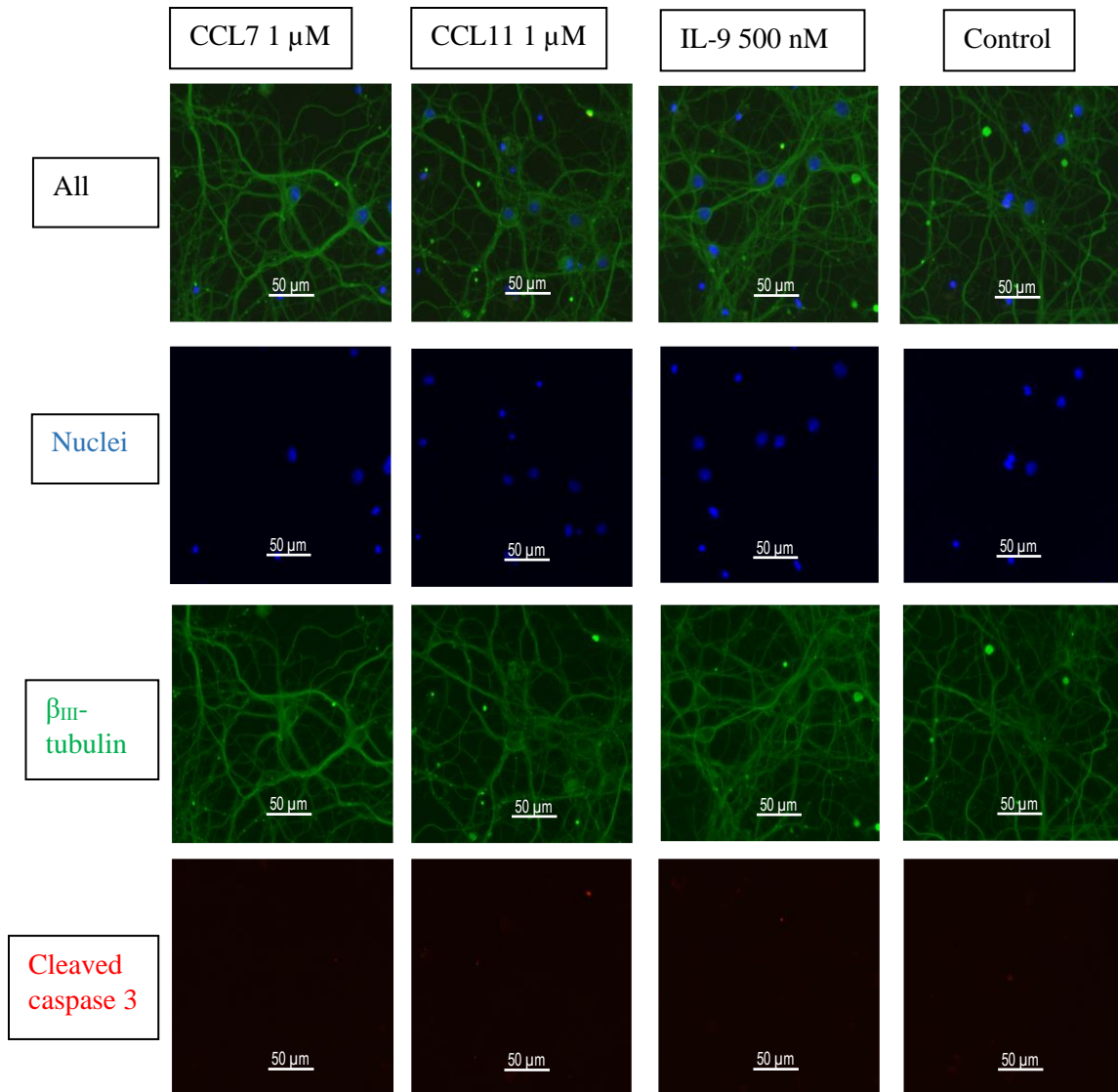


Figure 6: Neuronal morphology and apoptosis after incubation with CCL7, CCL11 and IL-9. Neurons E12 treated with AraC were incubated for 24 h with the cytokines at the indicated concentrations. The cells were then immunostained for their DNA (blue), neuronal β_{III} -tubulin (green) and cleaved caspase 3 (red). 5 images per condition were taken. Only a part of a single image is shown for better demonstration of the morphology of a single neuron. Neurites were compared between treated and control samples. No difference was detected. Cleaved caspase 3 stainings did not show any positivity. N= 1 nonAraC + 2 AraC for CCL7; n= 1 nonAraC + 2 AraC for CCL11 and n= 1 nonAraC + 1 AraC for IL-9. Additionally, the concentrations of 5nM, 50 nM and 500 nM (CCL7 and CCL11) and 5 nM and 30 nM (IL-9) were analyzed and demonstrated no difference in cell damage.

3.4 Analysis of the effect of defined cytokines and T_H9 cell conditioned imaging buffer on Ca²⁺ levels in cultured E16 mouse neurons using Ca²⁺-imaging

3.4.1 General notes regarding Ca²⁺-imaging

The following experiments were conducted using Ca²⁺-imaging. Neurons were stained with the Ca²⁺ fluorescent dye Fluo-4 AM. An increase in intracellular Ca²⁺ concentration is reflected by an increase in Fluo-4 AM fluorescence. Figure 7 shows examples of this increase in fluorescence in response to KCl or glutamate. Both lead to a depolarization in neurons. The reaction to these substances is very heterogeneous. While some neurons are already bright before the addition of a depolarizing agent (Figure 7, blue arrows), others are only bright after the addition (Figure 7, yellow arrows), with others not reacting at all or only slightly with an increase in fluorescence intensity (Figure 7, white arrows). In the analysis of the following experiments only neurons reacting to these stimulating substances with an increase in fluorescence of at least 50 % of baseline are included. Additionally, to account for the heterogeneous reactions, a large number of neurons is included in each analysis ranging from 50 to 300.

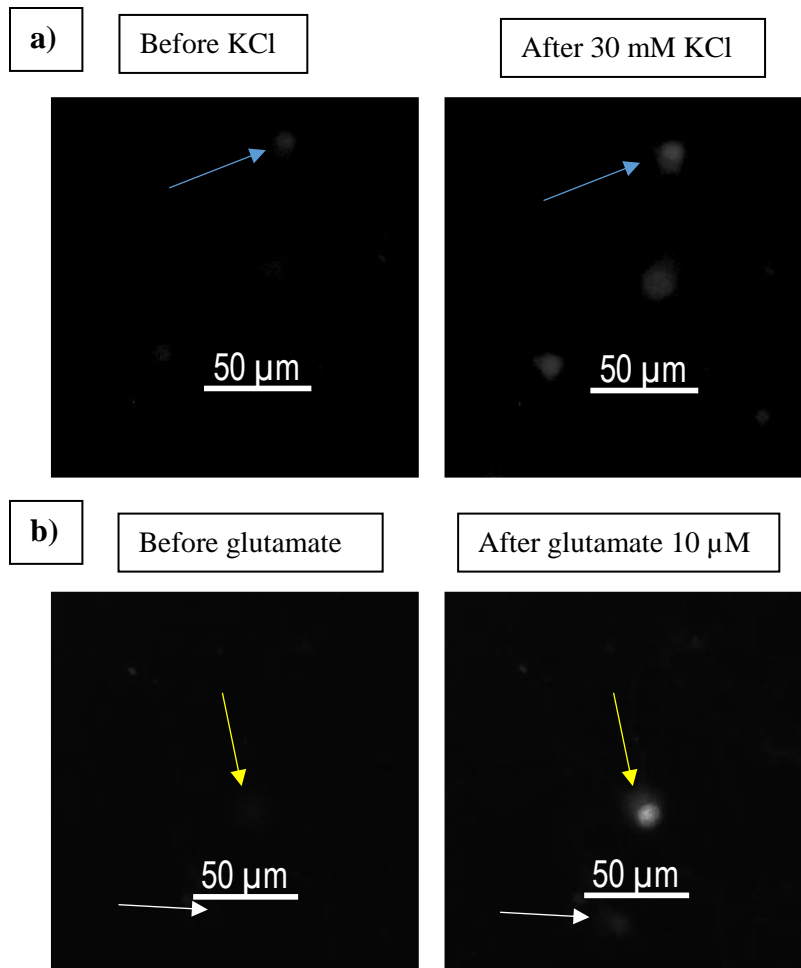


Figure 7: Examples of neurons stained with the Ca^{2+} fluorescent dye Fluo-4AM and their reaction to KCl and glutamate. Neurons DIV 14 were stained with Fluo-4AM. **a)** Neurons stained are shown before and after the addition of 30 mM KCl. Fluorescence intensity increases after the addition. The blue arrow marks a neuron already bright before the KCl addition. **b)** Neurons stained are shown before and after the addition of 10 μM glutamate. Fluorescence intensity increases after the addition. The yellow arrow marks a neuron reacting after the glutamate addition. The white arrow marks a neuron reacting only slightly to the glutamate addition.

3.4.2 Direct effect of the application of mouse T_h9 cell supernatant on Ca²⁺ levels in E16 mouse neurons

In order to analyze the hypothesis that T_h9 cells damage neurons via glutamate-mediated excitotoxicity, the Ca²⁺ levels of neurons were assessed upon exposure to Locke's Buffer in which T_h9 cells had been incubated (LB-T_h9).

The addition of the LB-T_h9 at approximately 3 min leads to a sharp increase in neuronal fluorescence intensity up to 3 times of the baseline levels (Figure 8 a, b and c). Blockage of the NMDA-receptor with MK-801 after this increase in fluorescence intensity leads to a sharp decrease in fluorescence intensity (Figure 8 c). The application of MK-801 before the recordings leads to no alteration of fluorescence intensity upon LB-T_h9 addition (Figure 8 b).

Two samples showed an increase in fluorescence upon KCl addition (Figure 8 b, c). This glutamate receptor independent depolarization served as a positive control. It indicates the functionality of the neurons used. One sample did not react to KCl but reacted to LB-T_h9 with an increase in fluorescence intensity (Figure 8 a).

The T_h9 cell culture was analyzed for its IL-9 production (see 3.1.1). The qPCR analysis for the culture used for Figure 8 is shown in 3.1.1.

Taken together, LB-T_h9 leads to an increase in Ca²⁺ levels of neurons DIV 14. This response can be blocked by the NMDA-receptor antagonist MK-801. Experiments were only conducted with two T_h9-cultures in total (one not shown, see 3.1.1 and 4.1.1).

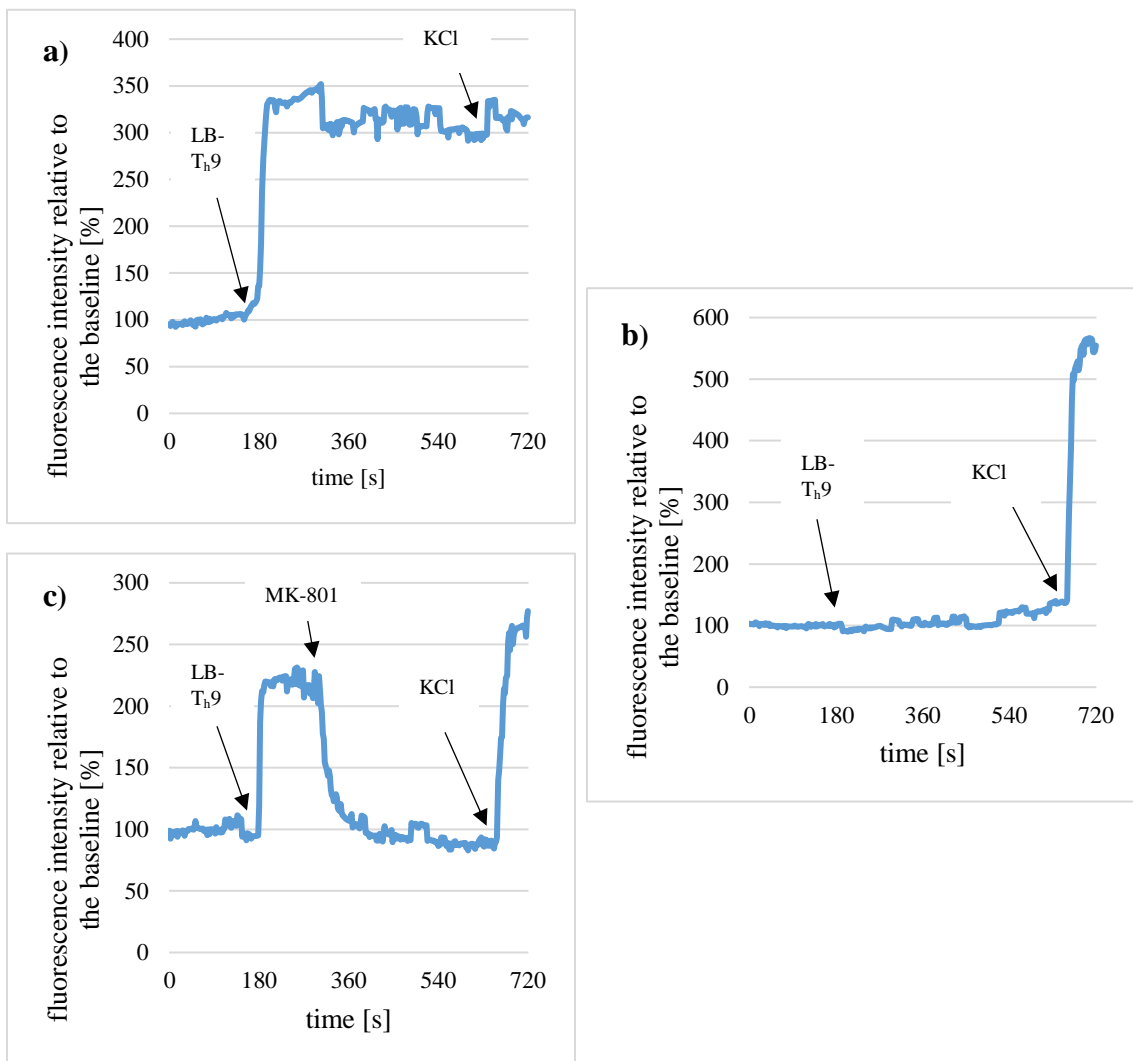


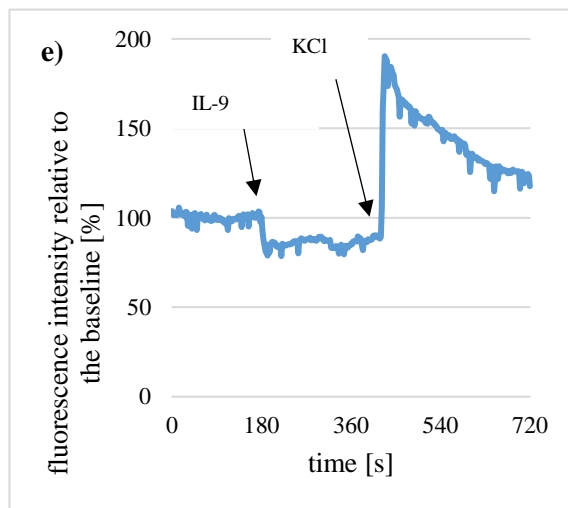
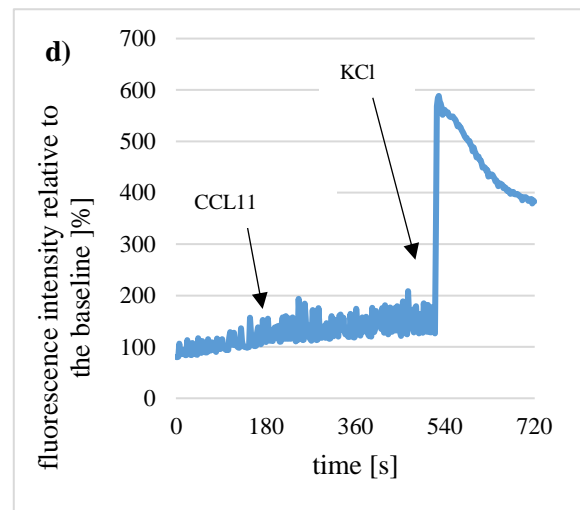
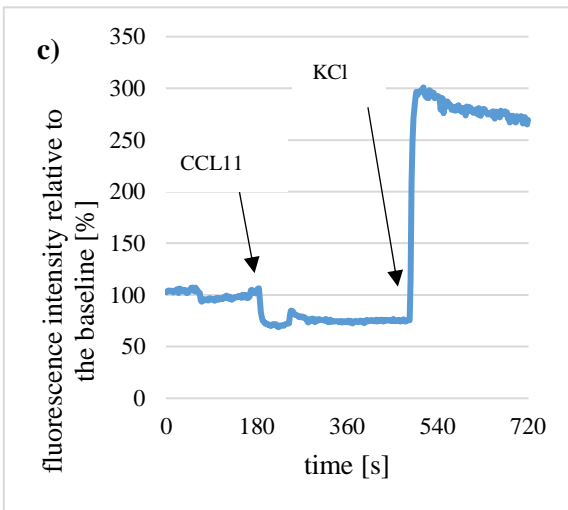
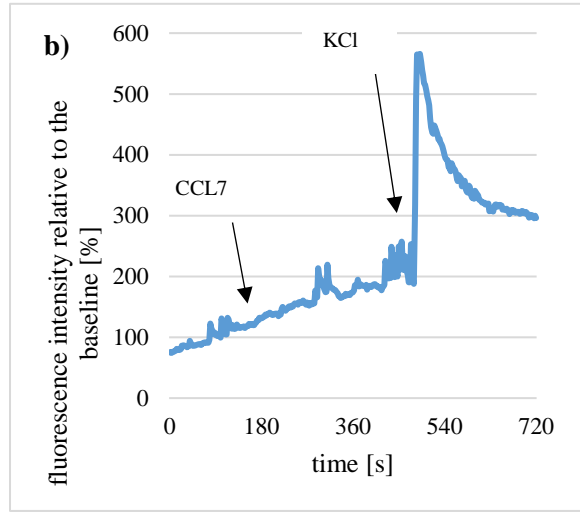
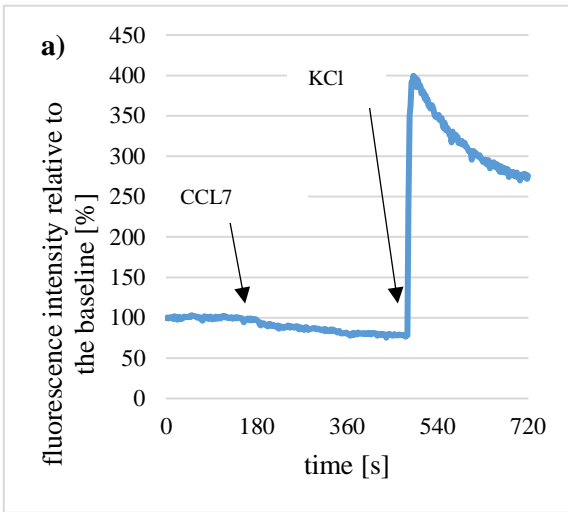
Figure 8: Effect of Th9 conditioned Locke's Buffer (LB-Th9) on Ca²⁺ levels in neurons and its antagonization by the NMDA-receptor antagonist MK-801. Fluorescence intensity over time is shown. The baseline fluorescence intensity was recorded from 0 s to 180 s and the fluorescence intensity is shown relative to the baseline. **a)** LB-Th9 was added at 180 s and 30 mM KCL at 660 s to neurons DIV 14. An increase in fluorescence intensity is visible upon LB- Th9 addition. **b)** Neurons DIV 14 were pretreated with 10 μ M MK-801 for 25 min. LB-Th9 was added at 180 s and 30 mM KCl at 660 s. An increase in fluorescence intensity is visible only upon KCl addition. **c)** LB-Th9 was added at 180 s, 10 μ M MK-801 was added at 300 s and 30 mM KCl at 660 s to neurons DIV 14. An increase in fluorescence intensity is visible upon LB-Th9 addition and upon KCl addition. A decrease in fluorescence intensity is visible upon MK-801 addition. N=1 for all experiments.

3.4.3 Direct effect of the application of CCL7, CCL11 and IL-9 on Ca²⁺ levels in E16 mouse neurons

After having established that CCL7, CCL11 and IL-9 do not directly damage neurons, the effect of these cytokines on intracellular Ca²⁺ levels was further investigated. Ca²⁺ is believed to play a role in T_H9 cell mediated neuronal damage, since previous data showed that neuronal damage is decreased by treating neuronal cells with the glutamate receptor antagonists MK-801 and NBQX (S. Ray, K. Forsberg, F. Bischof, unpublished results). Glutamate-induced excitotoxicity is discussed as the primary cause of this neuronal damage. In the following experiment, neuronal cells were stained with a Ca²⁺ sensitive dye and the effect of adding CCL7, CCL11 and IL-9 on intracellular Ca²⁺ levels was observed.

Neither CCL7, nor CCL11 or IL-9 have any direct effect on the fluorescence intensity in neurons DIV 7 or 14 in the concentrations applied (Figure 9). Small, sharp decreases in Ca²⁺ levels (Figure 9 c and e) are due to the LB itself or small shifts of the plate containing the neurons. Otherwise no changes in Ca²⁺ levels can be observed. The increase in fluorescence intensity upon KCl addition shows, that the neurons are still excitable and the non-reaction to the cytokines is not due to their inability to increase their Ca²⁺ levels. The imaging for IL-9 was only conducted for neurons DIV 7 (Figure 9 e).

In conclusion, none of the studied cytokines had any effect on short-term neuronal Ca²⁺ homoeostasis, when adding it directly to the neurons.



See the following page for the legend of this figure

Figure 9: Ca²⁺ levels in neurons (DIV 7 and 14) upon addition of CCL7, CCL11 and IL-9. Fluorescence intensity over time is shown. Baseline fluorescence intensity was recorded from 0 s to 180 s and the fluorescence intensity is shown relative to the baseline **a)** 50 nM CCL7 was added at 180 s and 30 mM KCl at 420 s to neurons DIV 7, AraC treated, n=3, one sample is shown. **b)** 50 nM CCL7 was added at 180 s and 30 mM KCl at 420 s to neurons DIV 14, AraC treated, n=8, one sample is shown. **c)** 50 nM CCL11 was added at 180 s and 30 mM KCl at 420 s to neurons DIV 7, AraC treated, n=3, one sample is shown. **d)** 50 nM CCL11 was added at 180 s and 30 mM KCl at 420 s to neurons DIV 14, AraC treated, n=2, one sample is shown. **e)** 50 nM CCL7 was added at 180 s and 30 mM KCl at 420 s to neurons DIV 7, AraC treated, n=2, one sample is shown. All samples show no increase in fluorescence intensity upon addition of the cytokines. All samples react to KCl with an increase in fluorescence intensity.

3.4.4 The effect of preincubation of E16 mouse neurons with CCL7, CCL11 and IL-9 on glutamate-induced Ca²⁺ influx

Next, the impact of the cytokines CCL7, CCL11 and IL-9 on glutamate-induced Ca²⁺-influx was assessed. This represents an indirect approach to the experiments demonstrated in 3.4.3, where the direct impact of CCL7, CCL11 and IL-9 on intracellular Ca²⁺ levels was assessed.

3.4.4.1 Notes for all samples

For each experiment, treated samples and their controls were matched in pairs. As already mentioned in 2.4.4, the fluorescence of the dye decreased during the day. Only samples taken at approximately the same time points can be compared. Each sample and its corresponding control are presented in the following tables.

Two different approaches to the analysis of the following experiments were performed: The absolute difference as the difference of the mean intensity values relative to the baseline of a treated sample and the corresponding control sample was calculated. Secondly, the relative difference at the time point 300 s is shown. Here, the mean intensity value relative to the baseline of the treated sample is shown relative to its corresponding control. In the following paragraphs these differences are abbreviated as the absolute and relative difference.

Additionally, due to the heterogeneity of the neuronal reactions to glutamate (see Figure 7) and the difference in between neuronal cultures, the standard deviations are very large.

Calculations of the significance have been performed on samples, which showed an increase or decrease of fluorescence intensity compared to the control after glutamate addition.

3.4.4.2 The effect of 50 nM CCL7 preincubation on glutamate-induced Ca²⁺ influx in neurons DIV 7

Exposure of neurons DIV7 to 50 nM CCL7 for 48 h and subsequent addition of glutamate does not lead to a change of the glutamate-mediated increase of intracellular Ca²⁺ levels compared to neurons not treated with CCL7. This is indicated by the lack of increase in fluorescence intensity relative to the baseline, recorded before glutamate addition, in Figure 10 compared to the control. The fluorescence intensity of both samples peaks at roughly 350 % of the baseline (Figure 10 a).

Figure 10 b) shows a single measurement at one time point after the glutamate addition. As already seen in Figure 10 a), neurons treated with CCL7 and control neurons show a similar reaction to glutamate. The large extent of the standard deviation is due to the variability of neuronal reactions to glutamate in our cultures (see 3.4.1 and 4.4.1).

In Table 6, all the measurements are listed separately, instead of determining the mean of all measurements as in Figure 10. This results in an average absolute difference of 0 % and an average relative difference of 12 %. Additionally, the difference in between single samples is rather small, ranging from -16 % to 11 % relative difference, with one outlier at 65 %. Therefore, both the absolute and the relative difference show no change in fluorescence intensity. The 50 nM CCL7 pretreatment of neurons DIV 7 appears to have no effect on the neuronal excitability through glutamate.

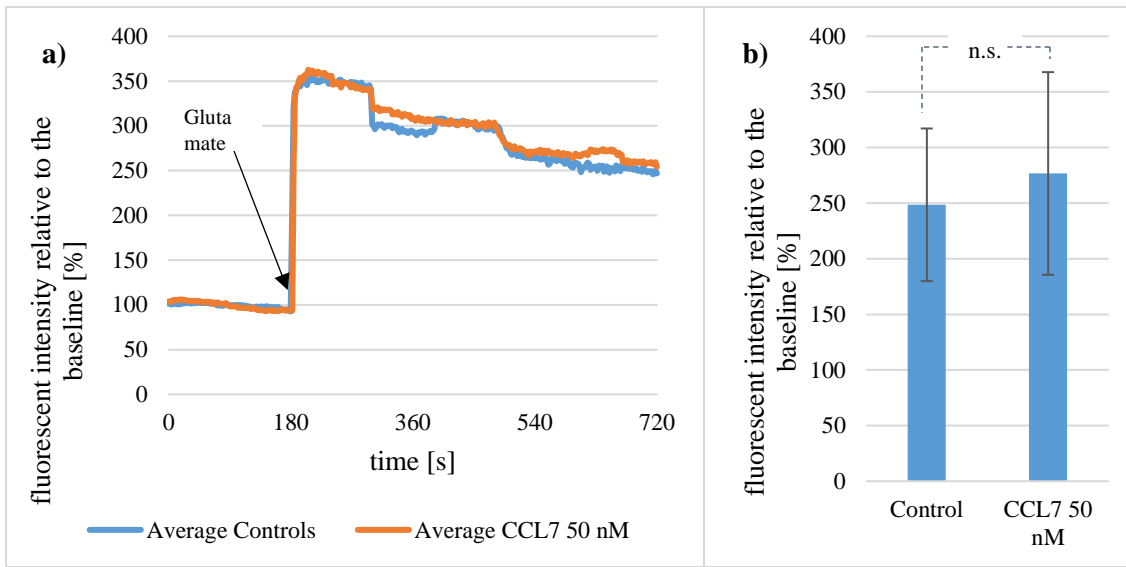


Figure 10: The effect of 50 nM CCL7 on glutamate-mediated Ca^{2+} rise in neurons DIV 7. Neurons DIV 7 were incubated with 50 nM CCL7 for 48 h and their Ca^{2+} levels were measured using Fluo-4 AM. **a)** Fluorescence intensity relative to the baseline, recorded from 0 to 180 s, over time is shown. 10 μM glutamate was added at 180 s. Averages of all samples and corresponding controls are shown, $n=4$ for each control and sample. No difference between CCL7 treated neurons and the control can be seen. **b)** Fluorescence intensity relative to the baseline of the time point 300 s is shown. Two samples are shown as the mean out of all cells measured in one trial. Error bars represent the standard deviation. n.s.=non-significant ($p>0,05$) as determined by student's t-test.

Table 6: The effect of 50 nM CCL7 on glutamate-mediated Ca²⁺ rise in neurons DIV 7. Neurons DIV 7 were incubated with 50 nM CCL7 for 48 h and their Ca²⁺ levels were measured using Fluo-4 AM. Fluorescence intensity relative to the baseline, recorded from 0 to 180 s, is shown at the time point 300 s. The absolute difference between the fluorescence intensity relative to the baseline of treated neurons and control neurons was calculated. The relative difference was calculated with the fluorescence intensity relative to the baseline of the control set as 100 % and with the fluorescence intensity of the treated sample, relative to the control. The first cypher of the numbering indicates the neuronal culture, the second indicates the sample number of this culture. Both the absolute and the relative difference between the CCL7 treated and control samples are very small.

	Control [%]	CCL7 50 nM [%]	Absolut difference in percent of the baseline [%]	Relative difference in percent of the control value at its peak [%]
1.1	488	412	-76	~-16
2.1	460	398	-62	~-13
3.1	249	277	28	~11
3.2	168	277	109	~65
Average of all samples	341,25	341	-0,25	~12

3.4.4.3 The effect of 50 nM CCL7 preincubation on glutamate-induced Ca²⁺ influx in neurons DIV 14

Pretreatment of neurons DIV 14 with 50 nM CCL7 leads to an enhanced intracellular Ca²⁺ rise upon glutamate addition compared to control samples (Figure 11 a), as indicated by the fluorescence intensity measured. Thereby, the increase in fluorescence intensity was roughly 140 % higher in CCL7 treated neurons. The difference in increase relative to the control value amounts to 42 % on average (Table 7).

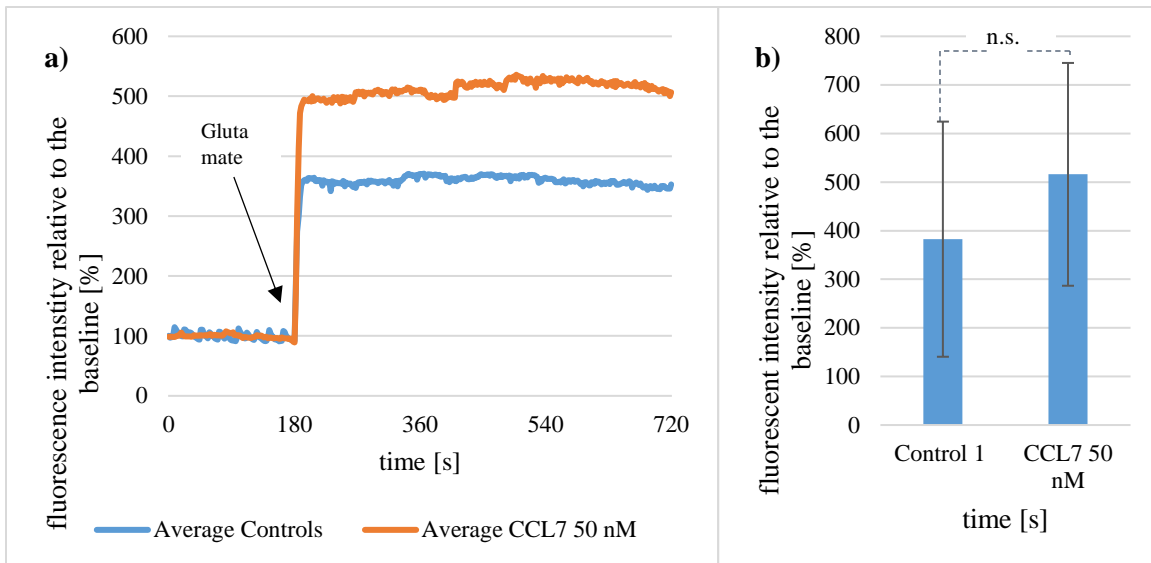


Figure 11: The effect of 50 nM CCL7 on glutamate-mediated Ca^{2+} rise in neurons DIV 14. Neurons DIV 14 were incubated with 50 nM CCL7 for 48 h and their Ca^{2+} levels were measured using Fluo-4 AM. **a)** Fluorescence intensity relative to the baseline, recorded from 0 to 180 s, over time is shown. 10 μM glutamate was added at 180 s. Averages of all samples and corresponding controls are shown, $n=5$ for each control and sample. **b)** Fluorescence intensity relative to the baseline of the time point 300 s is shown. One sample only is shown as the mean out of all cells measured in one trial. Error bars represent the standard deviation. n.s.=non-significant ($p>0,05$) as determined by student's t-test.

This increase is nonsignificant, see Figure 11 b). Here, a single measurement is shown at one time point after the glutamate addition. The standard deviation is very large, due to the very heterogenous reactions of the neurons to glutamate (see 3.4.1 and 4.4.1).

In Table 7, all the measurements are listed separately, instead of determining the mean of all measurements as in Figure 11. Out of 5 different samples with cells derived from 3 different cell cultures only one showed a slightly lower Ca^{2+} level after glutamate addition compared to its control. All other samples demonstrated an increase in fluorescence intensity higher than the corresponding control. The relative difference ranges from 33 % to 88 %.

All in all, the results show a consistent, albeit nonsignificant, increase in Ca^{2+} levels in CCL7 treated samples compared to controls. This indicates that 50 nM CCL7 pretreatment enhances the glutamate-mediated Ca^{2+} rise in neurons DIV 14.

Table 7: The effect of 50 nM CCL7 on glutamate-mediated Ca²⁺ rise in neurons DIV 14. Neurons DIV 14 were incubated with 50 nM CCL7 for 48 h and their Ca²⁺ levels were measured using Fluo-4 AM. Fluorescence intensity relative to the baseline, recorded from 0 to 180 s, is shown at the time point 300 s. The absolute difference between the fluorescence intensity relative to the baseline of treated neurons and control neurons was calculated. The relative difference was calculated with the fluorescence intensity relative to the baseline of the control set as 100 % and with the fluorescence intensity of the treated sample shown relative to the control. The first cypher of the numbering indicates the neuronal culture, the second indicates the sample number of this culture. Both the absolute and the relative difference between the CCL7 treated and control samples show a bigger increase in fluorescence intensity by CCL7 pretreatment.

	Control [%]	CCL7 50 nM [%]	Absolute difference in percent of the baseline [%]	Relative difference in percent of the control value at its peak [%]
1.1	368	693	325	~88
2.1	331	547	216	~66
2.2	361	481	120	~33
3.1	383	516	133	~34
3.2	340	306	-34	~-10
Average of all samples	356	509	153	~42

3.4.4.4 The effect of 5 nM CCL7 preincubation on glutamate-induced Ca²⁺ influx in neurons DIV 14

Exposure of neurons DIV 14 to 5 nM CCL7 for 48 h and subsequent addition of glutamate does not lead to changes in the glutamate-mediated increase of intracellular Ca²⁺ levels compared to control samples (Figure 12 a), as indicated by the fluorescence intensity. Both the CCL7 treated sample and the control show roughly the same increase in fluorescence intensity after glutamate addition up to about 480 % of the baseline.

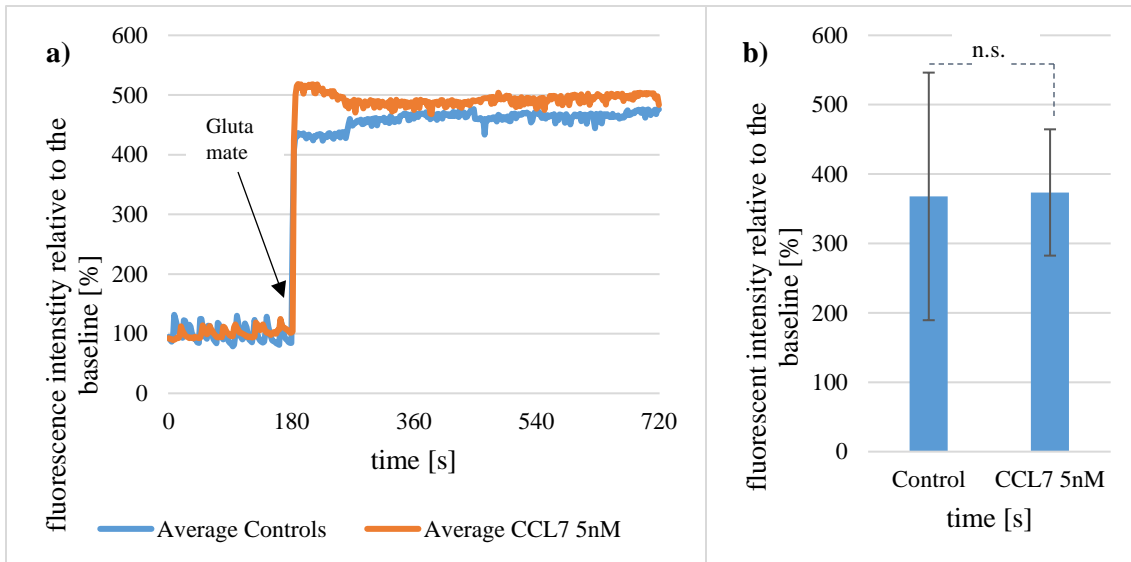


Figure 12: The effect of 5 nM CCL7 on glutamate-mediated Ca^{2+} rise in neurons DIV 14. Neurons DIV 14 were incubated with 5 nM CCL7 for 48 h and their Ca^{2+} levels were measured using Fluo-4 AM. **a)** Fluorescence intensity relative to the baseline, recorded from 0 to 180 s, over time is shown. 10 μM glutamate was added at 180 s. Averages of all samples and corresponding controls are shown, $n=2$ for each control and sample **b)** Fluorescence intensity relative to the baseline of the time point 300 s is shown. One sample only is shown as the out of all cells measured in one trial. Error bars represent the standard deviation. n.s.=non-significant ($p>0,05$) as determined by student's t-test.

Figure 12 b) shows a single measurement at one time point after the glutamate addition. In both samples the standard deviation is very large (see 3.4.1 and 4.4.1). The difference between the CCL7 treated sample and control is non-significant.

In Table 8, all the measurements are listed separately, instead of determining the mean of all measurements as in Figure 12. The relative changes in comparison between one control and one treated sample are small, ranging from 1 % to 15 %. This results in an average absolute difference of 42 % and an average relative difference of 8 %. Especially when considering the relative difference, this difference is negligible. Also, the absolute difference is rather small when comparing it with values seen in 50 nM CCL7 pretreatment (Table 7) of 150 % on average.

The results indicate that 5 nM CCL7 pretreatment does not enhance or reduce glutamate-mediated Ca^{2+} rise in neurons DIV 14.

Table 8: The effect of 5 nM CCL7 on glutamate-mediated Ca²⁺ rise in neurons DIV 14. Neurons DIV 14 were incubated with 5 nM CCL7 for 48 h and their Ca²⁺ levels were measured using Fluo-4 AM. Fluorescence intensity relative to the baseline, recorded from 0 to 180 s, is shown at the time point 300 s. The absolute difference between the fluorescence intensity relative to the baseline of treated neurons and control neurons was calculated. The relative difference was calculated with the fluorescence intensity relative to the baseline of the control set as 100 % and with the fluorescence intensity of the treated sample shown relative to the control. The first cypher of the numbering indicates the neuronal culture, the second indicates the sample number of this culture. Both the absolute and the relative difference between the CCL7 treated and control samples are very small.

	Control [%]	CCL7 5 nM [%]	Absolute difference in percent of the baseline [%]	Relative difference in percent of the control value at its peak [%]
1.1	368	374	6	~1
2.1	529	606	77	~15
Average of all samples	448	490	42	~8

3.4.4.5 The effect of 50 nM CCL11 preincubation on glutamate-induced Ca²⁺ influx in neurons DIV 7

Pretreatment of neurons DIV 7 with 50 nM CCL11 for 48 h and subsequent exposure to glutamate does not lead to changes in the glutamate-induced increase of intracellular Ca²⁺ levels compared to control samples (Figure 13 a), as indicated by the fluorescence intensity. Both the CCL11 treated and the control sample show roughly the same increase in fluorescence intensity after glutamate addition up to about 200 % of the baseline. The average of the control samples is slightly higher at 210 %.

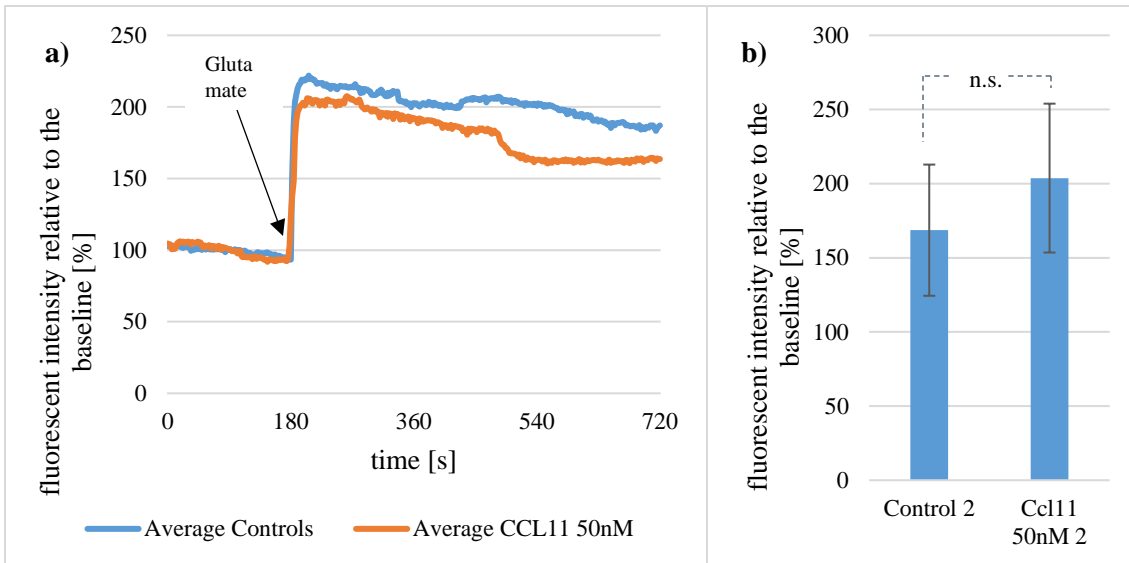


Figure 13: The effect of 50 nM CCL11 on glutamate-mediated Ca^{2+} rise in neurons DIV 7. Neurons DIV 7 were incubated with 50 nM CCL11 for 48 h and their Ca^{2+} levels were measured using Fluo-4 AM. **a)** Fluorescence intensity relative to the baseline, recorded from 0 to 180 s, over time is shown. 10 μM glutamate was added at 180 s. Averages of all samples and corresponding controls are shown, $n=2$ for each control and sample. **b)** Fluorescence intensity relative to the baseline of the time point 300 s is shown. One sample only is shown as the mean out of all cells measured in one trial. Error bars represent the standard deviation. n.s.=non-significant as determined by student's t-test.

Figure 13 b) shows a single measurement at one time point after the glutamate addition. The CCL11 treated sample is about 40 % higher and the standard deviation is very large (see 3.4.1 and 4.4.1). The difference between CCL11 treated sample and control is non-significant.

In Table 9, all the measurements are listed separately, instead of determining the mean of all measurements as in Figure 13 a). The relative difference between one control and one treated sample is rather small, ranging from -30 % to 21 %. This results in an average absolute difference of -19 % and an average relative difference of -5 %. Similar to Figure 12 and Table 8, this difference is negligible.

The results indicate that 50 nM CCL11 pretreatment does not enhance or reduce glutamate-mediated Ca^{2+} rise in neurons DIV 7.

Table 9: The effect of 50 nM CCL11 on glutamate-mediated Ca²⁺ rise in neurons DIV 7. Neurons DIV 7 were incubated with 50 nM CCL11 for 48 h and their Ca²⁺ levels were measured using Fluo-4 AM. Fluorescence intensity relative to the baseline, recorded from 0 to 180 s, is shown at the time point 300 s. The absolute difference between the fluorescence intensity relative to the baseline of treated neurons and control neurons was calculated. The relative difference was calculated with the fluorescence intensity relative to the baseline of the control set as 100 % and with the fluorescence intensity of the treated sample shown relative to the control. The first cypher of the numbering indicates the neuronal culture, the second indicates the sample number of this culture. The results are varying between an increase or a decrease of glutamate-induced Ca²⁺ rise.

	Control [%]	CCL11 50 nM [%]	Absolute difference in percent of the baseline [%]	Relative difference in percent of the control value at its peak [%]
1.1	249	174	-75	~-30
1.2	169	204	35	~21
Average of all samples	209	189	-19	~-5

3.4.4.6 The effect of 5 nM IL-9 preincubation on glutamate-induced Ca²⁺ influx in neurons DIV 7

Exposure of neurons DIV 7 to 5 nM IL-9 for 48 h and subsequent addition of glutamate shows inconclusive results, when comparing the increase of intracellular Ca²⁺ levels compared to the control (Figure 14 a) as indicated by the fluorescence intensity.

The control average shows an increase in Ca²⁺ levels after glutamate addition up to about 200 % of the baseline, with IL-9 treated samples being about 40 % higher.

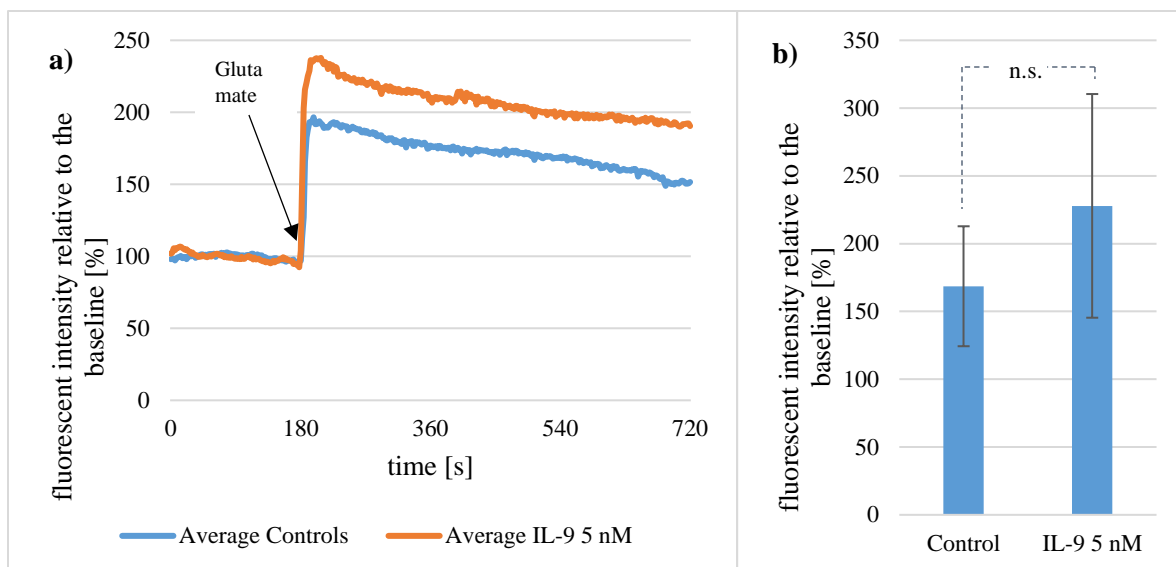


Figure 14: The effect of 5 nM IL-9 on glutamate-mediated Ca^{2+} rise in neurons DIV 7. Neurons DIV 7 were incubated with 5 nM IL-9 for 48 h and their Ca^{2+} levels were measured using Fluo-4 AM. **a)** Fluorescence intensity relative to the baseline, recorded from 0 to 180 s, over time is shown. 10 μM glutamate was added at 180 s. Averages of all samples and corresponding controls are shown, $n=2$ for each control and sample. **b)** Fluorescence intensity relative to the baseline of the time point 300 s is shown. One sample only is shown as the mean out of all cells measured in one trial. Error bars represent the standard deviation. n.s.=non-significant ($p>0,05$) as, determined by student's t-test.

Figure 14 b) shows a single measurement at one time point after the glutamate addition. The IL-9 treated sample is about 50 % higher than the control sample. The difference between the IL-9 treated sample and the control is non-significant due to the very large standard deviation (see 3.4.1 and 4.4.1).

In Table 10, all measurements are listed separately, instead of determining the mean of all measurements as in Figure 14 a). The fluorescence intensity increase relative to the control value differs, when comparing both samples. This results in an average absolute difference of 37 % and an average relative difference of 22 %.

Only two samples were analyzed. Both results differ by a large amount, one showing basically no increase, the other showing a larger increase of IL-9 treated neurons compared to control neurons. No conclusions can be drawn, whether 5 nM IL-9 pretreatment enhances or reduces glutamate-mediated Ca^{2+} rise in neurons DIV 7.

Table 10: The effect of 5 nM IL-9 on glutamate-mediated Ca²⁺ rise in neurons DIV 7. Neurons DIV 7 were incubated with 5 nM IL-9 for 48 h and their Ca²⁺ levels were measured using Fluo-4 AM. Fluorescence intensity relative to the baseline, recorded from 0 to 180 s, is shown at the time point 300 s. The absolute difference between the fluorescence intensity relative to the baseline of treated neurons and control neurons was calculated. The relative difference was calculated with the fluorescence intensity relative to the baseline of the control set as 100 % and with the fluorescence intensity of the treated sample shown relative to the control. The first cypher of the numbering indicates the neuronal culture, the second indicates the sample number of this culture. The results are inconclusive.

	Control [%]	IL-9 5nM [%]	Absolute difference in percent of the baseline [%]	Relative difference in percent of the control value at its peak [%]
1.1	169	228	59	~35
1.2	193	209	16	~8
Average of all samples	181	218	37	~22

3.4.4.7 The effect of 30 nM IL-9 preincubation on glutamate-induced Ca²⁺ influx in neurons DIV 14

Pretreatment of neurons DIV 14 with 30 nM IL-9 for 48 h and subsequent exposure to glutamate does not lead to an enhanced rise of intracellular Ca²⁺ levels compared to control samples (Figure 15 a), as indicated by the increase in fluorescence intensity. The average of the control neurons shows an increase in Ca²⁺ levels after glutamate addition of about 350 % of the baseline, with IL-9 treated samples being roughly the same.

Figure 15 b) shows a single measurement at one time point after the glutamate addition. Both treated sample and control show about the same amount of fluorescence intensity increase. No significant increase or decrease was calculated. The standard deviation is very large (see 3.4.1 and 4.4.1).

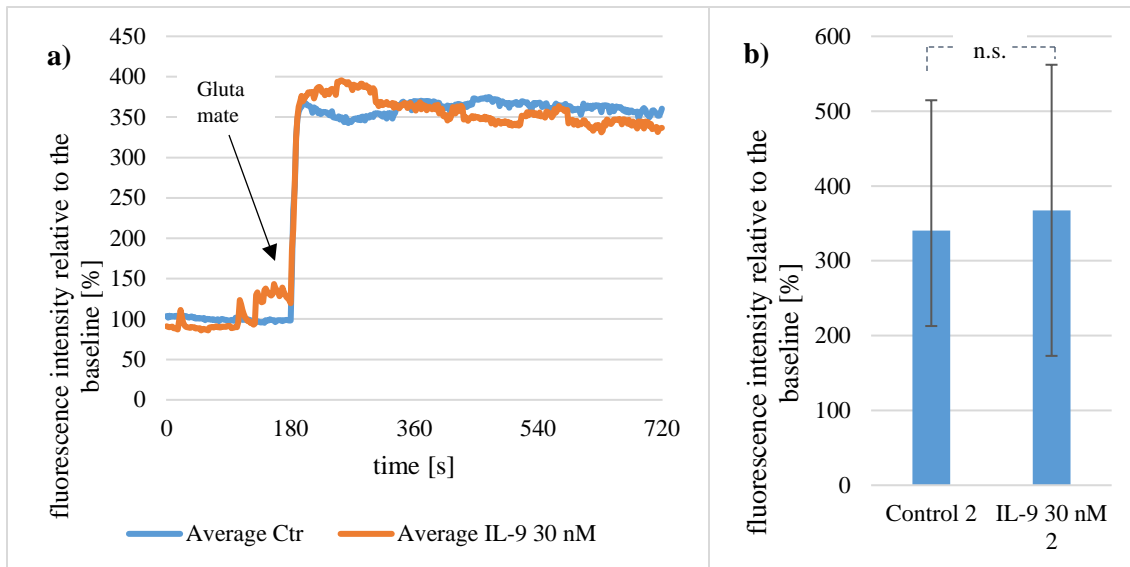


Figure 15: The effect of 30 nM IL-9 preincubation on glutamate-mediated Ca^{2+} rise in neurons DIV 14. Neurons DIV 14 were incubated with 30 nM IL-9 for 48 h and their Ca^{2+} levels were measured using Fluo-4 AM.

a) Fluorescence intensity relative to the baseline, recorded from 0 to 180 s, over time is shown. 10 μM glutamate was added at 180 s. Averages of all samples and corresponding controls are shown, $n=3$ for each control and sample.

b) Fluorescence intensity relative to the baseline of the time point 300 s is shown. One sample only is shown as the mean out of all cells measured in one trial. Error bars represent the standard deviation. n.s.=non-significant ($p>0,05$) as determined by student's t-test.

In Table 11, all the measurements are listed separately, instead of determining the mean of all measurements as in Figure 15 a). The relative changes in comparison between one control and one treated sample are varying, ranging from -15 % to 38 %. This results in an average absolute difference of 32 % and an average relative difference of 9 %. Similar to Figure 12 and Table 8, this difference is negligible.

This indicates, that 30 nM IL-9 pretreatment does not enhance or reduce the glutamate-mediated Ca^{2+} rise in neurons DIV 14.

Table 11: The effect of 30 nM IL-9 on glutamate-mediated Ca²⁺ rise in neurons DIV 14. Neurons DIV 14 were incubated with 30 nM IL-9 for 48 h and their Ca²⁺ levels were measured using Fluo-4 AM. Fluorescence intensity relative to the baseline, recorded from 0 to 180 s, is shown at the time point 300 s. The absolute difference between the fluorescence intensity relative to the baseline of treated neurons and control neurons was calculated. The relative difference was calculated with the fluorescence intensity relative to the baseline of the control set as 100 % and with the fluorescence intensity of the treated sample shown relative to the control. The first cypher of the numbering indicates the neuronal culture, the second indicates the sample number of this culture. On average, only a slight increase in glutamate-mediated Ca²⁺ rise in IL-9 treated samples can be observed.

	Control [%]	IL-9 30nM [%]	Absolute difference in percent of the baseline [%]	Relative difference in percent of the control value at its peak [%]
1.1	331	457	126	~38
2.1	383	324	-59	~-15
2.2	340	367	27	~8
Average of all samples	351	383	32	~16

3.4.4.8 The effect of 5 nM IL-9 preincubation on glutamate-induced Ca²⁺ influx in neurons DIV 14

Exposure of neurons DIV 14 to 5 nM IL-9 for 48 h and subsequent addition of glutamate leads to an enhanced increase of intracellular Ca²⁺ levels compared to the control (Figure 16 a), as indicated by the increase in fluorescence intensity.

The control average shows an increase in Ca²⁺ levels after glutamate addition up to about 360 % of the baseline. IL-9 treated samples show an increase which is 70 % higher.

This increase is non-significant however. Figure 16 b) shows a single measurement at one time point right after the glutamate addition. The IL-9 treated sample is higher than the control with 420 % compared to 370 % increase in fluorescence intensity. The standard deviation is very large (see 3.4.1 and 4.4.1).

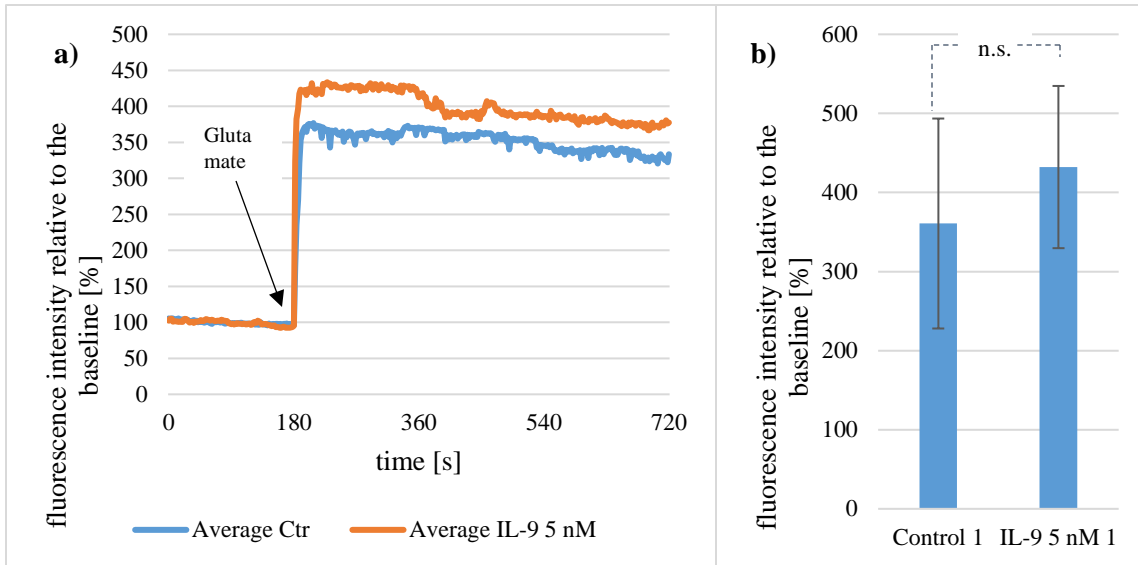


Figure 16: The effect of 5 nM IL-9 on glutamate-mediated Ca^{2+} rise in neurons DIV 14. Neurons DIV 14 were incubated with 5 nM IL-9 for 48 h and their Ca^{2+} levels were measured using Fluo-4 AM. **a)** Fluorescence intensity relative to the baseline, recorded from 0 to 180 s, over time is shown. 10 μM glutamate was added at 180 s. Averages of all samples and corresponding controls are shown, $n=3$ for each control and sample. **b)** Fluorescence intensity relative to the baseline of the time point 300 s is shown. One sample only is shown as the mean out of all cells measured in one trial. Error bars represent the standard deviation. n.s.=non-significant ($p>0,05$) as determined by student's t-test.

In Table 12, all measurements are listed separately. The fluorescence intensity increase relative to the control value in comparison between one control and one treated sample is similar in all samples compared, ranging from 17 % to 21 %.

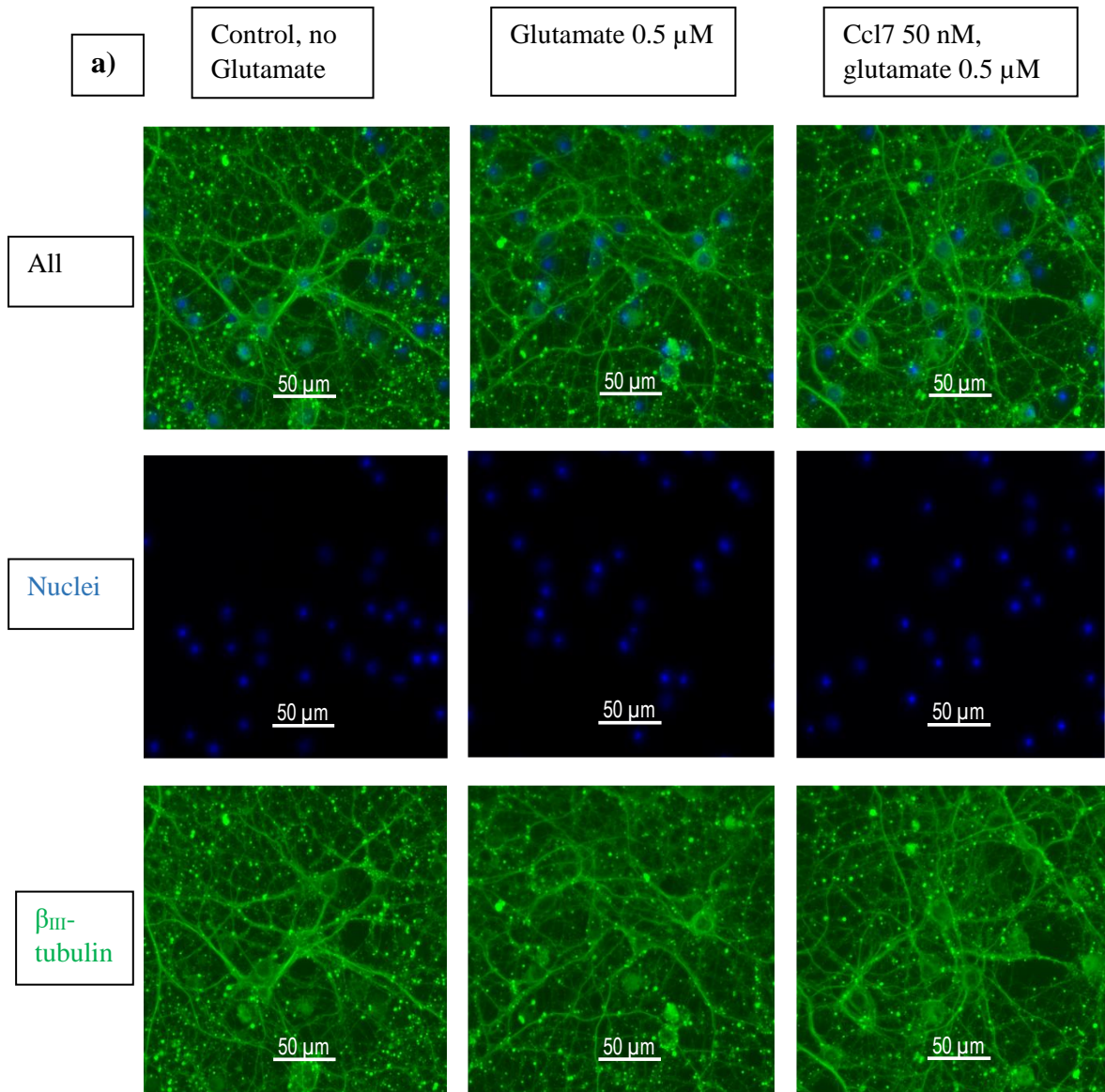
This indicates that 5 nM IL-9 pretreatment enhances glutamate-mediated Ca^{2+} rise in neurons DIV 14 non-significantly.

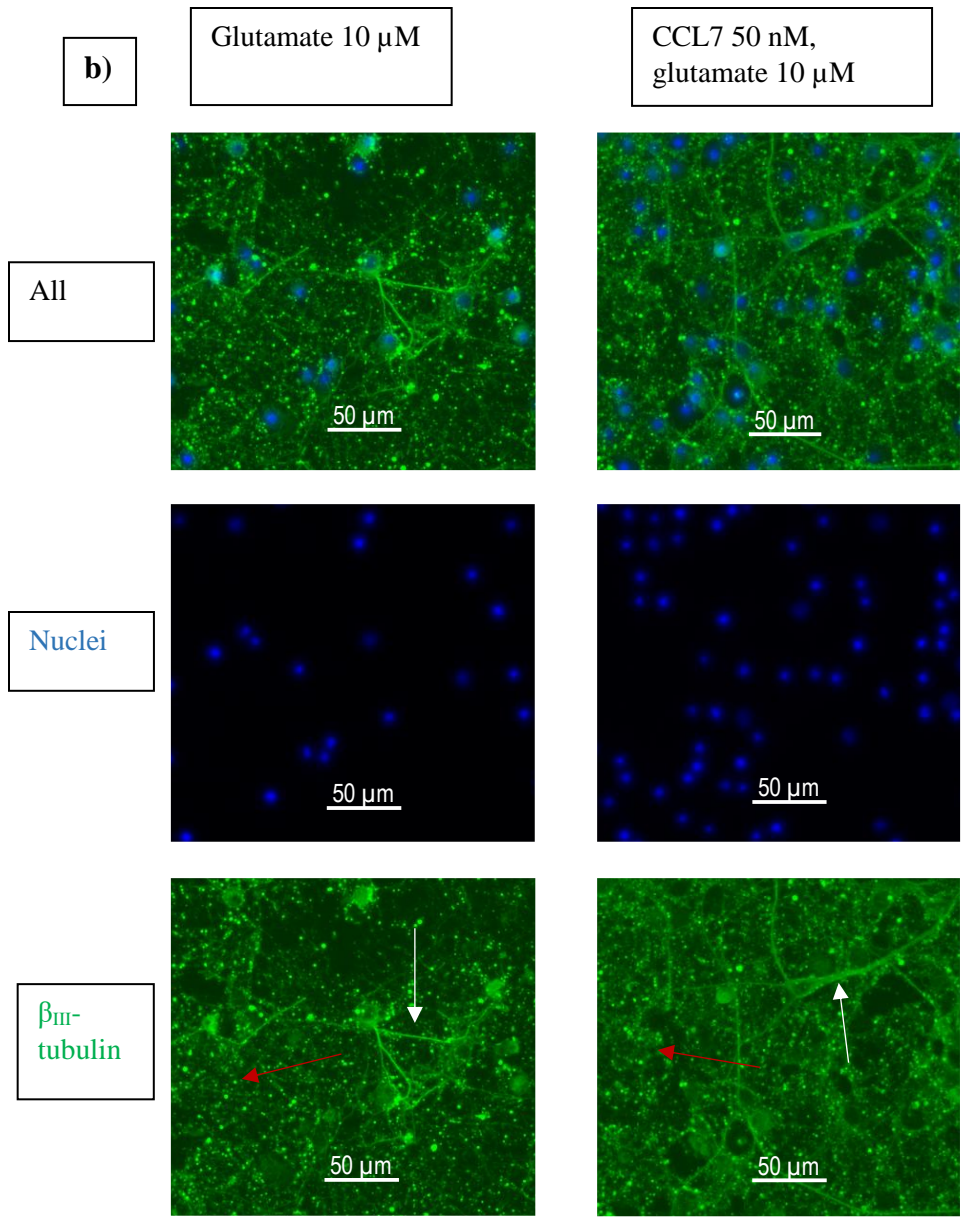
Table 12: The effect of 5 nM IL-9 on glutamate-mediated Ca²⁺ rise in neurons DIV 14. Neurons DIV 14 were incubated with 5 nM IL-9 for 48 h and their Ca²⁺ levels were measured using Fluo-4 AM. Fluorescence intensity relative to the baseline, recorded from 0 to 180 s, is shown at the time point 300 s. The absolute difference between the fluorescence intensity relative to the baseline between treated neurons and control neurons was calculated. The relative difference was calculated with the fluorescence intensity relative to the baseline of the control set as 100 % and with the fluorescence intensity of the treated sample shown relative to the control. The first cypher of the numbering indicates the neuronal culture, the second indicates the sample number of this culture. An increase in glutamate-mediated Ca²⁺ rise in IL-9 treated samples can be observed in both the absolute and relative difference.

	Control [%]	IL-9 5nM [%]	Absolute difference in percent of the baseline [%]	Relative difference in percent of the control value at its peak [%]
1.1	361	432	71 %	~20
2.1	383	448	65 %	~17
2.2	340	412	72 %	~21
Average of all samples	361	431	68 %	~19

3.5 The effect of CCL7, CCL11 and IL-9 preincubation on glutamate-mediated excitotoxicity in neurons

Since previous results showed that CCL7 and IL-9 pretreatment alters glutamate-mediated Ca²⁺ influx in neurons (see 3.4.4.3 and 3.4.4.8 respectively), we needed to determine, whether this alteration in Ca²⁺ influx was also accompanied by an alteration of glutamate-induced neuronal damage. Therefore, neurons were incubated with CCL7, CCL11 and IL-9 and then exposed to glutamate assessing their morphology and apoptosis thereafter.





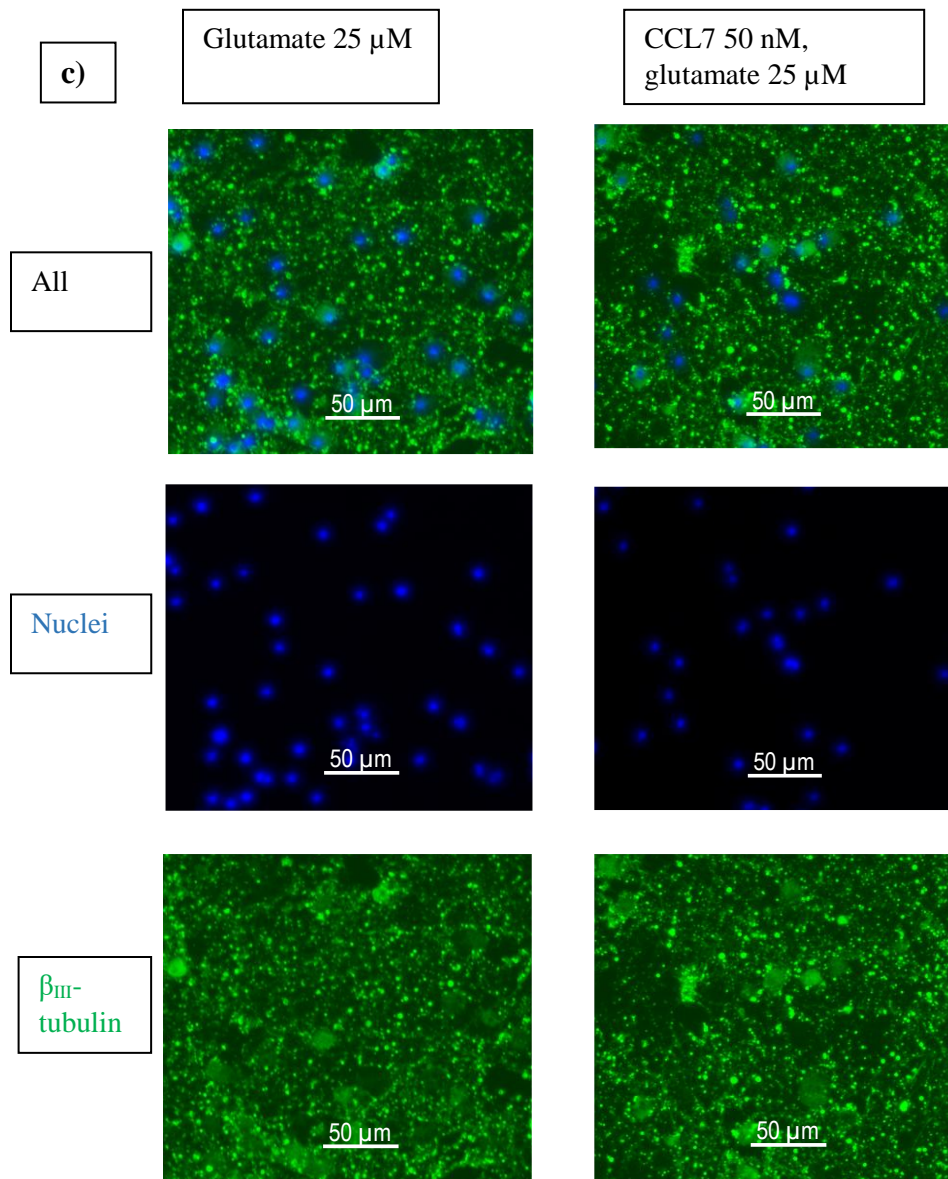


Figure 17: The effect of CCL7 pretreatment on glutamate induced excitotoxicity in neurons. Neurons E16, DIV 15 were incubated with 50 nM CCL7 for 24 h and then exposed to glutamate for 24 h. The cells were subsequently fixed and stained for DNA (blue) and β_{III} -tubulin (green). 5 images per condition were taken at set locations in each well. Only a part of a single image is shown for better demonstration of the morphology of single neurons. Single stainings and the combined stainings are shown in each column. The same experiment was conducted several times with different cytokines and different concentrations of these cytokines: n=3 for 50 nM CCL7, n=1 for CCL7 250 nM, n= 1 for 2,5 nM and 25nM CCL11, n=2 for 5 nM IL-9 and n=1 for 250 nM IL-9. **a)** Neurons were treated with 0.5 μ M glutamate or no glutamate. **b)** Neurons were treated with 10 μ M glutamate. White arrows mark examples of intact neurites, red arrows mark examples of fragmented neurites. **c)** Neurons were treated with 25 μ M glutamate. No difference between CCL7 treated samples and controls can be seen, while increasing amounts of glutamate lead to increased neuronal deterioration.

Neurons were incubated with CCL7 for 24 h and subsequently incubated with glutamate for another 24 h. They were then stained for DNA and cytoskeletal markers (Figure 17). As a correlation of neuronal damage, neuronal morphology in form of cytoskeletal deterioration was analyzed. Cleaved caspase 3 stainings showed no positivity even when neurites were heavily fragmented (see Figure 17 c, cleaved caspase 3 not shown). For each condition five pictures were taken and only small parts of one picture are presented in this figure. This ensures better visualization of neurites and nuclei on a singular cell level.

When comparing the morphology (Figure 17 a-c, β_{III} -tubulin staining), clear differences can be seen between conditions treated with different concentrations of glutamate. White arrows in the β_{III} -tubulin staining show examples of these intact neurites (see Figure 17 b). Damaged neurites can be distinguished by their fragmentation, marked with red arrows in Figure 17 b. In the samples treated with no glutamate or 0.5 μ M glutamate, neurites are mostly well preserved with few signs of bright green cell fragments. In the samples treated with 10 μ M glutamate the neurites are mostly fragmented. Still, some healthy neurites can be observed in this treatment group. Neurons treated with 25 μ M glutamate show no remaining intact neurites.

However, there were no differences in cell morphology observable between samples treated with CCL7 and control samples. The damage was always attributed to the glutamate exposure.

The same experiment was also conducted with 250 nM CCL7, 2.5 nM and 25 nM CCL11, as well as 5 nM and 250 nM IL-9. All experiments revealed the same results as described above.

All in all, glutamate induces neuronal damage with increasing concentrations. However, CCL7 and IL-9 do not alter neuronal damage induced by glutamate, despite altering glutamate-mediated Ca^{2+} influx in neurons.

3.6 Detection of CCL7, CCL11 and IL-9 in an experimental autoimmune encephalomyelitis (EAE) mouse model

Finally, we wanted to identify, whether the observed cytokines are also existent in the most commonly used EAE mouse model. The mRNA of the spinal cord of mice induced with EAE was analyzed by qPCR with special regards to the T_h9 cell signature cytokine IL-9. An increase in IL-9-mRNA expression would suggest an increase of T_h9 cells in EAE mice. This could indicate a relevance for MS disease.

When comparing the mRNA expression of CCL7, CCL11 and IL-9 in an EAE mouse model (Figure 18) with control mice not infected with EAE, one can see a significant ($p < 0,01$) increase in CCL7-mRNA expression in EAE mice. CCL11 does not show any difference between EAE and control and IL-9-mRNA is even lower in EAE mice compared to the control. This difference is not significant however.

Since no elevation of IL-9 was found, we refrained from further immunohistochemistry.

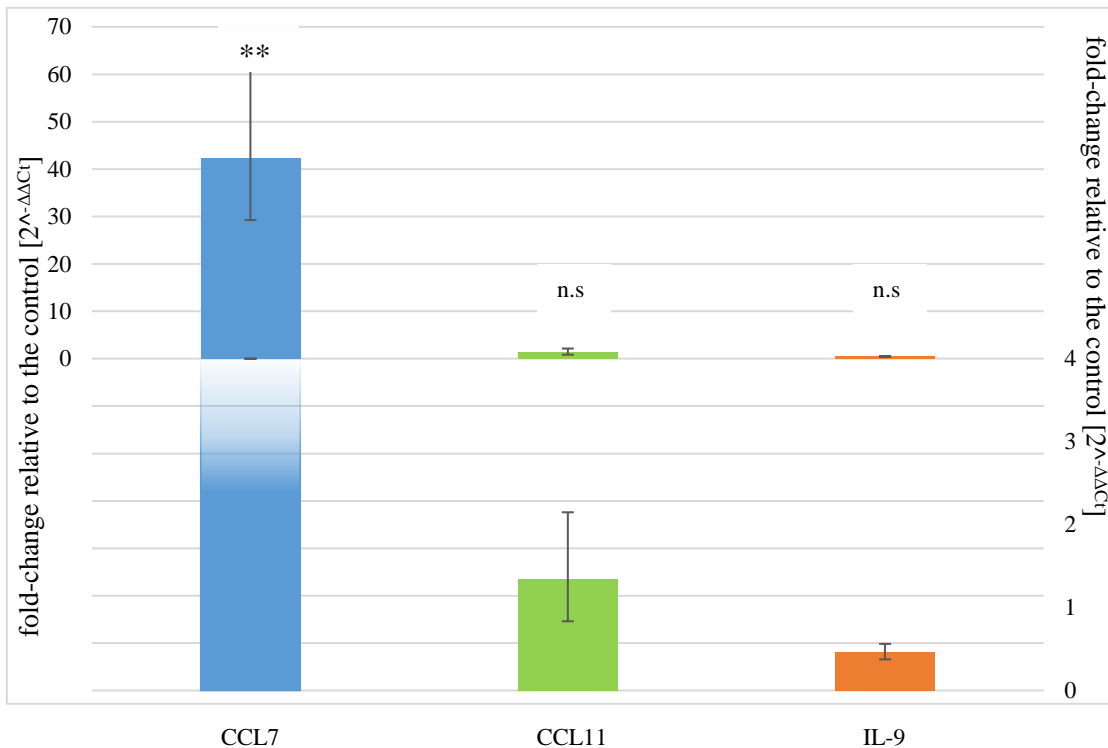


Figure 18: mRNA expression of CCL7, CCL11 and IL-9 in spinal cords of EAE-mice. EAE was induced in mice and at the first sign of EAE-specific symptoms, mice were sacrificed and their spinal cord dissected. cDNA was obtained from these spinal cords. qPCR was performed in triplicates for the targets *CCL7*, *CCL11* and *IL-9*. Fold-changes of treated samples versus control samples normalized to actin ($\Delta\Delta C_t$ -method) are shown. Data is presented in form of a patch panel: The lower part of the graph is represented by the secondary y-axis in order to better distinguish between low fold-changes. Error bars represent the positive and negative errors derived from the standard deviation. N=4 for control mice, n=3 for EAE mice. *** p<0.001, ** p<0.01, * p<0,05, n.s.=non-significant, determined by student's t-test.

3.7 Summary of the results

In summary, we determined the damaging potential of the cytokines CCL7, CCL11 and IL-9. None of these cytokines was found to damage the cultured neurons by itself. Similarly, none of the cytokines had any direct effect on neuronal Ca²⁺ levels upon addition, while T_H9 cell supernatant was found to increase neuronal Ca²⁺ levels upon addition. To observe long-term effect and modulation of existing changes in Ca²⁺ levels by these cytokines, neurons were treated with CCL7, CCL11 and IL-9 and subsequently exposed to glutamate. Thereby, 50 nM CCL7 and 5 nM IL-9 enhanced glutamate-mediated

Ca²⁺ rises in neurons DIV 14. However, none of the cytokines enhanced or reduced glutamate-mediated excitotoxicity.

Parallel to these experiments, mRNA of neuronal and astrocyte cultures was analysed. There, IL-9 treatment induced a CCL7-mRNA upregulation in astrocytes and a CCL7-mRNA downregulation in neurons. The general expression levels of CCL7 were higher in astrocytes than in neurons, but overall rather low. Finally, the mRNA expression of these cytokines was detected in an EAE mouse model. Here, CCL7 was strongly upregulated, CCL11 only slightly and IL-9 not at all.

4. Discussion

4.1 Culturing of neurons and of T_h9 cells

4.1.1 Assessment of the T_h9 cell cultures

As already mentioned in 3.1.1, T_h9-cultures were analysed for their purity with qPCR instead of FACS. T_h cells are characterized by their production of cytokines and T_h9 cells in particular are characterized by the production of their signature cytokine IL-9⁷. Other T_h cells such as T_h17 cells have the ability to produce IL-9 as well²¹. Importantly, T_h9 cells do not co-stain with any other cytokines typical for different T_h cell subsets, for example IL-4 for T_h2 cells or IL-17A for T_h17 cells⁷. Our qPCR controls of the cell culture only detect IL-9 gene expression of all cells combined (see 3.1.1). This IL-9 expression is not unique to T_h9 cells and can therefore not affirm, that the cells analysed are indeed of the T_h9 phenotype. Co-expression with other cytokines cannot be analysed by qPCR. FACS on the other hand, can stain cells on a singular cell level and thus determine co-expression of IL-9 with other cytokines of each cell. Exact percentages can be given of T_h9 cells, producing only IL-9, as well as exact percentages of other cell types, producing IL-9 as well as other cytokines.

As FACS analysis was not possible in our experiments due to problems with the machine and the staining, the qPCR data gathered has certain limitations: The results indicate that there are a high number of IL-9 producing cells, since the reference culture, which had been analysed with FACS, expressed less IL-9. However, our cells are not confirmed to be T_h9 cells. Nonetheless, since T_h9 cells are the main producers of IL-9 and the qPCR shows a high expression of IL-9, these results indicate that the cells analysed are in fact T_h9 cells.

4.1.2 Assessment of the neuronal cultures

The neuronal cultures used were analysed for their purity, as well as for cell damage by immunocytochemistry. Cultures were assessed for their morphology and rejected, if they were already damaged prior to any treatments. Neuronal morphology can both be applied

for assessment of a single sample as well as for comparison between two samples. Damage usually starts with the neurites and spreads to the soma later¹¹⁰. The analysis of the morphology though is only qualitative, not quantitative.

A quantitative analysis of neuronal damage could be performed by analyzing pyknotic nuclei and cleaved caspase 3 positivity. However, pyknotic nuclei count is not a viable method for neuronal damage analysis, since even in healthy cultures, a high amount of nuclei is classified as pyknotic¹⁰⁷.

This unusual number of pyknotic nuclei can be due to small dividing non-neuronal cells¹⁰⁷ present in neuronal cell cultures. AraC treatment as used in our cultures results in the death of these cells and pyknotic nuclei. Additionally, fragments of nuclei of cells that died during the preparation of the culture are still stained by DAPI¹⁰⁷. Taken together, this leads to a larger number of counted pyknotic nuclei than actual apoptotic neurons. It needs to be noted, that these non-neuronal cells do not have a correlating neuronal cell body.

Accordingly, we used a morphological analysis of neuronal cell bodies stained for β III-tubulin (see 2.5.2) as a means to assess neuronal cell death.

Cleaved caspase 3 is commonly used to evaluate apoptosis in neurons (see for example Kim et al.¹¹¹). Cleaved caspase 3 stainings did not reveal any positivity in our neuronal cultures, both when the cells looked morphologically very healthy (see 3.3) and when the staining of the neuronal cytoskeleton revealed heavy neurite fragmentation (see 3.5). This indicates, that in our experiments cleaved caspase 3 staining is also not a reliable way to assess neuronal damage.

Thus, both quantitative methods could not be used for our analysis. Nonetheless, the analysis of the neuronal morphology allows for a qualitative assessment of our neuron cultures. The fragmentation of neurites allowed for an assessment already at early stages of neuronal damage, as well as heavy cell damage.

4.2 CCL7- and CCL11-mRNA expression in neurons and astrocytes

The CCL7- and CCL11-mRNA expression was measured in astrocytes and neurons, which had been exposed to CCL7, CCL11 and IL-9, to determine cross regulation between these cytokines. Our results indicate that IL-9 upregulates CCL7-mRNA expression in astrocytes (see 3.2.1).

Recent studies revealed that CCL7 and CCL11 are not just expressed by immune cells, but are expressed in non-immune cells as well. Especially, after they were stimulated with certain cytokines. Expression of CCL7 has already been shown in cortical neurons upon TNF- α stimulation and in a GnRH producing neuronal cell line^{68,69}. CCL7 production by astrocytes was demonstrated as well. The production was constitutive and increased upon TNF- α stimulation^{63,112}.

CCL11 was shown to be secreted by activated astrocytes⁸⁶ and by neurons in the brain¹¹³.

However, the induction of CCL7- and CCL11-mRNA expression in neurons or astrocytes by CCL7, CCL11 or IL-9 has never been demonstrated. Our results are in line with a study from Luo et al.¹¹⁴, which shows a C-C chemokine dependant chemokine production in astrocytes. Additionally, IL-9 receptors were revealed to be highly expressed in astrocytes and upregulated during EAE. IL-9 could thus induce chemokine expression in astrocytes¹¹⁵. Our results now confirm these observations, by showing that CCL7-mRNA is expressed in astrocytes and is upregulated by IL-9. This implies that T_h9 cells can influence astrocytes by secreting IL-9 and thereby stimulating CCL7 expression. This in turn could attract further inflammatory cells and aggravate inflammation due to the chemotactic effect of CCL7. Additionally, CCL7 can directly influence CNS resident cell, which is discussed in the following pages (see 4.4.4 as well as 1.1.5.1).

A limitation to our results is the low fold-change, ranging from 1.5 to 4.5. Ding et al.¹¹⁵ observed similar fold-changes ranging up to 6, when inducing CCL20 and CXCL9 in mouse astrocytes with IL-9.

Further results include the downregulation of CCL7-mRNA expression in neurons by IL-9 and the upregulation of CCL11-mRNA expression in astrocytes. Both results have a very low expression in general with C_T -values >31 (see Table 4 and Table 3 respectively). This leads to very accident-sensitive measurements. As seen in Figure 3, none of the results is statistically significant. This might be due to this accident-sensitivity. Additionally, the low expression points out, that the amount of chemokine expression is very low and might not be relevant *in vivo*. Nonetheless, a downregulation of CCL7 in neurons (as seen Figure 4) could present a neuroprotective mechanism. Neurons have already been shown to have the ability to suppress neuroinflammation as shown in EAE⁴².

Finally, the CCL11-mRNA expression in neurons was analysed. Here, the results are very heterogeneous and do not allow for any conclusions.

All in all, these results indicate a novel induction of CCL7-mRNA expression by IL-9 in astrocytes. It points out the role of astrocytes in aggravating existing neuroinflammation⁴³.

4.3 The role of CCL7, CCL11 and IL-9 in neuronal damage

Neurons were treated with CCL7, CCL11 or IL-9 and the effect on their morphology was assessed. No neuronal damage after treatment with these cytokines could be observed (3.3).

With the discovery of the presence of chemokine receptors on neuronal cells in the brain, questions regarding the functional implications of these receptors arose. CCR2, which is mainly activated by CCL2 but also by CCL7, was shown to be constitutively expressed in neurons. CCL2 led to a transient Ca^{2+} rise in neurons upon stimulation⁵⁸. Since CCR are GPCRs, which can invoke an intracellular Ca^{2+} rise (for a review see Rollins⁵⁴), this indicates a direct effect of these chemokines on neurons.

Other experiments revealed chemokines to be neurotoxic or even neuroprotective: CXCL10 induces apoptosis via the activation of caspase 3 in cultured neurons¹¹⁶. CCR2 deficient mice were shown to develop a milder course of a viral neurological disease compared to their controls. Thereby CCL7-mRNA next to the mRNA of other chemokines was upregulated, but no infiltration of immune cells into the brain could be detected¹¹⁷. This

indicates a role of chemokines in neuronal pathogenesis independent of their effect on immune cells. In contrast to these experiments, other results showed that CCL2, secreted by astrocytes, has neuroprotective properties. It reduced both the release of glutamate from neurons as well as the damage mediated by oxygen-glucose deprivation¹¹⁸. Additionally, CCL2 was associated with neuroprotection in experimental glaucoma¹¹⁹.

CCL7 and CCL11 have not been studied as extensively as CCL2. CCL11 has already been associated with protection against neuroinflammation in rats⁸⁷. This process however, is seen in the context of a tighter BBB and thus decreased recruitment of immune cells into the brain⁸⁷. Also, CCL11 was shown to be neurotoxic via the production of reactive oxygen species in microglia⁸⁶. CCL7 has not been associated with neurotoxicity directly. Since it binds to the same receptor as CCL2 however, CCL7 might display similar characteristics as CCL2 regarding neuronal damage or neuroprotection.

IL-9 has not been associated with directly damaging neurons either. Generally regarded as an inflammatory cytokine, possible deterioration of neurons can be achieved through inflammatory mechanisms by IL-9. Patkai et al¹²⁰ found that IL-9 exacerbates excitotoxic brain lesions. In contrast, IL-9 was shown to protect neurons against developmental apoptosis²⁰.

Our results show no neuronal damage in our primary neuron cultures after exposure to CCL7, CCL11 and IL-9 (see 3.3). The concentrations of these cytokines ranged up to 1 μ M. Effective concentrations of these cytokines in other experiments are far below that amount. CCL2 was shown to already lead to Ca^{2+} rises in neurons at 10 nM⁵⁸. It is unlikely, that the lack of neurotoxicity is due to an insufficient amount of cytokines added.

Possible explanations for the lack of neuronal damage after exposure to CCL7, CCL11 and IL-9 are firstly, that these cytokines simply are not able to induce neuronal damage. In line with our results, Giuliani et al.⁴⁸ showed that CCL7 did not induce neuronal damage. In contrast though, their T cell supernatant did not induce neuronal damage either, while previous experiments in our lab (S. Ray, K. Forsberg, F. Bischof, unpublished results) detected a neurotoxic effect of T_h9 cell supernatant.

Secondly, the neurotoxic properties of certain cytokines discovered are often studied in animal models of inflammatory diseases or in cell cultures containing microglia and astrocytes in addition to neurons^{86,116,117,118,119}. Our cell cultures contained mostly neurons with very few astrocytes (see 3.1.2). Damaging mechanisms functioning via astrocytes or microglia could thus not work. Since we wanted to show the direct interaction of neurons with these cytokines, this experimental setup was selected on purpose. Nevertheless, this might explain the lack of damage, when comparing our results with other publications such as Parajuli et al.⁸⁶.

Thirdly, chemokine receptors are often upregulated by inflammatory stimuli¹²¹. Additional inflammatory stimuli might be necessary to induce a receptor upregulation, which is sufficient for our chemokines to unfold their damaging potential. Synergistic effects of different cytokines might be necessary to impair neuronal cells. In our experimental setup, only single cytokines were tested. *In vivo* there are always a multitude of inflammatory and regulatory cytokines working together. Thus, further experiments could determine, whether the cytokines we studied can damage neurons under inflammatory conditions or when adding a proinflammatory cytokine together with CCL7, CCL11 or IL-9.

Altogether, our results show no direct damage induced by either CCL7, CCL11 or IL-9. This does not mean that these cytokines are not damaging, but rather that under non-inflammatory conditions, these cytokines alone do not cause neurotoxicity.

4.4 Analysis of neuronal Ca²⁺ levels

4.4.1 General limitations of the Ca²⁺-imaging experiments

Since none of the studied cytokines had a neuro-damaging effect in the previous experiments, the effects of these cytokines on neuronal intracellular Ca²⁺ levels were observed. The method used for these experiments was Ca²⁺-imaging using a Ca²⁺ dependant fluorescent dye, namely Fluo-4 AM¹²². Due to the setup of the experiment, only the relative Ca²⁺ levels over time could be observed, instead of the absolute concentration. This entails some limitations. Naturally, no conclusions on the absolute intracellular Ca²⁺

concentrations can be drawn. Next, it is difficult to compare different samples, since the absolute fluorescence intensity is dependent on many different factors, such as the type of neurons present, the dilution of the dye and the photobleaching during subsequent uses among others¹²².

This was no problem for the experiments in 3.4.2 and 3.4.3, where only the relative Ca^{2+} changes of a single sample were relevant.

However, the experiments in 3.4.4 did depend on a comparison between sample and control. Here, the relative changes of the increase of intracellular Ca^{2+} after glutamate addition were compared between several samples. This allows for a quantification in form of the amount of the relative increase even without a measurement of the absolute Ca^{2+} concentration.

In order to minimize the disturbance factors mentioned above, samples, which were going to be compared, were always measured with the same dilution of the dye. Photobleaching of the dye led to a decrease in fluorescence during subsequent experiments and could result in samples measured previously to others showing a higher fluorescence intensity. Also, the relative difference could be affected. For that reason, samples, which we expected to have an increase in fluorescence intensity compared to the controls, were always measured right after the controls. This ensured, that any observable effect of an increase in fluorescence after cytokine pretreatment would not be due to the photobleaching of the dye.

Another limitation of our experiments is the heterogeneous neuronal reaction to Ca^{2+} . This heterogeneity is even greater, when comparing samples of different primary neuronal cultures. This is partly due to the difference in neurons present in the mouse cortex, which we used for our experiments. Different neuronal subtypes express different receptors. For example, the NMDA receptor was shown to not be equally distributed across all cortical layers¹²³ and the number of NMDA receptors was shown to differ between cortical neurons¹²⁴. This disparity in glutamate receptors leads to a disparity in reactions to glutamate. Another reason for these heterogeneous reactions, is due to unequal loading of the neurons with the cell permeable dye¹²², which depends on the distribution of cells in the

well amongst other reasons. Additionally, stages of neuronal development are not completely equal in one culture¹²⁵. The heterogeneity leads to large standard deviations of our measurements (see for example Figure 10).

Finally, experiments showed that astrocytes express functional NMDA receptors¹²⁶ and react to glutamate with an intracellular Ca^{2+} rise¹²⁷. The number of astrocytes in our cell cultures was very low (see 3.1.2), but might have influenced the results.

4.4.2 The effect of T_h9 supernatant on neuronal Ca^{2+} levels

The results from 3.4.2 showed an increase in neuronal intracellular Ca^{2+} upon addition of LB-T_h9. All cells reacted to KCl, thus showing they are able to have an increase in Ca^{2+} levels, except for one sample (see Figure 8 a). This could be due to the large Ca^{2+} increase upon LB-T_h9 addition, which could have led to cell death. Additionally, the dye might have already been at its saturation. At the saturation of the dye, further increase in Ca^{2+} cannot be expressed in an increase in fluorescence intensity.

This increase in fluorescence upon LB-T_h9 addition could be inhibited by pre-treatment with the NMDA receptor antagonist MK-801 or reversed by adding MK-801 after adding LB-T_h9 (see Figure 8). NMDA receptors are activated by glutamate and can be modulated by glycine¹²⁸. These results indicate that glutamate is secreted by T_h9 cells. Thus, the supernatant leads to the Ca^{2+} increase in neuronal cells. This mechanism is independent of cell to cell contacts between T cells and neurons, since only the supernatant of T_h9 cells induced the Ca^{2+} rise in our experiments. Cell to cell contacts have already been demonstrated to induce Ca^{2+} oscillations in neurons as well as neuronal cell death in a glutamate dependant way^{49,102}.

Secretion of glutamate has already been demonstrated for T cells in general¹²⁹ and T_h1 and T_h17 in particular¹⁰², but never for T_h9 cells. These results present a mechanism for T_h9 mediated neuronal damage through excitotoxicity. Blockage of the glutamate receptor AMPA, which can mediate excitotoxicity, in EAE mice led to an amelioration of the disease^{100,101}. Thereby, the degree of inflammation was not affected, but the

oligodendrocytes and neurons were influenced. Blockage of NMDA receptor in EAE mice also led to an amelioration of EAE. Here, the proposed mechanism was disruption of the BBB by NMDA receptor mediated mechanisms¹³⁰. In MS, it was shown that enhanced glutamate production in brain lesions correlated with increased axonal damage¹³¹.

Taken together, excitotoxicity is an important pathophysiological process in EAE and MS. Our experiment suggests a T_h9 mediated, neurodamaging mechanism in form of the secretion of glutamate. Previous results in our lab (S. Ray, K. Forsberg, F. Bischof unpublished results) showed that the supernatant of T_h9 cells is able to damage neurons. Glutamate as indicated in our experiments (see 3.4.2), is most likely one of the mediators of this damage. This mechanism could also play a role *in vivo* in diseases such as MS.

Further experiments might include the measurement of the secreted glutamate by T_h9 cells. Finally, the limitation of our T_h9 cell culture needs to be noted, as already discussed in 4.1.1.

4.4.3 The effect of CCL7, CCL11 and IL-9 on neuronal Ca²⁺ levels

Our experiments did not reveal any increase of intracellular Ca²⁺ by CCL7, CCL11 or IL-9. Chemokines bind to GPCRs and can invoke intracellular Ca²⁺ rise by the mobilization of Ca²⁺ from intracellular stores (for a review see Bokoch¹³²). Transient intracellular Ca²⁺ rises have been shown to be induced by chemokines such as CCL2 and CCL11 in cerebellar neurons¹³³ and dorsal root ganglia (DRGs)¹³⁴ in cultures derived from neonatal rats. CCL2-induction of an intracellular Ca²⁺ rise has also been demonstrated in a variety of neuronal cells such as neurons from the cortex, hypothalamus, hippocampus and mesencephalon⁵⁸. There, the Ca²⁺ increased directly after the addition of the chemokines and lasted less than a minute. Thus, it was connected to the direct activation of neuronal chemokine receptors. CXCL10 was shown to induce neuronal apoptosis via the induction of intracellular Ca²⁺ increases¹³⁵.

IL-9 has not been connected to induction of Ca^{2+} rise in neurons, but CCL11 has been shown to (see above). There are several explanations for the lack of effect in our experiments:

The lack of reaction could be explained by a lack of functional receptors on our neuronal cells. This could be due to the very low expression of these receptors in our cultures under non-inflammatory conditions as already described in 4.3. Additionally, Gillard et al.¹³³ as well as Oh et al.¹³⁴ used neuronal cultures different from the ones we used. Gillard et al.¹³³ already described that only a small percentage of all the cells reacted to the chemokines added. Maybe the cortical neurons from our experiments contained none of the neuron types expressing the receptors necessary for an activation by CCL11. Finally, although CCL2 has been shown by several groups to invoke a transient intracellular Ca^{2+} rise^{58,133,134}, another group failed to show this Ca^{2+} response using differentiated neurons, derived from undifferentiated human teratocarcinoma cells (NT2.N)¹³⁶. This again highlights the difference of either using rat, human or mouse cells. In line with our findings, Coughlan et al.¹³⁶ reported no rise in intracellular Ca^{2+} when adding CCL7.

Another explanation for the lack of effect might be the experimental setup. The imaging lasted for a maximum of 25 minutes after the addition of the cytokines. Long-term effects such as gene transcription of Ca^{2+} channels need a longer time. Especially IL-9 is known to activate the JAK-STAT pathway amongst others and influence transcriptional processes¹³⁷. Extending the imaging process might solve this problem.

4.4.4 The enhancement of the glutamate-mediated increase of neuronal Ca^{2+} levels by CCL7 and IL-9

Pretreatment of neurons with CCL7 and IL-9 led to an enhancement of a glutamate mediated Ca^{2+} -rise (see 3.4.4.3 and 3.4.4.8). This enhancement was non-significant. Other samples did not show an effect. The non-significance due to neuronal heterogeneity has already been discussed in 4.4.1.

A modulation of glutamate-mediated intracellular Ca^{2+} rise in neurons has not been shown for any of the cytokines we studied. However, IL-9 was demonstrated to increase Ca^{2+}

transients induced by cholecystokinin-8 in interstitial cells of Cajal¹³⁸. Similar to our experiments, IL-9 does not induce an intracellular Ca^{2+} rise by itself, but enhances the Ca^{2+} rise induced by another agent.

Other cytokines have been associated with the modulation of Ca^{2+} dynamics in cultured neurons. The C-C chemokine CCL2 was shown to enhance the Ca^{2+} response mediated by an agonist of a metabotropic glutamate receptor (mGluR)¹³⁹ at a concentration of 25 nM. Higher and lower concentrations of CCL2 did not evoke this enhanced Ca^{2+} response. Our results yielded similar observations. While CCL7 did not reveal any effect at a concentration of 5 nM, it showed an effect at 50 nM. Similarly, IL-9 revealed an effect at a concentration of 5 nM, but not at 30 nM. In reverse, this indicates that the other samples, which did not reveal any enhance or decrease, might need to be tested with a broader range of cytokine concentrations. Some effects might not have been detected, due to the small range of cytokine concentrations used.

Another implication of the findings of Van Gassen et al.¹³⁹ is based on the usage of agonists of a mGluR. In our experimental setup, we used glutamate and thus we could not distinguish, which receptors are the ones that led to our results. Glutamate binds to a variety of receptors. The activation of many of those results in an increase in intracellular Ca^{2+} , either by functioning as an ion channel (NMDA, AMPA/kainate) or by influencing intracellular pathways via GPCRs such as mGluRs. For example, mGluRs can lead to an activation of phospholipase C and a release of Ca^{2+} from intracellular stores¹⁴⁰. Chemokines bind to GPCRs as well. Interactions between GPCRs and their pathways were shown to lead to increased Ca^{2+} responses compared to only activating a single receptor (for a review see Werry et al.¹⁴¹). In transfer to our results, this means an activation of the chemokine receptor by CCL7 could lead to an activation of phospholipase C¹⁴². This synergizes with the phospholipase C activation by glutamate via a mGluR such as mGluR1¹⁴³. Thus, the Ca^{2+} release from intracellular stores, such as the endoplasmic reticulum, could be increased.

Also, other receptors could be influenced. IL-6 was shown to enhance NMDA mediated Ca^{2+} rise in neurons¹⁴⁴. In line with our experiments, IL-6 was applied for several days

before measuring the intracellular Ca^{2+} . This enables a long-term regulation of glutamate receptors. For example, CCL7 or IL-9 might upregulate the NMDA receptor expression, consequently leading to increased Ca^{2+} responses.

A short-term regulation is also possible. CCL2 was shown to inhibit γ -aminobutyric acid (GABA)-induced currents in rat neurons, after being applied together with GABA¹⁴⁵. This indicates a modulatory effect of a C-C chemokine on ion channels. Furthermore, short-term CCL2 application increased the NMDA and AMPA receptor activity in DRG mouse neurons¹⁴⁶. Both experiments additionally demonstrated the CCR2 receptor expression on their neurons. Since CCL7 also binds to CCR2, our effect could be attributed to a short-term modulation of NMDA or AMPA receptors. Considering our cultures contained almost exclusively neurons, our observed effect indicates a CCL7 receptor expression on neurons.

Our experiments could not detect the absolute Ca^{2+} concentrations, but only the relative increases or decreases of each sample. Changes of basal Ca^{2+} levels could not be detected. Additionally, the origin of the increase in intracellular Ca^{2+} could not be shown. Further experiments might include the usage of a setup, which allows for an exact quantification of intracellular Ca^{2+} . Antagonists for single glutamate receptors could be used to determine, which receptor mediates the effect of CCL7 and IL-9. A shorter incubation time for CCL7 could be utilized or both glutamate and CCL7 could be applied at the same time in order to show, whether the effect results from a short-term modulation of glutamate receptors or a long-term one. Finally, a broader range of cytokine concentrations could be adopted, maybe even together with an inflammatory cytokine, to further test the effects of CCL7, CCL11 and IL-9.

Since the detection of this increase in Ca^{2+} does not necessarily correlate with an increase in excitotoxicity, further experiments were conducted to test this hypothesis (see 3.5). Nonetheless, our experiments indicate the influences of CCL7 and IL-9 on neuronal Ca^{2+} levels. Ca^{2+} is an important second messenger inside of cells and modulates a variety of processes including receptor modulation and metabolic pathways¹⁴⁷.

In conclusion, our results show that CCL7 and IL-9 influence Ca^{2+} levels in neurons after glutamate addition. Possible mechanisms of this increase include the modulation of NMDA receptors or the co-activation of GPCRs.

4.5 The effect of CCL7, CCL11 and IL-9 on glutamate-mediated excitotoxicity

Pre-treatment of neuronal cells with CCL7, CCL11 or IL-9 did not lead to increased or decreased excitotoxicity upon application of glutamate (see 3.5) even though CCL7 and IL-9 increased glutamergic excitation in our experiments (see 3.4.4.3 and 3.4.4.8). CCL11 has already been shown to possess neuroprotective properties¹¹³. However, Adzemovic et al.¹¹³ attributed these properties largely to the effect of CCL11 on immune cells. IL-9 and CCL7 have not been connected to excitotoxicity. Nevertheless, other ILs such as IL-6 were shown to be neuroprotective¹⁴⁸.

Possible explanations for this lack of effect include a lack of receptors on our neurons under non-inflammatory conditions amongst others. They were already discussed in 4.3. However, in 4.4.4 we showed that CCL7 and IL-9 do effect neurons, so at least some functional receptors for CCL7 and IL-9 must be present. Nonetheless, neither CCL7 nor IL-9 are sufficient to exacerbate or ameliorate excitotoxicity on their own, but they might enhance it in addition to other cytokines. For all three cytokines studied, future experiments could include the pre-treatment of neurons with several cytokines together or the induction of inflammatory conditions, prior to the application of the cytokines.

4.6 Detection of CCL7-, CCL11- and IL-9-mRNA in an EAE mouse model

Having shown that IL-9 induces the mRNA expression of CCL7 in astrocytes, we wanted to investigate the localisation of these cytokines in a neuroinflammatory model *in vivo*, as well as determine the role of $\text{T}_\text{H}9$ cells in this model. The contribution of this relatively new T_H subtype to EAE has not been studied much. However, it was discovered that this cell

type can induce EAE upon adoptive transfer²⁷. T_h9 cells were also recently connected with MS disease¹⁴⁹.

IL-9 has been studied more extensively. IL-9 deficient mice were resistant to EAE¹⁵⁰ and neutralization of IL-9 led to an amelioration of EAE⁹⁷. Both studies connected the inhibition of IL-9 to a reduction in IL-17. In contrast, recent studies, determining the role of IL-9 in MS disease, associated elevated levels of IL-9 in the cerebrospinal fluid and serum with remission from relapse remitting MS^{149,151,152}. As opposed to the EAE model, in MS IL-9 reduces the expression of IL-17 in T_h17 cells, suggesting a protective role for IL-9¹⁴⁹. This highlights the difference between EAE and MS as well as the ambiguity of IL-9, functioning both as an inflammatory and an anti-inflammatory cytokine²¹.

Our results showed no significant change in IL-9-mRNA expression in EAE mice compared to the controls (see 3.6). This is in line with the reports of reduced IL-9 levels in MS patients, but stands in contrast to the EAE studies as explained above. However, these results do not contradict the presence of T_h9 cells in our EAE model. First of all, the whole spinal cord was analysed. At the early stage of disease mice were sacrificed at, only a part of the spinal cord is affected by the inflammation. IL-9 could still be upregulated in this part of the spinal cord, while being downregulated in the rest, resulting effectively in no fold change visible in our graph. Secondly, IL-9 is produced by a variety of cells (see 1.1.2). Again, downregulation of IL-9 in some cell types could conceal an increase of IL-9 by an increase in T_h9 cells. Nonetheless, we refrained from further immunohistochemistry: While there was no definite indication of T_h9 cells not contributing to EAE, there was no indication of T_h9 cells contributing either.

Finally, CCL7-mRNA was increased in EAE mice significantly, while CCL11 was elevated non-significantly (see 3.6). Both CCL7¹⁵³ and CCL11¹¹³ have been detected in an EAE mouse model. Our results are in line with these observations. It is not surprising that these chemokines are upregulated, since they are needed to recruit inflammatory cells to the sites of inflammation in the early stages of the disease. In this experimental setup, the producers of these cytokines could not be detected and we could not connect the results of our

induction of CCL7 by IL-9 in astrocytes (see 3.2.1) of our *in vitro* experiments to the *in vivo* model.

5. Summary

Neuroinflammatory mechanisms play a crucial part in various diseases such as multiple sclerosis and stroke. Interactions of neuronal and immune cells result in impairment of the nervous system. A better understanding of these interactions could serve as the basis for better treatments of various neuroinflammatory disorders. T cells in general and T helper cells (T_h) in particular, contribute to this damaging process. One particular subset of IL-9 producing T_h cells, namely T helper type 9 (T_h9) cells has been recently characterized as a distinct subset of T_h cells^{7,8} and was found to cause neuronal deterioration in a T_h9 cell neuronal co-culture (S. Ray, K. Forsberg, F. Bischof, unpublished results). Thereby, a diversity of cytokines is upregulated in this co-culture including the C-C chemokines CCL7 and CCL11.

This work aims at identifying the potential roles of the cytokines CCL7, CCL11 and IL-9 in this T_h9 cell mediated neuronal damage. Primary neurons derived from embryonic or postnatal mice were cultured. Neuronal damage was assessed in form of cytoskeletal deterioration in an immunostaining and calcium (Ca^{2+}) levels of neurons were measured with a Ca^{2+} dependent fluorescent dye.

The results reveal that none of the studied cytokines damaged neurons by itself when exposing neurons to these cytokines. Also, none of the cytokines enhanced or decreased neuronal Ca^{2+} levels upon addition. However, CCL7 and IL-9 were observed to increase the glutamate-mediated Ca^{2+} rise in neurons after incubation for 48 h. Intracellular Ca^{2+} rise and overstimulation of neurons can lead to excitotoxicity and cell⁴⁵ death. However, neither CCL7 and CCL11 nor IL-9 were found to increase glutamate-mediated excitotoxicity.

All in all, these results show the potential of CCL7 and IL-9 to play a part in neurodamaging processes, while not being able to damage neurons on their own.

6. Summary (native language of the faculty)

Neuroinflammatorische Mechanismen spielen eine Schlüsselrolle in der Pathophysiologie verschiedener Krankheiten wie z.B. Multiple Sklerose oder Schlaganfall. Interaktionen zwischen neuronalen und Immunzellen führen zu einer Schädigung des Nervensystems. Ein besseres Verständnis dieser Interaktionen kann als Basis neuartiger Therapiemöglichkeiten dieser Krankheiten dienen. T-Zellen und speziell T-Helferzellen (T_h) tragen zu diesen schädigenden Mechanismen bei. Es wurde gezeigt, dass T-Helferzellen Typ 9 (T_h9), ein IL-9 produzierender Subtyp von T_h der kürzlich charakterisiert wurde^{7,8}, zu neuronaler Schädigung in einer Co-Kultur, bestehend aus Neuronen und T_h9 Zellen, führen (S. Ray, K. Forsberg, F. Bischof, unpublished results). Hierbei wurden die Gene diverser Zytokine hochreguliert, unter anderem die C-C Chemokine CCL7 und CCL11.

Die vorliegende Arbeit hat das Ziel die potentielle Rolle der Zytokine CCL7, CCL11 und IL-9 im Rahmen des T_h9 Zell-verursachten, neuronalen Schadens zu identifizieren. Hierfür wurden primäre Mausneuronen aus embryonalen und postnatalen Mäusen kultiviert. Neuronaler Schaden wurde mithilfe einer Immunfärbung des Zytoskeletts beurteilt. Zusätzlich wurden intrazelluläre, neuronale Calcium (Ca^{2+})-Level gemessen, mithilfe eines Ca^{2+} -abhängigen, fluoreszenten Farbstoffs.

Die Ergebnisse ergaben, dass keines der untersuchten Zytokine Neurone schädigt, wenn diese den Zytokinen ausgesetzt wurden. Ebenfalls führte keines der Zytokine zu einem Ca^{2+} -Einstrom in Neuronen. Weitere Ergebnisse zeigten einen Anstieg des Glutamat-induzierten Ca^{2+} -Einstroms durch Vorbehandlung mit CCL7 und IL-9 für 48 h. Ein Anstieg von intrazellulärem Ca^{2+} , in Form einer Überstimulation, kann zu Exzitotoxizität und Zelltod führen⁴⁵. Jedoch verursachten weder CCL7, noch CCL11 oder IL-9 eine Zunahme der durch Glutamat ausgelösten Exzitotoxizität

Zusammenfassend demonstrieren die vorliegenden Ergebnisse das Potential von CCL7 und IL-9 eine Rolle in Prozessen der neuronalen Schädigung zu spielen, auch wenn sie nicht in der Lage sind Neuronen selbst zu schädigen.

7. Literature

1. Rassow, J., Hauser, K., Netzker, R. & Deutzmann, R. *Duale Reihe Biochemie*. 3rd Edition, p. 677-680 (Georg Thieme Verlag KG, Stuttgart, 2012).
2. Murphy, K. M., Travers, P. & Walport, M. *Janeway Immunologie*. 7th Edition, p. 442-443 (Springer Spektrum, Berlin-Heidelberg, 2009).
3. Mosmann, T. R., Cherwinski, H., Bond, M. W., Giedlin, M. A. & Coffman, R. L. Two Types of Murine Helper T Cell Clone I. Definition According to Profiles of Lymphokine Activities and Secreted Proteins. *J. Immunol.* **136**, 2348–2357 (1986).
4. Schmitt, E., Van Brandwijk, R., Fischer, H. G. & Rude, E. Establishment of different T cell sublines using either interleukin 2 or interleukin 4 as growth factors. *Eur. J. Immunol.* **20**, 1709–1715 (1990).
5. Fiorentino, D. F., Bond, M. W. & Mosmann, T. R. Two types of mouse T helper cell. IV. Th2 clones secrete a factor that inhibits cytokine production by Th1 clones. *J. Exp. Med.* **170**, 2081–95 (1989).
6. Vahedi, G., Poholek, A., Hand, T. W., Laurence, A., Kann, Y., O’Shea, J. J. & Hirahara, K. Helper T Cell Identity and Evolution of Differential Transcriptomes and Epigenomes. *Immunol. Rev.* **252**, 24–40 (2013).
7. Veldhoen, M., Uyttenhove, C., Snick, J. Van, Helmby, H., Westendorf, A., Buer, J., Martin, B., Wilhelm, C. & Stockinger, B. Transforming growth factor- β ‘reprograms’ the differentiation of T helper 2 cells and promotes an interleukin 9 – producing subset. *Nat. Immunol.* **9**, 1341–1346 (2008).
8. Dardalhon, V., Awasthi, A., Kwon, H., Galileos, G., Gao, W., Sobel, R. A., Mitsdoerffer, M., Strom, T. B., Elyaman, W., Ho, I., Khoury, S., Oukka, M., Kuchroo, V. K., Street, L., Hospital, B. I. & Alto, P. Interleukin 4 inhibits TGF- β -induced-Foxp3⁺ T cells and generates, in combination with TGF- β , Foxp3⁻ effector T cells that produce interleukins 9 and 10. *Nat. Immunol.* **9**, 1347–1355 (2008).
9. Chang, H., Sehra, S., Goswami, R., Yao, W., Yu, Q., Stritesky, L., Jabeen, R., Mckinley, C., Ahyi, A., Han, L., Evelyn, T., Robertson, M. J., Perumal, N. B., Tepper, R. S., Stephen, L. & Kaplan, M. H. The transcription factor PU.1 is required for the development of interleukin 9-producing T cells and allergic inflammation. *Nat. Immunol.* **11**, 527–534 (2010).
10. Uyttenhove, C., Simpson, R. J. & Van Snick, J. Functional and structural characterization of P40, a mouse glycoprotein with T-cell growth factor activity. *Proc. Natl. Acad. Sci. U. S. A.* **85**, 6934–6938 (1988).
11. Van Snick, J., Goethals, A., Renauld, J. C., Van Roost, E., Uyttenhove, C., Rubira, M. R., Moritz, R. L. & Simpson, R. J. Cloning and characterization of a cDNA for a

- new mouse T cell growth factor (P40). *J. Exp. Med.* **169**, 363–368 (1989).
12. Hültner, L., Moeller, J., Schmitt, E., Jäger, G., Reisbach, G., Ring, J. & Dörmer, P. Thiol-sensitive mast cell lines derived from mouse bone marrow respond to a mast cell growth-enhancing activity different from both IL-3 and IL-4. *J. Immunol.* **142**, 3440–3446 (1989).
 13. Hültner, L., Druetz, C., Moeller, J., Uyttenhove, C., Schmitt, E., Rude, E., Dörmer, P. & Van Snick, J. Mast cell growth-enhancing activity (MEA) is structurally related and functionally identical to the novel mouse T cell growth factor P40/TCGFIII (interleukin 9). *Eur. J. Immunol.* **20**, 1413–1416 (1990).
 14. Moeller, J., Hültner, L., Schmitt, E., Breuer, M. & Dörmer, P. Purification of MEA, a mast cell growth-enhancing activity, to apparent homogeneity and its partial amino acid sequencing. *J. Immunol.* **144**, 4231–4234 (1990).
 15. Nowak, E. C., Weaver, C. T., Turner, H., Begum-Haque, S., Becher, B., Schreiner, B., Coyle, A. J., Kasper, L. H. & Noelle, R. J. IL-9 as a mediator of Th17-driven inflammatory disease. *J. Exp. Med.* **206**, 1653–60 (2009).
 16. Beriou, G., Bradshaw, E. M., Lozano, E., Costantino, C. M., Hastings, W. D., Orban, T., Elyaman, W., Khoury, S. J., Kuchroo, V. K., Baecher-Allan, C. & Hafler, D. A. TGF- Induces IL-9 Production from Human Th17 Cells. *J. Immunol.* **185**, 46–54 (2010).
 17. Stassen, M., Arnold, M., Hültner, L., Müller, C., Neudörfl, C., Reineke, T. & Schmitt, E. Murine bone marrow-derived mast cells as potent producers of IL-9: costimulatory function of IL-10 and kit ligand in the presence of IL-1. *J. Immunol.* **164**, 5549–5555 (2000).
 18. Gounni, A. S., Nutku, E., Koussih, L., Aris, F., Louahed, J., Levitt, R. C., Nicolaides, N. C. & Hamid, Q. IL-9 expression by human eosinophils: Regulation by IL-1 beta and TNF-alpha. *J. Allergy Clin. Immunol.* **106**, 460–466 (2000).
 19. Williams, D. E., Morrissey, P. J., Mochizuki, D. Y., de Vries, P., Anderson, D., Cosman, D., Boswell, H. S., Cooper, S., Grabstein, K. H. & Broxmeyer, H. E. T-cell growth factor P40 promotes the proliferation of myeloid cell lines and enhances erythroid burst formation by normal murine bone marrow cells in vitro. *Blood* **76**, 906–911 (1990).
 20. Fontaine, R. H., Cases, O., Lelièvre, V., Mesplès, B., Renaud, J.-C., Loron, G., Degos, V., Dournaud, P., Baud, O. & Gressens, P. IL-9/IL-9 receptor signaling selectively protects cortical neurons against developmental apoptosis. *Cell Death Differ.* **15**, 1542–1552 (2008).
 21. Elyaman, W., Bradshaw, E. M., Uyttenhove, C., Dardalhon, V., Awasthi, A., Imitola, J., Bettelli, E., Oukka, M., van Snick, J., Renaud, J.-C., Kuchroo, V. K. & Khoury, S. J. IL-9 induces differentiation of TH17 cells and enhances function of FoxP3+ natural regulatory T cells. *Proc. Natl. Acad. Sci. U. S. A.* **106**, 12885–12890

(2009).

22. Dugas, B., Renauld, J. C., Pène, J., Bonnefoy, J. Y., Peti-Frère, C., Braquet, P., Bousquet, J., Van Snick, J. & Mencia-Huerta, J. M. Interleukin-9 potentiates the interleukin-4-induced immunoglobulin (IgG, IgM and IgE) production by normal human B lymphocytes. *Eur. J. Immunol.* **23**, 1687–92 (1993).
23. Stephens, G. L., Swerdlow, B., Benjamin, E., Coyle, A. J., Humbles, A., Kolbeck, R. & Fung, M. IL-9 is a Th17-derived cytokine that limits pathogenic activity in organ-specific autoimmune disease. *Eur. J. Immunol.* **41**, 952–962 (2011).
24. Faulkner, H., Renauld, J., Snick, J. Van, Grecis, R. K. & Snick, J. V. a N. Interleukin-9 Enhances Resistance to the Intestinal Nematode *Trichuris muris*. *Infect. Immun.* **66**, 3832–3840 (1998).
25. Staudt, V., Bothur, E., Klein, M., Lingnau, K., Reuter, S., Grebe, N., Gerlitzki, B., Hoffmann, M., Ulges, A., Taube, C., Dehzad, N., Becker, M., Stassen, M., Steinborn, A., Lohoff, M., Schild, H., Schmitt, E. & Bopp, T. Interferon-Regulatory Factor 4 Is Essential for the Developmental Program of T Helper 9 Cells. *Immunity* **33**, 192–202 (2010).
26. Nicolaides, N. C., Holroyd, K. J., Ewart, S. L., Eleff, S. M., Kiser, M. B., Dragwa, C. R., Sullivan, C. D., Grasso, L., Zhang, L. Y., Messler, C. J., Zhou, T., Kleeberger, S. R., Buetow, K. H. & Levitt, R. C. Interleukin 9: a candidate gene for asthma. *Proc. Natl. Acad. Sci. U. S. A.* **94**, 13175–80 (1997).
27. Jäger, A., Dardalhon, V., Sobel, R. A., Bettelli, E. & Vijay Kuchroo. Th1, Th17, and Th9 effector cells induce experimental autoimmune encephalomyelitis with different pathological phenotypes. *J. Immunol.* **183**, 7169–7177 (2009).
28. Galea, I., Bechmann, I. & Perry, V. H. What is immune privilege (not)? *Trends Immunol.* **28**, 12–18 (2007).
29. Hauser, S. L., Bhan, A. K., Gilles, F. H., Hoban, C. J., Reinherz, E. L., Schlossman, S. F. & Weiner, H. L. Immunohistochemical staining of human brain with monoclonal antibodies that identify lymphocytes, monocytes, and the Ia antigen. *J. Neuroimmunol.* **5**, 197–205 (1983).
30. Wekerie, H., Linington, C., Lassmann, H. & Meyermann, R. Cellular immune reactivity within the CNS. *Trends Neurosci.* **9**, 271–277 (1986).
31. Hickey, W. F., Hsu, B. L. & Kimura, H. T-lymphocyte entry into the central nervous system. *J. Neurosci. Res.* **28**, 254–260 (1991).
32. Joseph, J., Lublin, F. D. & Knobler, R. L. Modulation of T cell-endothelial adhesion by astrocyte conditioned medium. *Glia* **21**, 408–412 (1997).
33. Ifergan, I., Kebir, H., Alvarez, J. I., Marceau, G., Bernard, M., Bourbonnere, L., Poirier, J., Duquette, P., Talbot, P. J., Arbour, N. & Prat, A. Central nervous system recruitment of effector memory CD8⁺ T lymphocytes during neuroinflammation is

dependent on $\alpha 4$ integrin. *Brain* **134**, 3560–3577 (2011).

34. Grabovsky, V., Feigelson, S., Chen, C., Bleijs, D. a, Peled, A., Cinamon, G., Baleux, F., Arenzana-Seisdedos, F., Lapidot, T., van Kooyk Y, Lobb, R. R. & Alon, R. Subsecond induction of alpha4 integrin clustering by immobilized chemokines stimulates leukocyte tethering and rolling on endothelial vascular cell adhesion molecule 1 under flow conditions. *J. Exp. Med.* **192**, 495–505 (2000).
35. Mauerhoff, T., Pujol-Borrell, R., Mirakian, R. & Bottazzo, G. F. Differential expression and regulation of major histocompatibility complex (MHC) products in neural and glial cells of the human fetal brain. *J. Neuroimmunol.* **18**, 271–289 (1988).
36. Maehlen, J., Schröder, H. D., Klareskog, L., Olsson, T. & Kristensson, K. Axotomy induces MHC class I antigen expression on rat nerve cells. *Neurosci. Lett.* **92**, 8–13 (1988).
37. Lindå, H., Hammarberg, H., Cullheim, S., Levinovitz, A., Khademi, M. & Olsson, T. Expression of MHC Class I and $\beta 2$ -Microglobulin in Rat Spinal Motoneurons: Regulatory Influences by IFN-Gamma and Axotomy. *Exp. Neurol.* **150**, 282–295 (1998).
38. Corriveau, R. a, Huh, G. S. & Shatz, C. J. Regulation of class I MHC gene expression in the developing and mature CNS by neural activity. *Neuron* **21**, 505–520 (1998).
39. Huh, G. S., Boulanger, L. M., Du, H., Riquelme, P. A., Brotz, T. M. & Shatz, C. J. Functional Requirement for Class I MHC in CNS Development and Plasticity. *Science (80-.)*. **290**, 2155–2159 (2015).
40. Hayes, G. M., Woodroffe, M. N. & Cuzner, M. L. Microglia are the major cell type expressing MHC class II in human white matter. *J. Neurol. Sci.* **80**, 25–37 (1987).
41. Wong, G. H. W., Bartlett, P. F., Clark-Lewis, I., McKimm-Breschkin, J. L. & Schrader, J. W. Interferon- γ induces the expression of H-2 and Ia antigens on brain cells. *Nature* **310**, 688–691 (1984).
42. Liu, Y., Teige, I., Birnir, B. & Issazadeh-Navikas, S. Neuron-mediated generation of regulatory T cells from encephalitogenic T cells suppresses EAE. *Nat. Med.* **12**, 518–525 (2006).
43. Yang, J. F., Tao, H. Q., Liu, Y. M., Zhan, X. X., Liu, Y., Wang, X. Y., Wang, J. H., Mu, L. L., Yang, L. L., Gao, Z. M., Kong, Q. F., Wang, G. Y., Han, J. H., Sun, B. & Li, H. L. Characterization of the interaction between astrocytes and encephalitogenic lymphocytes during the development of experimental autoimmune encephalomyelitis (EAE) in mice. *Clin. Exp. Immunol.* **170**, 254–265 (2012).
44. Mizuno, T., Zhang, G., Takeuchi, H., Kawanokuchi, J., Wang, J., Sonobe, Y., Jin, S., Takada, N., Komatsu, Y. & Suzumura, A. Interferon-gamma directly induces

- neurotoxicity through a neuron specific, calcium-permeable complex of IFN-gamma receptor and AMPA GluR1 receptor. *FASEB J.* **22**, 1797–1806 (2008).
45. Kandel, E. R., Schwartz, J. H., Jessell, T. M., Siegelbaum, S. A. & Hudspeth, A. J. *Principles of Neural Science*. 5th Edition, p. 1134 (McGraw-Hill Education Medical, 2013).
 46. Benveniste, H., Drejer, J., Schousboe, a & Diemer, N. H. Elevation of the extracellular concentrations of glutamate and aspartate in rat hippocampus during transient cerebral ischemia monitored by intracerebral microdialysis. *J. Neurochem.* **43**, 1369–1374 (1984).
 47. Kebir, H., Kreymborg, K., Ifergan, I., Dodelet-Devillers, A., Cayrol, R., Bernard, M., Giuliani, F., Arbour, N., Becher, B. & Prat, A. Human TH17 lymphocytes promote blood-brain barrier disruption and central nervous system inflammation. *Nat. Med.* **13**, 1173–1175 (2007).
 48. Giuliani, F., Goodyer, C. G., Antel, J. P. & Yong, V. W. Vulnerability of human neurons to T cell-mediated cytotoxicity. *J. Immunol.* **171**, 368–379 (2003).
 49. Nitsch, R., Pohl, E. E., Smorodchenko, A., Infante-Duarte, C., Aktas, O. & Zipp, F. Direct Impact of T Cells on Neurons Revealed by Two-Photon Microscopy in Living Brain Tissue. *J. Neurosci.* **24**, 2458–2464 (2004).
 50. Kaltschmidt, C., Kaltschmidt, B. & Baeuerle, P. A. Stimulation of ionotropic glutamate receptors activates transcription factor NF-kappa B in primary neurons. *Proc. Natl. Acad. Sci. U. S. A.* **92**, 9618–22 (1995).
 51. Kerschensteiner, M., Gallmeier, E., Behrens, L., Leal, V. V., Misgeld, T., Klinkert, W. E., Kolbeck, R., Hoppe, E., Oropeza-Wekerle, R. L., Bartke, I., Stadelmann, C., Lassmann, H., Wekerle, H. & Hohlfeld, R. Activated human T cells, B cells, and monocytes produce brain-derived neurotrophic factor in vitro and in inflammatory brain lesions: a neuroprotective role of inflammation? *J. Exp. Med.* **189**, 865–870 (1999).
 52. Moalem, G., Leibowitz-Amit, R., Yoles, E., Mor, F., Cohen, I. R. & Schwartz, M. Autoimmune T cells protect neurons from secondary degeneration after central nervous system axotomy. *Nat. Med.* **5**, 49–55 (1999).
 53. Ishii, H., Jin, X., Ueno, M., Tanabe, S., Kubo, T., Serada, S., Naka, T. & Yamashita, T. Adoptive transfer of Th1-conditioned lymphocytes promotes axonal remodeling and functional recovery after spinal cord injury. *Cell Death Dis.* **3**, e363 (2012).
 54. Rollins, B. J. Chemokines. *Blood* **90**, 909–928 (1997).
 55. Huang, D. R., Wang, J., Kivisakk, P., Rollins, B. J. & Ransohoff, R. M. Absence of monocyte chemoattractant protein 1 in mice leads to decreased local macrophage recruitment and antigen-specific T helper cell type 1 immune response in experimental autoimmune encephalomyelitis. *J. Exp. Med.* **193**, 713–726 (2001).

56. McManus, C., Berman, J. W., Brett, F. M., Staunton, H., Farrell, M. & Brosnan, C. F. MCP-1, MCP-2 and MCP-3 expression in multiple sclerosis lesions: An immunohistochemical and in situ hybridization study. *J. Neuroimmunol.* **86**, 20–29 (1998).
57. Banisadr, G., Queraud-Lesaux, F., Boutterin, M. C., Pelaprat, D., Zalc, B., Rostene, W., Haour, F. & Parsadaniantz, S. M. Distribution, cellular localization and functional role of CCR2 chemokine receptors in adult rat brain. *J. Neurochem.* **81**, 257–269 (2002).
58. Banisadr, G., Gosselin, R. D., Mechighel, P., Rostene, W., Kitabgi, P. & Parsadaniantz, S. M. Constitutive neuronal expression of CCR2 chemokine receptor and its colocalization with neurotransmitters in normal rat brain: Functional effect of MCP-1/CCL2 on calcium mobilization in primary cultured neurons. *J. Comp. Neurol.* **492**, 178–192 (2005).
59. Bezzi, P., Domercq, M., Brambilla, L., Galli, R., Schols, D., De Clercq, E., Vescovi, a, Bagetta, G., Kollias, G., Meldolesi, J. & Volterra, a. CXCR4-activated astrocyte glutamate release via TNF α : amplification by microglia triggers neurotoxicity. *Nat. Neurosci.* **4**, 702–710 (2001).
60. Vyshkina, T., Shugart, Y. Y., Birnbaum, G., Leist, T. P. & Kalman, B. Association of haplotypes in the beta-chemokine locus with multiple sclerosis. *Eur. J. Hum. Genet.* **13**, 240–247 (2005).
61. Van Damme, J., Proost, P., Lenaerts, J. P. & Opdenakker, G. Structural and functional identification of two human, tumor-derived monocyte chemotactic proteins (MCP-2 and MCP-3) belonging to the chemokine family. *J. Exp. Med.* **176**, 59–65 (1992).
62. Pype, J. L., Dupont, L. J., Menten, P., Coillie, E. Van, Opdenakker, G., Damme, J. Van, Chung, K. F., Demedts, M. G., Verleden, G. M., Chung, K. F., Demedts, M. G. & Expression, G. M. V. MCP-3 by Human Airway Smooth-Muscle Cells Modulation by Corticosteroids and T-Helper 2 Cytokines likely to play a critical role in the generation and regulation of the inflammatory response characteristic of. *Am. J. Respir. Cell Mol. Biol.* **21**, 528–536 (1999).
63. Renner, N. A., Ivey, N. S., Redmann, R. K., Lackner, A. A. & MacLean, A. G. MCP-3/CCL7 production by astrocytes: Implications for SIV neuroinvasion and AIDS encephalitis. *J. Neurovirol.* **17**, 146–152 (2011).
64. Loetscher, P., Seitz, M., Clark-Lewis, I., Baggiolini, M. & Moser, B. Monocyte chemotactic proteins MCP-1, MCP-2, and MCP-3 are major attractants for human CD4⁺ and CD8⁺ T lymphocytes. *FASEB J.* **8**, 1055–1060 (1994).
65. Sozzani, S., Sallusto, F., Luini, W., Zhou, D., Piemonti, L., Allavena, P., Van Damme, J., Valitutti, S., Lanzavecchia, A. & Mantovani, A. Migration of dendritic cells in response to formyl peptides, C5a, and a distinct set of chemokines. *J.*

- Immunol.* **155**, 3292–3295 (1995).
66. Sozzani, S., Rieppi, M., Locati, M., Zhou, D., Bussolino, F., Proost, P., Damme, J. Van & Mantovani, A. Synergism between platelet activating factor and c-c chemokines for arachidonate release in human monocytes. *Biochem. Biophys. Res. Commun.* **199**, 761–766 (1994).
 67. Loetscher, P., Seitz, M., Clark-Lewis, I., Baggiolini, M. & Moser, B. Activation of NK cells by CC chemokines. Chemotaxis, Ca²⁺ mobilization, and enzyme release. *J. Immunol.* **156**, 322–327 (1996).
 68. Bandyopadhyay, S., Jeong, K.-H., Hansen, J. T., Vassilev, P. M., Brown, E. M. & Chattopadhyay, N. Calcium-Sensing Receptor Stimulates Secretion of an Interferon- γ -Induced Monokine (CXCL10) and Monocyte Chemoattractant Protein-3 in Immortalized GnRH Neurons. *J. Neurosci. Res.* **85**, 882–895 (2007).
 69. Karrer, M., Lopez, M. A., Meier, D., Mikhail, C., Ogunshola, O. O., Müller, A. F., Strauss, L., Tafti, M. & Fontana, A. Cytokine-induced sleep: Neurons respond to TNF with production of chemokines and increased expression of Homer1a in vitro. *Brain. Behav. Immun.* **47**, 186–192 (2015).
 70. Bhardwaj, D., Náger, M., Camats, J., David, M., Benguria, A., Dopazo, A., Cantí, C. & Herreros, J. Chemokines induce axon outgrowth downstream of Hepatocyte Growth Factor and TCF/ β -catenin signaling. *Front. Cell. Neurosci.* **7**, 2–10 (2013).
 71. Edman, L. C., Mira, H. & Arenas, E. The beta-chemokines CCL2 and CCL7 are two novel differentiation factors for midbrain dopaminergic precursors and neurons. *Exp. Cell Res.* **314**, 2123–2130 (2008).
 72. Ying, S., Tabordabarata, L., Meng, Q., Humbert, M. & Kay, A. B. The Kinetics of Allergen-Induced Transcription of Messenger-Rna for Monocyte Chemotactic Protein-3 and Rantes in the Skin of Human Atopic Subjects: Relationship to Eosinophil, T-Cell, and Macrophage Recruitment. *J. Exp. Med.* **181**, 2153–2159 (1995).
 73. Jose, P. J., Griffiths-Johnson, D. A., Collins, P. D., Walsh, D. T., Moqbel, R., Totty, N. F., Truong, O., Hsuan, J. J. & Williams, T. J. Eotaxin: a potent eosinophil chemoattractant cytokine detected in a guinea pig model of allergic airways inflammation. *J. Exp. Med.* **179**, 881–887 (1994).
 74. Garcia-Zepeda, E. A., Rothenberg, M. E., Ownbey, R. T., Celestin, J., Leder, P. & Luster, A. D. Human eotaxin is a specific chemoattractant for eosinophil cells and provides a new mechanism to explain tissue eosinophilia. *Nat. Med.* **2**, 449–456 (1996).
 75. Ponath, P. D., Qin, S., Ringler, D. J., Clark-Lewis, I., Wang, J., Kassam, N., Smith, H., Shi, X., Gonzalo, J. A., Newman, W., Gutierrez-Ramos, J. C. & Mackay, C. R. Cloning of the human eosinophil chemoattractant, eotaxin: Expression, receptor binding, and functional properties suggest a mechanism for the selective recruitment

- of eosinophils. *J. Clin. Invest.* **97**, 604–612 (1996).
76. Bartels, J., Schlueter, C., Richter, E., Noso, N., Kulke, R., Christophers, E. & Schroeder, J.-M. Human Dermal Fibroblasts Express Eotaxin : Molecular Cloning , mRNA Expression , and Identification of Eotaxin Sequence Variants. *Biochem. Biophys. Res. Commun.* **225**, 1045–1051 (1996).
 77. Sozzani, S., Luini, W., Borsatti, A., Polentarutti, N., Zhou, D., Piemonti, L., D’Amico, G., Power, C. A., Wells, T. N., Gobbi, M., Allavena, P. & Mantovani, A. Receptor expression and responsiveness of human dendritic cells to a defined set of CC and CXC chemokines. *J. Immunol.* **159**, 1993–2000 (1997).
 78. Ugucioni, M., Mackay, C. R., Ochensberger, B., Loetscher, P., Rhee, S., LaRosa, G. J., Rao, P., Ponath, P. D., Baggiolini, M. & Dahinden, C. A. High expression of the chemokine receptor CCR3 in human blood basophils. Role in activation by eotaxin, MCP-4, and other chemokines. *J. Clin. Invest.* **100**, 1137–1143 (1997).
 79. Elsner, J., Hochstetter, R., Kimmig, D. & Kapp, A. Human eotaxin represents a potent activator of the respiratory burst of human eosinophils. *Eur J Immunol* **26**, 1919–1925 (1996).
 80. Hohki, G., Terada, N., Hamano, N. & Konno, A. The effects of eotaxin on the surface adhesion molecules of endothelial cells and on eosinophil adhesion to microvascular endothelial cells. *Biochem. Biophys. Res. Commun.* **241**, 136–141 (1997).
 81. Lamkhioued, B., Renzi, P. M., Abi-Younes, S., Garcia-Zepeda, E. A., Allakhverdi, Z., Ghaffar, O., Rothenberg, M. D., Luster, A. D. & Hamid, Q. Increased expression of eotaxin in bronchoalveolar lavage and airways of asthmatics contributes to the chemotaxis of eosinophils to the site of inflammation. *J. Immunol.* **159**, 4593–4601 (1997).
 82. Minshall, E. M., Cameron, L., Lavigne, F., Leung, D. Y., Hamilos, D., Garcia-Zepeda, E. a, Rothenberg, M., Luster, a D. & Hamid, Q. Eotaxin mRNA and protein expression in chronic sinusitis and allergen-induced nasal responses in seasonal allergic rhinitis. *Am. J. Respir. Cell Mol. Biol.* **17**, 683–90 (1997).
 83. Tanaka, M., Matsushita, T., Tateishi, T., Ochi, H., Kawano, Y., Mei, F. J., Minohara, M., Murai, H. & Kira, J. I. Distinct CSF cytokine/chemokine profiles in atopic myelitis and other causes of myelitis. *Neurology* **71**, 974–981 (2008).
 84. Maysami, S., Nguyen, D., Zobel, F., Heine, S., Hoepfner, M. & Stangel, M. Oligodendrocyte precursor cells express a functional chemokine receptor CCR3: Implications for myelination. *J. Neuroimmunol.* **178**, 17–23 (2006).
 85. Villeda, S. a, Luo, J., Mosher, K. I., Zou, B., Britschgi, M., Bieri, G., Stan, T. M., Fainberg, N., Ding, Z., Eggel, A., Lucin, K. M., Czirr, E., Park, J.-S., Couillard-Després, S., Aigner, L., Li, G., Peskind, E. R., Kaye, J. a, Quinn, J. F., *et al.* The ageing systemic milieu negatively regulates neurogenesis and cognitive function.

Nature **477**, 90–94 (2011).

86. Parajuli, B., Horiuchi, H., Mizuno, T., Takeuchi, H. & Suzumura, A. CCL11 enhances excitotoxic neuronal death by producing reactive oxygen species in microglia. *Glia* **63**, 2274–2284 (2015).
87. Adzemovic, M. Z., Öckinger, J., Zeitelhofer, M., Hochmeister, S., Beyeen, A. D., Paulson, A., Gillett, A., Hedreul, M. T., Covacu, R., Lassmann, H., Olsson, T. & Jagodic, M. Expression of Ccl11 associates with immune response modulation and protection against neuroinflammation in rats. *PLoS One* **7**, 1–12 (2012).
88. Mumenthaler, M. & Mattle, H. *Neurologie*. 12th Edition, pp. 401 (Georg Thieme Verlag KG, Stuttgart, 2008).
89. Robinson, A. P., Harp, C. T., Noronha, A. & Miller, S. D. The experimental autoimmune encephalomyelitis (EAE) model of MS: utility for understanding disease pathophysiology and treatment. *Handb Clin Neurol*. **122**, 173–189 (2014).
90. Stromnes, I. M. & Goverman, J. M. Active induction of experimental allergic encephalomyelitis. *Nat. Protoc.* **1**, 1810–1819 (2006).
91. Stromnes, I. M. & Goverman, J. M. Passive induction of experimental allergic encephalomyelitis. *Nat. Protoc.* **1**, 1952–1960 (2006).
92. Ben-Nun, A., Wekerle, H. & Cohen, I. R. The rapid isolation of clonable antigen-specific T lymphocyte lines capable of mediating autoimmune encephalomyelitis. *Eur. J. Immunol.* **11**, 195–199 (1981).
93. Ando, D. G., Clayton, J., Kono, D., Urban, J. L. & Sercarz, E. E. Encephalitogenic T cells in the B10.PL model of experimental allergic encephalomyelitis (EAE) are of the Th-1 lymphokine subtype. *Cell. Immunol.* **124**, 132–143 (1989).
94. Langrish, C. L., Chen, Y., Blumenschein, W. M., Mattson, J., Basham, B., Sedgwick, J. D., McClanahan, T., Kastelein, R. A. & Cua, D. J. IL-23 drives a pathogenic T cell population that induces autoimmune inflammation. *J. Exp. Med.* **201**, 233–40 (2005).
95. O'Connor, R. A., Prendergast, C. T., Sabatos, C. A., Lau, C. W. Z., Leech, M. D., Wraith, D. C. & Anderton, S. M. Cutting edge: Th1 cells facilitate the entry of Th17 cells to the central nervous system during experimental autoimmune encephalomyelitis. *J. Immunol.* **181**, 3750–3754 (2008).
96. Cua, D. J., Sherlock, J., Chen, Y., Murphy, C. a, Joyce, B., Seymour, B., Lucian, L., To, W., Kwan, S., Churakova, T., Zurawski, S., Wiekowski, M., Lira, S. a, Gorman, D., Kastelein, R. a & Sedgwick, J. D. Interleukin-23 rather than interleukin-12 is the critical cytokine for autoimmune inflammation of the brain. *Nature* **421**, 744–748 (2003).
97. Li, H., Nourbakhsh, B., Ciric, B., Zhang, G.-X. & Abdolmohamad Rostami. Neutralization of IL-9 ameliorates experimental autoimmune encephalomyelitis by

- decreasing the effector T cell population. *J. Immunol.* **185**, 4095–4100 (2010).
98. Vogt, J., Paul, F., Aktas, O., Mueller-Wielsch, K., Doerr, J., Doerr, S., Suman Bharathi, B., Glumm, R., Schmitz, C., Steinbusch, H., Raine, C. S., Tsokos, M., Nitsch, R. & Zipp, F. Lower motor neuron loss in multiple sclerosis and experimental autoimmune encephalomyelitis. *Ann. Neurol.* **66**, 310–322 (2009).
 99. Yu, W. & Miller, R. F. NBQX, an improved non-NMDA antagonist studied in retinal ganglion cells. *Brain Res.* **692**, 190–194 (1995).
 100. Pitt, D., Werner, P. & Raine, C. S. Glutamate excitotoxicity in a model of multiple sclerosis. *Nat. Med.* **6**, 67–70 (2000).
 101. Smith, T., Groom, a, Zhu, B. & Turski, L. Autoimmune encephalomyelitis ameliorated by AMPA antagonists. *Nat. Med.* **6**, 62–66 (2000).
 102. Siffrin, V., Radbruch, H., Glumm, R., Niesner, R., Paterka, M., Herz, J., Leuenberger, T., Lehmann, S. M., Luenstedt, S., Rinnenthal, J. L., Laube, G., Luche, H., Lehnardt, S., Fehling, H. J., Griesbeck, O. & Zipp, F. In Vivo Imaging of Partially Reversible Th17 Cell-Induced Neuronal Dysfunction in the Course of Encephalomyelitis. *Immunity* **33**, 424–436 (2010).
 103. Yednock TA , Cannon C , Fritz LC , Sanchez-Madrid F , Steinman L, K. N. Prevention of experimental autoimmune encephalomyelitis by antibodies against alpha 4 beta 1 integrin. *Nature* **356**, 63–66 (1992).
 104. Gold, R., Linington, C. & Lassmann, H. Understanding pathogenesis and therapy of multiple sclerosis via animal models: 70 Years of merits and culprits in experimental autoimmune encephalomyelitis research. *Brain* **129**, 1953–1971 (2006).
 105. Selmaj, K., Raine, C. S. & Cross, A. H. Anti-tumor necrosis factor therapy abrogates autoimmune demyelination. *Ann. Neurol.* **30**, 694–700 (1991).
 106. Van Oosten, B. W., Barkhof, F., Truyen, L., Boringa, J. B., Bertelsmann, F. W., Von Blomberg, B. M. E., Woody, J. N., Hartung, H. P. & Polman, C. H. Increased MRI activity and immune activation in two multiple sclerosis patients treated with the monoclonal anti-tumor necrosis factor antibody cA2. *Neurology* **47**, 1531–1534 (1996).
 107. Beaudoin, G. M. J., Lee, S.-H., Singh, D., Yuan, Y., Ng, Y.-G., Reichardt, L. F. & Arikath, J. Culturing pyramidal neurons from the early postnatal mouse hippocampus and cortex. *Nat. Protoc.* **7**, 1741–1754 (2012).
 108. Livak, K. J. & Schmittgen, T. D. Analysis of relative gene expression data using real-time quantitative PCR and the 2⁻deltadeltaCt Method. *Methods* **25**, 402–408 (2001).
 109. Miller, S. D., Karpus, W. J. & Davidson, T. S. Experimental Autoimmune Encephalomyelitis in the Mouse. *Curr Protoc Immunol.* 1–26 (2007).

110. Iliev, A. I., Stringaris, A. K., Nau, R. & Neumann, H. Neuronal injury mediated via stimulation of microglial toll-like receptor-9 (TLR9). *FASEB J.* **18**, 412–414 (2004).
111. Kim, Y., Kim, Y. S., Noh, M., Lee, H., Joe, B., Kim, H. Y., Kim, J., Kim, S. H. & Park, J. Neuroprotective effects of a novel poly (ADP- - ribose) 289 , in hypoxic rat cortical neurons. *Clin. Exp. Pharmacol. Physiol.* **44**, 671–679 (2017).
112. Thompson, W. L. & Van Eldik, L. J. Inflammatory cytokines stimulate the chemokines CCL2/MCP-1 and CCL7/MCP-3 through NFκB and MAPK dependent pathways in rat astrocytes. *Brain Res.* **1287**, 47–57 (2009).
113. Adzemovic, M. Z., Öckinger, J., Zeitelhofer, M., Hochmeister, S., Beyeen, A. D., Paulson, A., Gillett, A., Hedreul, M. T., Covacu, R., Lassmann, H., Olsson, T. & Jagodic, M. Expression of Ccl11 associates with immune response modulation and protection against neuroinflammation in rats. *PLoS One* **7**, e39794 (2012).
114. Luo, Y., Berman, M. A., Zhai, Q., Fischer, F. R., Abromson-Leeman, S. R., Zhang, Y., Kuziel, W. A., Gerard, C. & Dorf, M. E. RANTES stimulates inflammatory cascades and receptor modulation in murine astrocytes. *Glia* **39**, 19–30 (2002).
115. Ding, X., Cao, F., Cui, L., Ciric, B., Zhang, G. X. & Rostami, A. IL-9 signaling affects central nervous system resident cells during inflammatory stimuli. *Exp. Mol. Pathol.* **99**, 570–574 (2015).
116. Sui, Y., Potula, R., Dhillon, N., Pinson, D., Li, S., Nath, A., Anderson, C., Turchan, J., Kolson, D., Narayan, O. & Buch, S. Neuronal apoptosis is mediated by CXCL10 overexpression in simian human immunodeficiency virus encephalitis. *Am. J. Pathol.* **164**, 1557–1566 (2004).
117. Peterson, K. E., Errett, J. S., Wei, T., Derek, E., Ransohoff, R., Kuziel, W. A., Chesebro, B., Dimcheff, D. E. & Evans, L. MCP-1 and CCR2 Contribute to Non-Lymphocyte-Mediated Brain Disease Induced by Fr98 Polytopic Retrovirus Infection in Mice : Role for Astrocytes in Retroviral Neuropathogenesis MCP-1 and CCR2 Contribute to Non-Lymphocyte-Mediated Brain Disease Induced by. *J. Virol.* **78**, 6449–6458 (2004).
118. Madrigal, J. L., Leza, J. C., Polak, P., Kalinin, S. & Feinstein, D. L. Astrocyte-derived MCP-1 mediates neuroprotective effects of noradrenaline. *J Neurosci* **29**, 263–267 (2009).
119. Chiu, K., Yeung, S.-C., So, K.-F. & Chang, R. C.-C. Modulation of morphological changes of microglia and neuroprotection by monocyte chemoattractant protein-1 in experimental glaucoma. *Cell. Mol. Immunol.* **7**, 61–8 (2010).
120. Patkai, J., Mesples, B., Dommergues, M. a, Fromont, G., Thornton, E. M., Renauld, J. C., Evrard, P. & Gressens, P. Deleterious effects of IL-9-activated mast cells and neuroprotection by antihistamine drugs in the developing mouse brain. *Pediatr. Res.* **50**, 222–230 (2001).

121. Weber, K. S. C., Nelson, P. J., Gro, H. & Weber, C. Expression of CCR2 by Endothelial Cells: Implications for MCP-1 Mediated Wound Injury Repair and In Vivo Inflammatory Activation of Endothelium. *Arter. Thromb Vasc Biol.* **19**, 2085–2093 (1999).
122. Gee, K. R., Brown, K. A., Chen, W. N., Bishop-Stewart, J., Gray, D. & Johnson, I. Chemical and physiological characterization of fluo-4 Ca(2+)-indicator dyes. *Cell Calcium* **27**, 97–106 (2000).
123. Aoki, C., Venkatesan, C., Go, C.-G., Mong, J. A. & Dawson, T. M. Cellular and Subcellular Localization of NMDA-RI Subunit Immunoreactivity in the Visual Cortex of Adult and Neonatal Rats. *J. Neurosci.* **14**, 5202–5222 (1994).
124. Conti, F., Minelli, A., Molnar, M. & Brecha, N. C. Cellular localization and laminar distribution of NMDAR1 mRNA in the rat cerebral cortex. *J. Comp. Neurol.* **343**, 554–565 (1994).
125. Kaech, S. & Banker, G. Culturing hippocampal neurons. *Nat. Protoc.* **1**, 2406–2415 (2007).
126. Schipke, C. G., Ohlemeyer, C., Matyash, M., Nolte, C., Kettenmann, H. & Kirchhoff, F. Astrocytes of the mouse neocortex express functional N-methyl-D-aspartate receptors. *FASEB J.* **15**, 1270–1272 (2001).
127. Jensen, A. M. & Chiu, S. Y. Fluorescence measurement of changes in intracellular calcium induced by excitatory amino acids in cultured cortical astrocytes. *J. Neurosci.* **10**, 1165–1175 (1990).
128. Johnson, J. W. & Ascher, P. Glycine potentiates the NMDA response in cultured mouse brain neurons. *Nature* **325**, 529–531 (1987).
129. Garg, S. K., Banerjee, R. & Kipnis, J. Neuroprotective immunity: T cell-derived glutamate endows astrocytes with a neuroprotective phenotype. *J. Immunol.* **180**, 3866–3873 (2008).
130. Bolton, C. & Paul, C. MK-801 limits neurovascular dysfunction during experimental allergic encephalomyelitis. *J. Pharmacol. Exp. Ther.* **282**, 397–402 (1997).
131. Werner, P., Pitt, D. & Raine, C. S. Multiple sclerosis: Altered glutamate homeostasis in lesions correlates with oligodendrocyte and axonal damage. *Ann. Neurol.* **50**, 169–180 (2001).
132. Gary M. Bokoch. Chemoattractant Signaling and Leukocyte Activation. *Blood* **86**, 1649–1660 (1995).
133. Gillard, S. E., Lu, M., Mastracci, R. M. & Miller, R. J. Expression of functional chemokine receptors by rat cerebellar neurons. *J. Neuroimmunol.* **124**, 16–28 (2002).
134. Oh, S. B., Tran, P. B., Gillard, S. E., Hurley, R. W., Hammond, D. L. & Miller, R. J. Chemokines and glycoprotein120 produce pain hypersensitivity by directly exciting

- primary nociceptive neurons. *J. Neurosci.* **21**, 5027–5035 (2001).
135. Sui, Y., Stehno-Bittel, L., Li, S., Loganathan, R., Dhillon, N. K., Pinson, D., Nath, A., Kolson, D., Narayan, O. & Buch, S. CXCL10-induced cell death in neurons: Role of calcium dysregulation. *Eur. J. Neurosci.* **23**, 957–964 (2006).
 136. Coughlan, C. M., McManus, C. M., Sharron, M., Gao, Z., Murphy, D., Jaffer, S., Choe, W., Chen, W., Hesselgesser, J., Gaylord, H., Kalyuzhny, a, Lee, V. M., Wolf, B., Doms, R. W. & Kolson, D. L. Expression of multiple functional chemokine receptors and monocyte chemoattractant protein-1 in human neurons. *Neuroscience* **97**, 591–600 (2000).
 137. Knoops, L. & Renauld, J.-C. IL-9 and its receptor: from signal transduction to tumorigenesis. *Growth factors* **22**, 207–215 (2004).
 138. Gong, Y., Huang, L., Cheng, W., Li, X., Lu, J., Lin, L. & Si, X. Roles of Interleukin-9 in the Growth and Cholecystokinin-Induced Intracellular Calcium Signaling of Cultured Interstitial Cells of Cajal. *PLoS One* **9**, 1–9 (2014).
 139. Van Gassen, K. L. I., Netzeband, J. G., De Graan, P. N. E. & Gruol, D. L. The chemokine CCL2 modulates Ca²⁺ dynamics and electrophysiological properties of cultured cerebellar Purkinje neurons. *Eur. J. Neurosci.* **21**, 2949–2957 (2005).
 140. Heinrich, P., Müller, M. & Graeve, L. *Löffler/Petrides Biochemie und Pathobiochemie*. 9th Edition, p. 976-977 (Springer-Verlag, Berlin Heidelberg, 2014).
 141. Werry, T. D., Wilkinson, G. F. & Willars, G. B. Mechanisms of cross-talk between G-protein-coupled receptors resulting in enhanced release of intracellular Ca²⁺. *Biochem. J.* **374**, 281–296 (2003).
 142. Wu, D., Huang, C. K. & Jiang, H. Roles of phospholipid signaling in chemoattractant-induced responses. *J. Cell Sci.* **113**, 2935–2940 (2000).
 143. Netzeband, J. G., Parsons, K. L., Sweeney, D. D. & Gruol, D. L. Metabotropic glutamate receptor agonists alter neuronal excitability and Ca²⁺ levels via the phospholipase C transduction pathway in cultured Purkinje neurons. *J. Neurophysiol.* **78**, 63–75 (1997).
 144. Qiu, Z. & Gruol, D. L. Interleukin-6, beta-amyloid peptide and NMDA interactions in rat cortical neurons. *J. Neuroimmunol.* **139**, 51–57 (2003).
 145. Gosselin, R. D., Varela, C., Banisadr, G., Mechighel, P., Rostene, W., Kitabgi, P. & Melik-Parsadaniantz, S. Constitutive expression of CCR2 chemokine receptor and inhibition by MCP-1/CCL2 of GABA-induced currents in spinal cord neurones. *J. Neurochem.* **95**, 1023–1034 (2005).
 146. Gao, Y., Zhang, L., Samad, O. A., Suter, M. R., Yasuhiko, K., Xu, Z., Park, J., Lind, A., Ma, Q. & Ji, R. JNK-induced MCP-1 production in spinal cord astrocytes contributes to central sensitization and neuropathic pain. *J. Neurosci.* **29**, 4096–4108 (2009).

147. Rassow, J., Hauser, K., Netzker, R. & Deutzmann, R. *Duale Reihe Biochemie*. 3rd Edition, p. 544 (Georg Thieme Verlag KG, Stuttgart, 2012).
148. Peng, Y. P., Qiu, Y. H., Lu, J. H. & Wang, J. J. Interleukin-6 protects cultured cerebellar granule neurons against glutamate-induced neurotoxicity. *Neurosci. Lett.* **374**, 192–196 (2005).
149. Ruocco, G., Rossi, S., Motta, C., Macchiarulo, G., Barbieri, F., De Bardi, M., Borsellino, G., Finardi, A., Grasso, M. G., Ruggieri, S., Gasperini, C., Furlan, R., Centonze, D., Battistini, L. & Volpe, E. T helper 9 cells induced by plasmacytoid dendritic cells regulate interleukin-17 in multiple sclerosis. *Clin. Sci.* **129**, 291–303 (2015).
150. Li, H., Nourbakhsh, B., Cullimore, M., Zhang, G. X. & Rostami, A. IL-9 is important for T-cell activation and differentiation in autoimmune inflammation of the central nervous system. *Eur. J. Immunol.* **41**, 2197–2206 (2011).
151. Matsushita, T., Tateishi, T., Isobe, N., Yonekawa, T., Yamasaki, R., Matsuse, D., Murai, H. & Kira, J. I. Characteristic Cerebrospinal Fluid Cytokine/Chemokine Profiles in Neuromyelitis Optica, Relapsing Remitting or Primary Progressive Multiple Sclerosis. *PLoS One* **8**, e61835 (2013).
152. Kürtüncü, M., Tüzün, E., Türkoğlu, R., Petek-Balci, B., İçöz, S., Pehlivan, M., Birişik, Ö., Ulusoy, C., Shugaiv, E., Akman-Demir, G. & Eraksoy, M. Effect of short-term interferon- β treatment on cytokines in multiple sclerosis: Significant modulation of IL-17 and IL-23. *Cytokine* **59**, 400–402 (2012).
153. Godiska, R., Chantry, D., Dietsch, G. & Gray, P. Chemokine expression in murine experimental allergic encephalomyelitis. *J. Neuroimmunol.* **58**, 167–176 (1995).

8. Declaration of Authorship

This work was conducted at *Hertie Institut für klinische Hirnforschung, Tübingen* and supervised by PD Dr. Felix Bischof. The experiments were designed by myself together with PD Dr. F. Bischof and Dr. Kirsi Forsberg (postdoc).

All experiments were conducted by myself after an orientation by Dr. K. Forsberg and Mrs. Evelyn Dubois. Neuronal and astrocyte cultures were prepared by myself together with Ms. Simone Burkhardt (Master Student) and subsequently shared with her. The preparation of T helper type 9 cell cultures was performed by myself together with Dr. K. Forsberg and E. Dubois. The induction of experimental autoimmune encephalomyelitis was conducted by PD Dr. F. Bischof. Dissection of the spinal cord was performed by myself under the supervision of Dr. K. Forsberg. The statistical analysis of the experiments was performed by myself after an introduction by Dr. K. Forsberg.

I assure that I autonomously wrote the manuscript and that no other than the indicated references were used.

Hamburg,

[signature]

9. Danksagung

Insbesondere möchte ich mich bei meinem Doktorvater PD Dr. Felix Bischof für die gute Betreuung und Unterstützung dieser Arbeit bedanken. Zudem gilt mein Dank Dr. Kirsi Forsberg für die Betreuung und Anleitung im Labor. Des Weiteren spreche ich Evelyn Dubois, Simone Burkhardt und Lisa Grönnert meinen Dank für ihre tatkräftige Unterstützung aus.

Ein herzliches Danke gilt zuletzt meiner Familie und meinen Freunden, die mich bei der Erstellung dieser Arbeit und auch abseits davon unterstützten.

10. Curriculum Vitae

Personal Details:

- Name: Nakov, Philipp
- Date and Place of Birth: 08/December/1992, Worms
- Nationality: German

Education:

- | | |
|---|---|
| Studies of medicine at Eberhard Karls Universität Tübingen | October/2011 until presumably July/2011 |
| - Second state examination, grade: Very Good | 06/April/2017 |
| - First state examination, grade: Very Good | 06/September/2013 |
| - Dissertation at <i>Hertie-Institut für klinische Hirnforschung</i> , Tübingen supported by a grant from the IZKF-Promotionskolleg | since June 2014 |
| Graduation with the German Abitur | March/2011 |
| - Carl-Bosch-Gymnasium, Ludwigshafen | August/2009 – March/2011 |
| - International student at Nayland College, Nelson, New Zealand | July/2008 – July/2009 |

Clinical Experience:

Practical year:

- | | |
|---|-------------------------------|
| - Psychiatry, Universitätsklinikum Hamburg | December/2017 – April/2018 |
| - Surgery, Tygerberg Hospital, Kapstadt, South Africa | October/2017 – December/2017 |
| - Surgery, Universitätsklinikum Tübingen | September/2016 – October/2017 |
| - Internal medicine, Universitätsklinikum Tübingen | May/2017 – September/2017 |

Internships:

- | | |
|--|----------------------------|
| - Cardiology, Belfast City Hospital, Belfast, Northern Ireland | August/2016 |
| - Neurology, Universitätsklinikum Tübingen | March/2016 – April/2016 |
| - Psychiatry, Universitätsklinikum Tübingen | March/2016 |
| - Internal medicine, Universitätsklinikum Tübingen | August/2014 |
| - General practitioner, Praxis Dr. Erlenwein, Limburgerhof | February/2014 – March/2014 |